Heterogeneity Consideration in Centrifuge Experiments and Simulations for Capillary Pressure Curve Measurements

by © Guming Zhou A thesis submitted

to the School of Graduate Studies in partial fulfillment of the

requirements for the degree of

Master of Engineering Faculty of Engineering and Applied Science

Memorial University of Newfoundland

February 2022

St. John's Newfoundland and Labrador

Abstract

Capillary pressure curves are one of the most important inputs for reservoir characterization and modelling in oil and gas industry. Using centrifuge experiments for capillary pressure measurements is an efficient method for obtaining such curves. With the rapid development of modelling methods for centrifuge experiments, a challenge is now faced by researchers that the assumption of a one-dimensional and homogeneous core is required. The major objective of this research is to investigate the impacts of core-scale heterogeneity on phase saturation predictions by using a centrifuge simulation method that allows a two-dimensional fluid flow in the core. The streamline tracing method that considers capillary pressure numerically is applied to visualize and quantify effects of heterogeneity. Significant differences in phase saturation predictions have been observed between homogeneous and heterogeneous cores. For example, when a low permeability area is present in a core plug during a drainage centrifuge simulation, less wetting phase is displaced at some capillary pressure condition as compared to a homogeneous/randomly distributed core. Therefore, higher average saturations can be obtained and the maximum mean squared error of it is about 0.0013. A capillary pressure curve with a positive bias can be calculated and taken as an input for reservoir simulation to describe the distribution of reservoir fluids and the fluids contacts. When a high permeability area is present, the maximum mean squared error of the deviated saturation is 0.0004. This study revealed that it is necessary to consider core-scale heterogeneity in the modelling of centrifuge experiments since an inaccurate capillary pressure curve can produce results with considerable errors in reservoir simulations.

Keywords: Centrifuge measurement of capillary pressure curves, Core heterogeneity, Streamline tracing method, Phase saturation prediction

Acknowledgements

It is my great privilege to have pursued a master's degree at Memorial University of Newfoundland. This has been an exceptional learning and personal experience for me. I take this opportunity to thank those who helped me and contributed to making this experience wonderful.

I deeply indebted to my research supervisors, Dr. Lesley James and Dr. Jie Cao; without their guidance, help and support, this thesis would never have been completed. Beyond the valuable advice they give, I am grateful for the manner in which we interacted. They work closely with me during difficult times. I also thank Norah for careful revision of my draft thesis. I address my sincere gratitude to all the engineers and researchers in the Hibernia Enhance Oil Recovery Laboratory for their tremendous help in assisting me. I thank the faculty members of the Faculty of Engineering and Applied Science, who taught me so much. I also thank the department staff for assisting me with all the administrative matters.

Finally, to my dear parents and girlfriend, I would like to thank you for all your love and support throughout my life. Without your support I could not complete my study far abroad. Thank you to my sister and friends, you have also been the best of support along this study.

Table of Contents

List of Tables

List of Figures

List of Nomenclature

Symbols	Meaning
P_c	Capillary pressure, [Pa]
P_{c_1}, P_{c_2}	Capillary pressure at the inlet and outlet face, respectively
P_{cd}	Threshold capillary pressure when the wetting phase begins to be displaced
P_c^{eq}	Capillary pressure at equilibrium
P_{nw}, P_w	Nonwetting/wetting phase capillary pressure
P_{th}	Threshold capillary pressure
σ	Interfacial tension between two phases/ normalizing factor
R_1, R_2	Radii of curvature of the interface between two fluids
r_c	Radius of the capillary tube
r_{th}	Location/radius of the threshold capillary pressure
K	Permeability, [m^2]
K_{avg}/K^*	Average permeability, [m^2]
k_r	Relative permeability
F	lithology factor accounting for differences between the fluid flow properties of a hypothetical porous medium and naturally occurring rocks
$\emptyset$	Porosity
S_{nw}	Nonwetting phase saturation as a fraction of bulk volume
S_w	Wetting phase saturation as a fraction of bulk volume

S_{wi}	Irreducible wetting phase saturation
$\bar{S}$	Average saturation
$\bar{S}_i$	Initial average saturation (at start of test)
ΔS_{eq}	Saturation variation during the considered speed step
S_w^{eq}	Water saturation at equilibrium
S_{wn}	Normalized water saturation
$aveS_w$	Average wetting phase saturation
$inletS_w$	Wetting phase saturation at the inlet face
S_{or}	Residual oil saturation
V_p	Pore volume, [cc]
$V_{dispalced}$	Volume of displaced fluid, [cc]
RPM	Revolutions per minute
r_1	Distance from the center of rotation to the outer face of the core plug
r_2	Distance from center of rotation to the inner face of the core plug
ω	Angular velocity
ω_c	Critical value of angular velocity
L	Length of the core
A	Area
T_1, T_2	Characteristic times of the exponential functions
w	Affected weight
f_w	Water fractional flow function
q	Volumetric outflow/inflow rate
λ	Mobility
T	Transmissibility, $[m^3/(s \cdot Pa)]$
W	Volume rate of water produced or injected by internal sources and sinks per

	unit volume of aquifer
Q	Volume flow rate across a cell face
Q_s	Sources or sinks in the grid block
q_r	Reference flow rate
g	Gravitational acceleration, $[m/s^2]$
SSE	Sum of squared errors
MSE	Mean squared errors
u_T	Drainge rate
R	Flow resistance
bc	Bounary condition

Greek Symbols	**Meaning**
θ	Contact angle, [°]
v	Velocity
u	Darcy velocity
ξ	Streamline arc-length, [m]
ψ	Stream function
τ	Time-of-flight, [s]
ρ	Density of the fluid, $[kg/m^3]$

Others	**Meaning**
$\times$	Cross product
∇	Gradient operator
$\nabla \cdot$	Divergence operator
Δ	Difference operator

1 Introduction

Capillary pressure curves are essential to understanding fluid distribution in a reservoir. They can be determined through a variety of laboratory methods and there are many methods to model capillary pressure measurement experiments; however, one-dimensional (1D) flow is not always assumed in these modelling methods, which is not representative. The work described in this thesis seeks to investigate the impacts of core-scale heterogeneity on phase saturation predictions by using a centrifuge simulation method that allows a two-dimensional (2D) flow in the rotated core. This chapter provides background information about rock, pore distribution, capillary pressure, capillary pressure measuring and modelling methods. This chapter also presents the challenges of centrifuge simulation methods when considering heterogeneity, and defines the objectives, motivation and outline of this thesis.

1.1 Pore Size Distribution

A rock is a solid mass made up of unconsolidated and consolidated grains of different minerals with pores in between (Panchuk, 2019). Figure 1 shows a typical porous rock. Rocks are usually grouped into three types based on how they form: sedimentary rocks, igneous rocks and metamorphic rocks. Sedimentary rocks form when rock fragments are buried, compressed and cemented together, or when minerals precipitate from solution. Igneous rocks form when melted rock cools down and becomes solid. Metamorphic rocks form when a previously existing rock is subject to very high temperature and pressure. Oil and gas may exist in any types of porous rock, but it is generally found in sedimentary rocks, such as sandstone or limestone. Figure 2 shows a sandstone that contains grains of quartz (white), calcite and feldspar (shades as brown). This rock

sample was injected with blue epoxy that is seen here filling interconnected pores and the arrow indicates a possible pathway for fluid movement. Figure 3 shows a limestone taken from a core sample and the circular grains composed of calcite and dolomite are totally cemented by medium crystalline calcite.

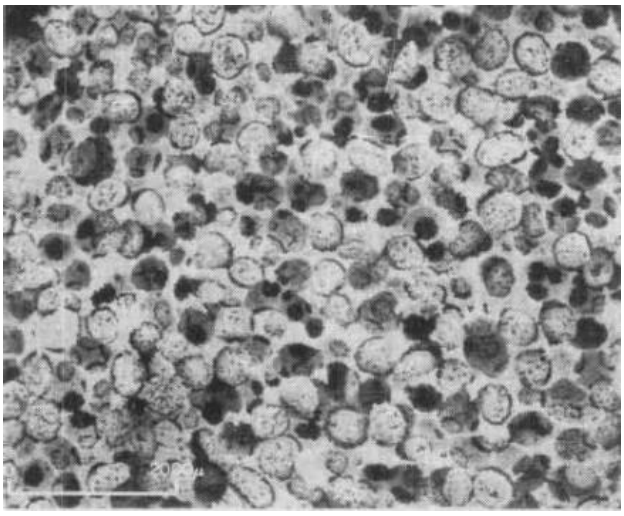

Figure 1 A rock with pores (from Swanson, 1979)

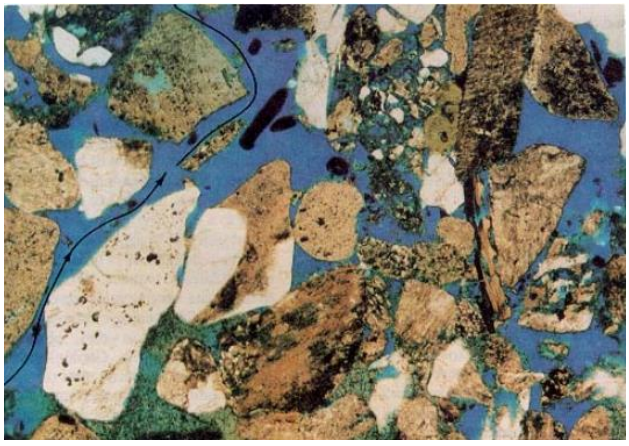

Figure 2 A magnified image of a sandstone (from Kansas Geological Survey and Baars, 1989)

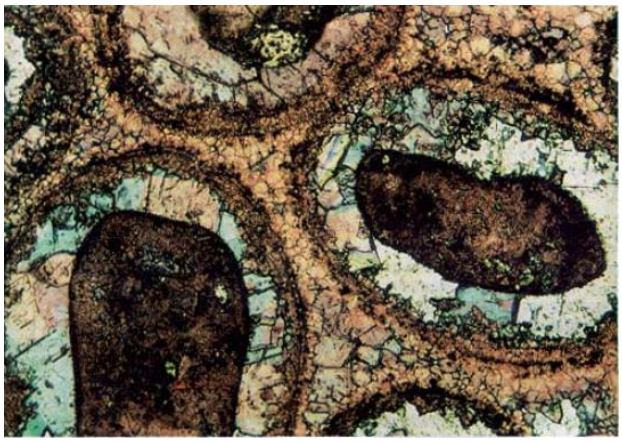

Figure 3 A thin-section photomicrograph of a Pennsylvanian limestone taken from a core sample of a producing zone in Victory field, Haskell County, Kansas (from Kansas Geological Survey and Baars, 1989)

In a rock sample with different sizes of pores, pore size distribution is the relative abundance of each pore size in a representative volume of rock (Nimmo, 2004). Figure 4 shows the pore size distributions for different rocks and voxel is a unit of graphic information that defines a point in three-dimensional space. Mt Gambier, Estaillades and Ketton are formations that contain carbonate rocks. Doddington and Bentheimer are formations that contain sandstones.

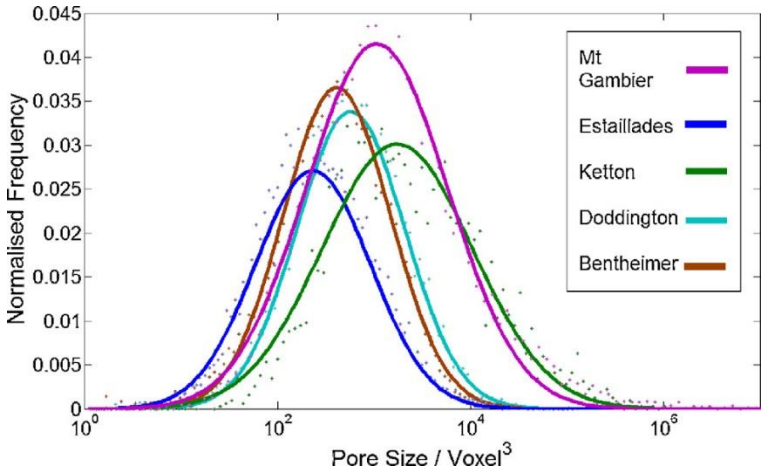

Figure 4 Pore size distributions for different types of rocks (from Andrew et al., 2014)

1.2 Capillary Pressure

The difference in pressure between two immiscible fluids is called capillary pressure, which

contributes to the equilibrium of the system (Tiab and Donaldson, 2015). The interface between the two phases is curved because each phase has a preference for wetting of the capillary wall. When a polar liquid is placed into a capillary, impacted by intermolecular forces it tends to rise against gravity, which is called capillary action. Namely, water will be drawn up into the capillary that is put in a dish of water. The entering angle of the tube will not influence the height of the water, which mainly depends on the diameter of the tube and the water temperature. Accordingly, a smaller diameter will make the liquid rise higher. Figure 5 shows the capillary tubes with different radius that occur between the wetting and non-wetting fluid reservoirs. This capillary tube model is analogous to illustrate the influence of pore size distribution on the characteristics of reservoir fluid saturation (Ng and Pang, 2000). Capillary action is the result of two opposing sets of forces: the intermolecular forces holding a liquid together (cohesive forces) and the attractive forces between a liquid and the capillary substances (adhesive forces). Meniscus is the upper surface of a liquid in a tube, the shape of which depends on the ratio of cohesive and adhesive forces (Batchelor, 1982). The rise of the liquid column can be described physically by a vertical capillary pressure model. The movement of fluid is caused by the potential between the liquid surface inside and outside the tube and will stop when the potential drops to zero (Evans and Guerrero, 1979).

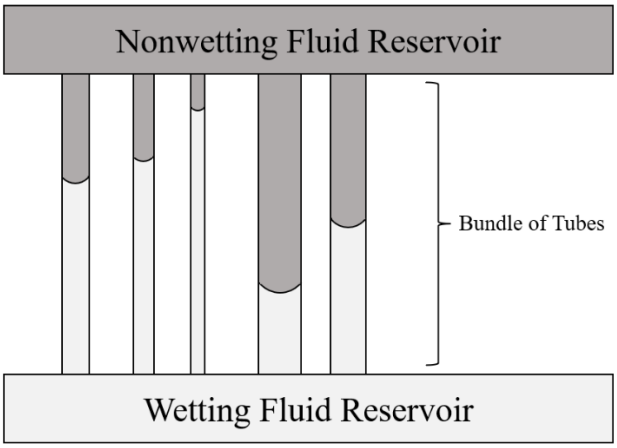

Figure 5 Buddle of capillary tubes (after Dahle et al., 2005)

The pressure within the wetting phase is always less than the pressure in the non-wetting phase leading to the curvature of the interface. The capillary pressure is therefore defined as the pressure difference between the non-wetting and wetting phases:

$$P_c = P_{nw} - P_w \tag{1.1}$$

where P_c is the capillary pressure, P_{nw} is the pressure in the non-wetting phase and P_w is the pressure in the wetting phase.

Mineralogy and pore size distribution, plus wetting and non-wetting fluids, define the capillary pressure. The application of capillary pressure to porous media is described by Equation (1.2), considering the capillary pressure as a function of interfacial tension and radius curvature (Leverett, 1941):

$$P_c = \sigma(\frac{1}{R_1} \pm \frac{1}{R_2}) \tag{1.2}$$

where σ is interfacial tension between two phases, and R_1, R_2 are radii of curvature of the interface between two fluids. Due to the mathematical relationship between the radius of capillary tube and that of spherical interface, the contact angle is defined as:

$$\cos\theta = \frac{r_c}{R_i} \tag{1.3}$$

where r_c is radius of the capillary tube and R_i is radius of the spherical interface. Substituting Equation (1.3) into Equation (1.2), a new expression for capillary pressure that relates contact angle, radius of the capillary tube and interfacial tension is yielded:

$$P_c = \frac{2\sigma\cos\theta}{r_c} \tag{1.4}$$

The pores of different sizes and wettability in the reservoir means that capillary pressure is a function of fluid saturation and wettability. The mathematical description between capillary pressure and wetting phase saturation is called the capillary pressure curve, the measurement of which is essential in petroleum industry.

1.3 Relevance to Petroleum Industry

Capillary pressure is one of the most important properties of a porous medium and many scientists have proved that it is necessary to include capillary pressure in research of phase behavior, multi-phase fluid displacement and reservoir simulation. Multi-phase flow problems in porous media are often encountered in important petroleum applications, such as enhanced oil recovery, oil production and gas storage techniques. It is difficult to obtain a theoretical solution of multi-phase fluid flow because the generic multiphase flow model has a complicated mathematical character and a changeable balance of different physical forces (Lie, 2019). The characteristics and individual strengths of this model also vary in different flow regimes. Thus, the multi-phase flow problem can be solved by using macroscopic equations based on capillary pressure and relative permeability (Dullien, 1992; Marle, 1981). In multi-phase system, the ability of flow for each phase in the

presence of other phases need be determined by calculating relative permeability. The currently used calculation methods of relative permeability curves from capillary pressure data are based on a model proposed by Purcell (1949). Combing the Poiseuille's equation and Darcy's Law for a hypothetical model composed of a large number of capillary tubes, he presented the following equation:

$$K = 2F(\sigma \cos\theta)^2 \emptyset \int_0^1 \frac{dS_{nw}}{{P_c}^2} \tag{1.5}$$

where K is permeability, F is a lithology factor accounting for differences between the fluid flow properties of a hypothetical porous medium and naturally occurring rocks, σ is interfacial tension, θ is contact angle, $\emptyset$ is porosity, P_c is capillary pressure and S_{nw} is nonwetting phase saturation as a fraction of bulk volume.

Capillary pressure in a reservoir can determine the saturation distribution and thus the total in-situ volumes of fluids (McPhee et al., 2015). Thus, it is essential to have an accurate knowledge of the capillary pressure in the estimation of hydrocarbon reserves. Ediriweera and Halvorsen (2015) studied the impacts of the relative permeability on oil recovery and found that total oil production and water breakthrough time are significantly influenced by relative permeability. Capillary pressure curves and relative permeability curves are often used as inputs for reservoir simulations to predict ultimate oil productions.

In reservoir engineering and oil production practice, the permeability of the rock is one of the most important properties. To measure this property, a rock sample of regular shape and appreciable dimensions is required; the costly operating process is also needed for the measurement. In order

to simplify permeability estimation, Purcell (1949) introduced an approach that relates capillary pressure curves to permeabilities of porous media. The calculation of permeability using this method is easily achievable. Gates and Lietz (1950) furthered this relationship so that it can be used to perform relative permeability calculations for multiphase fluid flow in porous media. However, it is almost impossible to get exact values of tortuosity factors in the equation because of the enormous number of variables. Therefore, a method to approximate tortuosity factors in terms of fluid saturations and petrophysical properties was introduced by Burdine (1953). In Brooks and Corey's' (1966) research, a modified method was proposed to represent capillary pressure by using a power law function of the wetting phase saturation. Instead of inputting reservoir permeability data directly, Li and Horne (2003) proposed a numerical simulation approach to compute corresponding relative permeabilities from capillary pressure data by some correlations, which increases the computational efficiency. Many scientists have devoted themselves to correlating capillary pressure to permeability. Honarpour et al. (2018) reviewed literature on correlations between permeability and capillary pressure in drainage.

Capillary pressure curves play a significant role in the description of a core's wettability. The contacts between oil, gas and water deviate from the normal situation because interfacial tensions between two phases are different from one another in capillary spaces where gas, oil and water coexist. Furthermore, to obtain the distribution of fluids in initial-state reservoirs, capillary pressure versus saturation data must be converted into height-saturation data so that the overall situation in the transition zone can be thoroughly understood (McPhee et al., 2015). The conversion process requires knowledge of capillary pressure as well as wetting characteristics, which is significant in

tertiary recovery and necessary in the facilitation of the oil removal. In addition, the wettability of the reservoir should be determined before normalizing the data from mercury injection experiments (Tiab and Donaldson, 2015). Therefore, scientific interest in research of using capillary to measure wettability was triggered (Anderson, 1986). Tiab and Donaldson (2015) proposed a method to determine the rock wettability by comparing the work required to displace water by oil with that required to displace oil by water according to the area enclosed by the drainage curve and the abscissa and that enclosed by the imbibition curve and the abscissa respectively. This finding has validated that capillary pressure curves can be applied to determine the rock wettability.

Capillary pressure curves have broad potential in the field of reservoir simulation; for example, capillary pressures between different immiscible phases at a specific saturation computed in the simulator can be used to calculate the phase pressure in one phase once the pressures in the other phases are known (Evans and Guerrero, 1979). It is also commonly believed that a clear understanding of both drainage and imbibition capillary pressure curves can result in better estimation and evaluation of the reservoir performance. In the model building process of reservoir simulation, saturation in each grid cell should be pre-defined within a plausible range because it determines the initial fluid distributions. The saturation limits can be calculated by setting different transition zones according to drainage capillary pressures (Lie, 2019). To determine the effect of capillary pressure on the numerical simulation of a reservoir producing under different recovery processes, Shams et al. (2013) studied both fractured and non-fractured reservoirs by constructing several numerical reservoir simulation models. They found that capillary pressure may affect the accuracy of fractured reservoir simulation studies, as imbibition capillary pressure is a dominant

driving force in these types of reservoirs. Several indicators have been proposed to evaluate the effects of capillary pressure on average reservoir pressure, water cut and gas-oil ratio; and the Dykstra-Parsons coefficient of permeability variation is used to indicate the degree of heterogeneity in models. Shams et al. (2015) concluded that the importance of capillary pressure effects differs from different recovery processes in all types of reservoirs, and they presented the conclusion maps that can be utilized as the reference to decide whether the capillary pressure should be considered in the numerical reservoir simulation. Wang et al. (2006) noted that to get satisfactory results, reservoir simulation models should incorporate different types of data including capillary pressure, relative permeabilities and pressure-volume-temperature (PVT). Thus, a procedure to incorporate the capillary pressure-saturation data was developed and a capillary pressure-saturation correlation was proposed. To investigate the importance of capillary pressure in waterflooding experiments, Alzayer et al. (2017) conducted a Numerical Coreflood Experiment (NCFE) to generate numerical experimental data (cumulative production, pressure). The flow functions (relative permeability, capillary pressure) can then be estimated and compared to the input flow functions. He discovered that the effects of capillary pressure in multiphase displacements appear to show on breakthrough time, flat length of the oil production and oil recovery.

The mathematical investigation of capillary pressure on the phase envelope was initiated by Brusllovsky (1992). Nojabaei et al. (2013) concluded that capillary pressure in nanometer pores can greatly affect the phase behavior and the physical properties of fluids, such as saturation pressures, fluid densities and viscosities. The interfacial tension in the capillary pressure equation is the key parameter contributing to the variation of bubble point and dew point pressure. The

pressure drop across coarse grid blocks is often larger than the capillary pressure in a reservoir-scale simulation, which makes the capillary pressure negligible (Alzayer et al., 2017). However, it has been shown that oil recovery in reservoir simulation can be enhanced when capillary pressure is input in the simulator (Purcell, 1950). To calculate bubble-point pressure suppression based on capillary pressure and solution gas-oil ratio, a correlation was developed by Firincioglu et al. (2012). They concluded that capillary pressure has a significant influence on bubble point pressure suppression. Wang et al. (2006) indicate that capillary pressure versus water saturation data should be considered in reservoir simulation when converting a fine scale reservoir model to a flow simulation model to ensure that it keeps the right geological and physical parameters.

Capillary pressure curve can be applied to evaluate the pore size distribution of reservoirs. It is known that the sorting of grains and the pore sizes have an influence on the shapes of the capillary pressure curves (Leal et al., 2001). The largest pore size can be calculated by substituting the threshold pressure acquired from the capillary pressure curve into the Equation (1.4) and the calculated r_c is the size of the largest pore. Pore size distribution is also a crucial indicator in selecting the diverting agent for heterogeneous reservoirs, which is a chemical agent used in simulation treatments to ensure uniform injection over the area to be treated (Harrison, 1972). Evans and Guerrero (1979) found that capillary pressure curves can show relative sorting of the grains that suggests the depositional environment. The capillary pressure and saturation data from mercury injection method are commonly used to determine the pore size distribution. This can be achieved by using the capillary pressure to calculate the pore size and then a histogram can be drawn to deduce pore geometry characteristics (Pickell et al., 1966; Swanson, 1979).

1.4 Capillary Pressure Measurement Methodologies

The pressure difference between the two different phases during the equilibrium displacement of the wetting phase by the non-wetting phase is the drainage capillary pressure, which is observed as a function of wetting phase saturation. If the non-wetting phase is displaced by wetting phase, the pressure difference is called imbibition capillary pressure (Tiab and Donaldson, 2015). Both drainage and imbibition capillary pressure curves are measured in the laboratory and in this thesis, only primary capillary drainage is considered. There are several special core analysis laboratory (SCAL) techniques to determine capillary pressure curves: the semi-permeable diaphragm/porous plate, mercury injection, and high-speed centrifuge methods. These methods usually give different capillary pressure curves and consequently residual oil/water concentration due to the underlying differences in the theoretical principles (Amyx et al., 1960).

1.4.1 Porous Plate Method

Diaphragm was the first tool that people used to measure capillary pressure curves, which can also be referred to as the porous plate method, semi-permeable membrane method, and restored-state technique (McPhee et al., 2015). Figure 6 shows the apparatus for capillary pressure measurement using a porous plate.

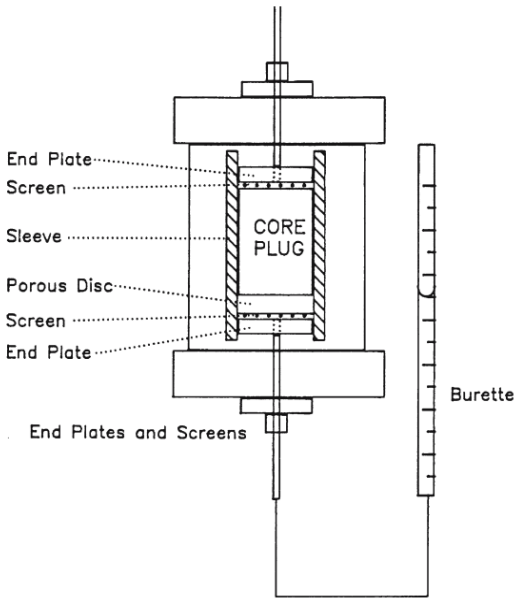

Figure 6 Porous plate method for measurement of capillary pressure (from Li and Williams, 2007)

This method involves placing a brine-saturated core sample on a porous membrane and then increasing the pressure of an immiscible displacing fluid incrementally. The displacement is complete when the water saturation has reached its irreducible value. The capillary pressure versus water saturation curve is then plotted using the experimental data. Core samples can be processed on a batch basis or in individual core holders in the diaphragm method. The displacement is reversible by placing the core on another oil saturated porous disk and the core is then covered with water. The porous plate method is often considered the most accurate of the three common methods for capillary pressure curve measurements, because it prevents a saturation gradient (Shikhov and Arns, 2015). The porous plate can also be used to condition the core sample for relative permeability tests and to provide saturation data at equilibrium for resistivity index measurements. Nonetheless, this method is very slow, and can take more than 20 weeks to obtain an oil-water drainage curve (Wilson et al., 2001). To shorten the time required for the experiment when it comes

to the low permeability membrane, a laminated diaphragm was developed to reduce the time for drainage capillary pressure of relatively homogeneous samples to 35-35 days (Wilson and Skjæveland, 2002). To accelerate the data collection process of this experiment, several mathematical models have been proposed such that the fluids do not need to reach equilibrium at the time of measurement (Fleury et al., 1997; Shafer and Lasswell, 2007; Dernaika et al., 2010).

1.4.2 Mercury Injection Method

Another capillary pressure measurement method involves injecting incremental volumes of mercury into an evacuated core sample while recording the injection pressure of each increment, which is called mercury injection method (McPhee et al., 2015). Figure 7 shows the equipment for mercury injection method for capillary pressure curve measurements. When mercury intrusion stops, the pressure can be decreased incrementally to achieve the imbibition capillary pressure curve. The capillary pressure data generated by the mercury injection method can provide information about the pore structures of rock samples (Yuan and Swanson, 1989). O'Meara et al. (1992) found that capillary pressure curves calculated from the mercury injection method are good representations of capillary pressure curves of water-wet reservoirs from other measuring method. Mercury injection is rapid (< 1 day) compared to the porous plate method (4-8 weeks) and can be implemented in pores with small diameters (Purcell, 1949). This mercury injection is analogous to a real drainage process for the strong non-wetting behavior of mercury; thus, it can be used to determine the connectivity of the pore structure but may not accurately represent partially wetting fluids. There are several other disadvantages in using this method to measure capillary pressure curves (McPhee et al., 2015). For sample, high pressures and interfacial tension can destroy

sensitive clays lining or filling pores; lack of standards to calibrate the experimental apparatus at high pressure resulting in errors in capillary pressure or water saturation measurements; no irreducible wetting phase saturation as air can be compressed at high pressure and the pore space will be totally filled with mercury; cores subject to mercury injection tests are contaminated preventing their further use for other tests and causing environmental issues.

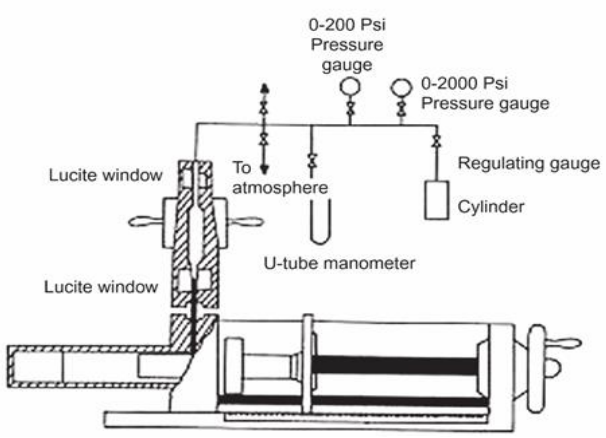

Figure 7 Equipment for mercury injection capillary pressure measurement (Tiab and Donaldson, 2015)

1.4.3 Centrifuge Method

Efficiency of the capillary pressure measurement methods is important since a great number of core plugs need to be tested for the evaluation of oil reservoirs. Slobod et al. (1951) introduced the centrifuge experiment and it is now a widely used method to measure capillary pressure in routine core analysis. Figure 8 shows the typical centrifuge machine for centrifuge experiments in McPhee et al. (2015). A cup involving a calibrated holder is used as a part of the experimental device and the centrifugal force can result in the fluids displacement from the core inside tube so that denser fluids will be forced away from the rotational center while lighter fluids have an opposite moving direction. Figure 9 shows a core holder with a graduated glass tube collecting the displaced fluids in Tiab and Donaldson (2015). During the experiment, the core sample is placed either towards the

rotation center to allow a denser fluid to be produced or away from it so that a lighter fluid will be forced out of the core plug. Thus, it is very important to take fluid density into consideration when determining the position of the core plug and gas should not be included in experiments due to its compressibility and diffusion problems. The rotational speed is increased incrementally and the volume of produced fluid is measured when the fluids in the core are at equilibrium. Accordingly, the displaced volumes of fluid and angular velocities at each incremental speed can be converted to average wetting-phase saturation versus capillary pressure data, which can then be used to generate the capillary pressure curve. Thus, the choice of the data conversion method can have a strong influence on the final capillary pressure curves. Figure 10 shows a typical plot of drainage capillary pressure curve.

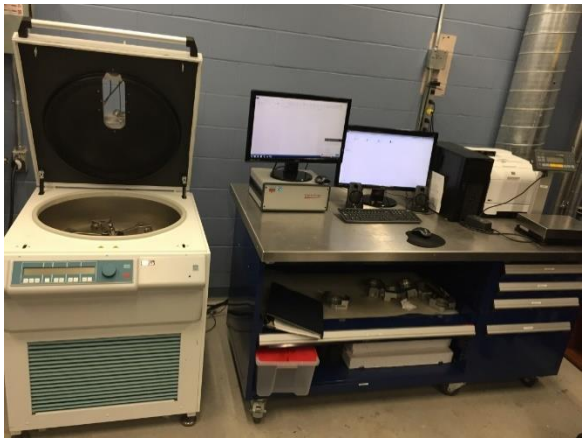

Figure 8 Ultra-centrifuge machine in Hibernia Enhanced Oil Recovery (EOR) Laboratory

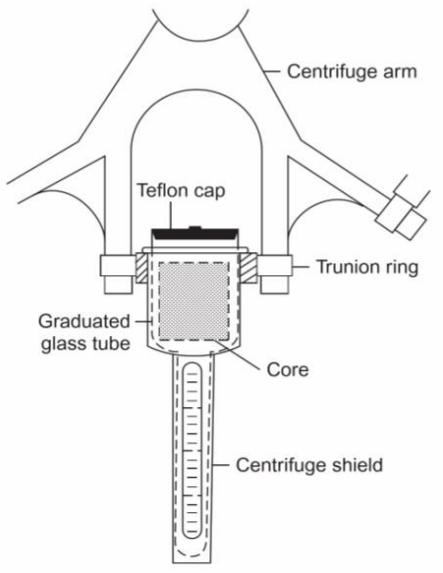

Figure 9 Equipment for centrifuge experiment (from Tiab and Donaldson, 2015)

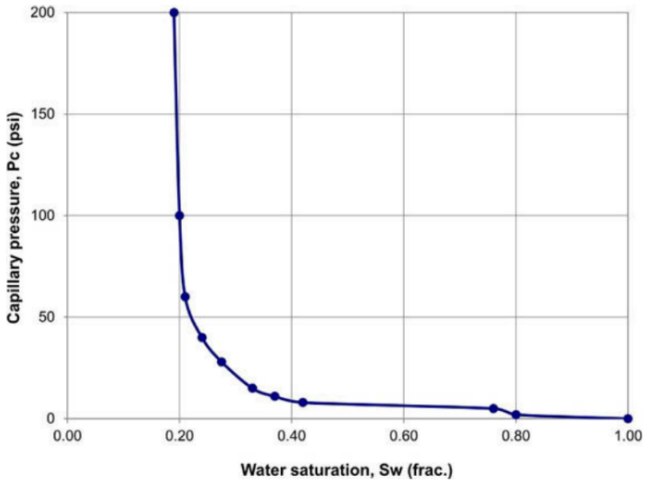

Figure 10 Linear plot of capillary pressure versus water saturation (from McPhee et al., 2015)

Procedures for centrifuge experiments were first introduced by Donaldson et al (1980). They are:

1. Measure pore and bulk volume of the core and saturate the core with brine.
2. Immerse the brine-saturated core sample in the capillary coreholder filled with non-wetting fluid, i.e. oil.
3. Rotate the core at the first angular velocity and collect the displaced fluid in the graduated tube.

4. Repeat Step 3 for each incremental pre-determined rotational speed and use a stroboscopic light to capture the illusion of the system, allowing the displaced volumes to be recorded.
5. Bond number should be calculated and plotted as a function of saturation to validate critical boundary conditions. For strongly water-wet systems, a bond number limit of 10^{-5} is usually used but it can also be directly determined using the correlation (Hagoort, 1980).
6. Once the drainage centrifuge test is completed, decelerate the spin gradually to avoid sample failure.

1.4.4 Comparison of Measurement Methods

Each method for capillary pressure measurement has advantages and drawbacks. A summary of the advantages, drawbacks and issues of the various capillary pressure methods is presented in Table 1. The porous plate method is considered the best method to duplicate the original displacing state in the reservoir (Tiab and Donaldson, 2015), but some scientists insist that the centrifuge method can produce better results (Slobod et al., 1951; Ayappa et al., 1989). Although this technique is thought to have the best simulation of the wetting condition of the rock sample, refined mineral oil and prepared salt water are generally used in the experiments rather than reservoir fluid samples (Evans and Guerrero, 1979). Also, this diaphragm method is time consuming, varying from 10 to 40 days for a single sample. The mercury injection method is simple, cheaper, and less time consuming than the diaphragm and centrifuge methods. It can appreciably increase the range of pressure being investigated and can be carried out on cuttings or sidewall samples. However, the mercury injection method has two disadvantages: the permanent loss of the core samples because the mercury cannot be safely removed after the injection, and the rigorous safety

precautions required (Shams et al., 2015). As a fast and relatively simple method, the centrifuge experiment has the potential for widespread application in oil industries as it is suitable for almost all types of reservoir rocks and is a non-destructive test (McPhee et al., 2015). Hence, high-speed centrifuge for capillary pressure measurements is carefully considered and modeled in this research.

Table 1 Pros and cons of capillary pressure methods (from McPhee et al., 2015)

Method	**Advantages**	**Drawbacks**
Centrifuge	• Relatively simple and quick • Use reservoir appropriate (synthetic) fluids • Desaturation is more rapid than for the porous fluid • Tests at reservoir overburden pressure and elevated temperature are possible • Non-destructive test, re-usable samples	• It is the most expensive method • Raw production data is corrected by the test lab to account for the capillary pressure gradient across sample. This the main source of inaccuracy of the method. • High speed centrifuge needed to reproduce pressures at crests of thick column reservoirs • At high sin speeds desaturation effects due to excessive viscous forces can cause changes in the capillary pressure • The method creates an unusual stress regime • Primary drainage curves require the samples to be water wet • The time allowed to achieve capillary equilibrium can completely govern the shape of the resultant curve • Stopping and restarting the centrifuge is not accepted as can lead to sample fracturing and produce saturation hysteresis effects • Benign cleaning is required to preserve delicate clay structure
Porous Plate	• It is the best method to achieve a uniform saturation profile during the drainage phase • Uses reservoir appropriate fluids • If the sample is relatively clay rich, the method is preferable to others • Nor destructive test, reusable samples • Test can be run in conjunction with resistivity index • In general, cheaper than centrifuge	• The main disadvantage lies in its length of time for the description of a complete curve. There are limitations on the maximum attainable capillary pressure values, depending on the system • Curves require the samples to be water wet • Time to achieve capillary equilibrium can completely govern the shape of the resultant curve • Benign cleaning is required to preserve delicate clay structure
Mercury injection	• It is a relatively low-cost technique • Capillary equilibrium is attained after a short period hence tests are very rapid • Provides data on pore throat size distribution • Provide useful input data to properly design pressure steps for centrifuge and porous plate tests • The mercury injection technique is well suited for low permeability samples and samples from high relief gas reservoirs • Dual porosity systems can be identified given the high resolution of the test	• Air-mercury tests are not strictly capillary pressure tests since there is no strong wetting phase involved and irreducible saturation is never attained • Not suited for samples with sensitive and/or reactive clays • The method is not representative of reservoir fluids • Tests are sensitive to sample size • The test is destructive so that the sample cannot be used for any other tests • The method is not recommended for unconsolidated samples • A closure correction is often required.

1.5 Modelling of Centrifuge Experiment

1.5.1 Effect of Rock Heterogeneity

Rock heterogeneity has long been regarded as an important factor in determining the physics of fluid flow in porous media and reservoir performance. However, core heterogeneity is often neglected in the modeling of centrifuge experiments for capillary pressure measurements. The assumption that the core is homogeneous leads to an assumption that flow is one-dimensional, which may result in significant deviations in the subsequent data interpretation process (Lenormand, 2017). Therefore, it is necessary to describe heterogeneity for better understanding (Lake et al., 1991). Many scientists have studied the effects of heterogeneity on viscous fingering. Kelkar and Gupta (1991) developed a numerical simulator with fine grids to study the viscous instabilities and the numerical results from the simulator was validated with the analytical solution for the displacement with unit mobility ratio. They concluded that heterogeneity contributes to the instabilities of displacement and that instabilities increase with increases in the degree of heterogeneity and permeability variance. Tchelepi et al. (1993) investigated how viscous fingering, dispersion and heterogeneous permeability interact with each other in the miscible displacement and they found that displacements with mobility less than unity diminish the effect of heterogeneity. Fayers et al. (1990) discovered that the three empirical methods for the modelling of viscous fingering produce results with similar degrees of accuracy in one-dimensional simulation, whereas their applications in two-dimensional cases differ from each other. They also found that heterogeneity has a strong influence on the accuracy of the models for viscous fingering simulations, which can be improved by adding an additional diffusive term. Recently, several

studies focused on the influences of heterogeneity on immiscible displacements. Watson et al. (1985) studied the effects of heterogeneity on the pressure drop profile in high-rate displacements. The presence and corresponding location of the heterogeneous section can be approximately determined in a two-phase miscible displacement. Araktingi and Orr (1988) have studied the effects of large-scale heterogeneities on mobility, pressure, and flow velocity. To study the effects of pore-scale heterogeneity, Chang and Yortsos (1992) completed a numerical Buckley-Leverett displacement process by varying permeability in the displacement direction. They conclude that the effects of heterogeneity on the saturation profile are significant even for displacements under large flow rates. Zeybek et al. (1995) proposed a study about the effects of heterogeneous permeability on spontaneous imbibition process by considering both the deterministic and stochastic heterogeneity profiles. They found that if a heterogeneous section is present in a two-dimensional flow system, recovery curves and saturation profiles will be seriously affected. Through these studies about rock heterogeneity, it is tacitly accepted that the importance of the heterogeneity of core plugs cannot be easily underestimated (Hamon and Vidal, 1986). Thus, it is necessary to include the rock heterogeneities in the modelling of centrifuge experiments because heterogeneity and anisotropy often exist in a core plug due to small-scale laminae or cross bedding (Mannseth et al., 1998).

1.5.2 Previous Studies on Centrifuge Modelling

Most of the centrifuge modelling methods over the length of the core are one-dimensional without the consideration of core heterogeneity. O' Meara and Crump (1985) presented a numerical simulator for the history-matching of the fluid production data in centrifuge experiments and

attempted to measure relative permeability and capillary pressure in a single experiment. They assumed the walls of the core as a no-flow boundary so the fluid flow inside is in one dimension. Andersen et al. (2017) developed an analytical model to analyze centrifuge experiments for drainage process and this model can be applied to estimate average water saturations at equilibrium. However, the derivations of the general partial differential equations describing the model setup were done based on the premise that the core is sealed in the directions normal to the displacement direction, meaning the system is one-dimensional. The major commercial software for centrifuge experiments, such as CYDAR, PORLAB, SCORES and SENDRA, can only assume a one-dimensional fluid flow system, which means they all neglect the fluid flow in the radial direction when heterogeneity exists (Lenormand, 2017). Shikhov and Arns (2015) made an evaluation of three laboratory techniques for capillary pressure measurements via a digital core generated from mathematical morphology and a digital sample representation by assuming that a core is homogeneous. This assumption indicates that they assume a one-dimensional fluid flow in the digital rock (Adachi, 1986). Although these centrifuge simulation methods are effective, they cannot describe the fluid flow accurately and account for the deviation in phase saturation predictions. These modelling methods predicted the average wetting phase saturation in the core by integrating the mass balance equation with the boundary conditions in a one-dimensional system, which apparently neglected core heterogeneity. Hence, a two-dimensional centrifuge simulation method is presented in this thesis to study the impacts of core-scale heterogeneity on phase saturation prediction.

1.6 Research Objectives and Motivation

The motivation for this research originates from the assumption in centrifuge data reducing methods that the rotated core is homogeneous (Christiansen and Cerise, 1992). Many scientists have developed centrifuge models based on the premise that the core is sealed in the directions normal to the displacement direction, which means the system is only one-dimensional (O'Meara and Crump, 1985; Andersen et al., 2017). Most commercial simulation methods available for the modelling centrifuge experiments assume a one-dimensional fluid flow in the core (Lenormand, 2017). Shikhov and Arns (2015) evaluated capillary pressure methods using the numerical simulation of the drainage process on a homogeneous core sample. When the core is homogeneous, the fluid flow in the core is only in one dimension (Adachi, 1986). The challenge for modelling the centrifuge experiment for phase saturation predictions is that the assumption of one-dimensional flow in a homogeneous core has been made. Our hypothesis is that fluid flow and saturation predictions in the core will be affected if heterogeneous regions exist.

Therefore, a two-dimensional centrifuge simulation model is needed to explain the heterogeneity effects on fluid flow and capillary pressure curves. This simulation technology has a potential to be improved to predict more accurate phase saturation with the consideration of heterogeneity as demonstrated in this thesis. This research builds a new two-dimensional, two-phase centrifuge simulation model to meet the following three objectives:

1. Model centrifuge experiments for capillary pressure measurements in two dimensions using streamline tracing method that considers capillary pressure numerically. The simulation results are compared with the observed results from lab-scale centrifuge experiments to

demonstrate the effectiveness of the two-dimensional centrifuge simulation method.

2. Visualize the effects of heterogeneities on fluid flow during the centrifuge experiment.
3. Validate and demonstrate the effects of heterogeneities on capillary pressure curves by comparing the simulations results from homogeneous porous media and that from heterogeneous porous media.

The above objectives are important since two-dimensional centrifuge simulation for phase saturation prediction is a relatively new method to researchers and engineers.

Core scale heterogeneity and two-dimensional system have never been introduced in the modelling of centrifuge experiments for capillary pressure curve measurements. My contribution to the centrifuge simulation technology is to develop a two-dimensional centrifuge simulation method for phase saturation prediction that takes core scale heterogeneity into consideration. In this thesis, the importance of accurate modelling of heterogeneities for the determination of capillary pressure curves is addressed. The centrifuge simulation method for phase saturation predictions proposed in this thesis has advantages over other methods presented by O'Meara and Crump (1985) and Andersen et al. (2017) since it considers core heterogeneity and allows fluids in the core model to flow in two dimensions. The procedures of a new centrifuge simulation method that allows saturation predictions from centrifuge experiments are introduced and rigorously examined in this thesis. Sufficiently accurate numerical results can be effectively obtained by the new centrifuge simulation method applying a semi-analytical streamline tracing method. The application of streamline or stream tube modelling is popular in petroleum reservoir simulation. The capillary pressure in during streamline simulation is assumed to be constant in each time step when the

centrifuge system is at equilibrium. Then the saturation distribution can be determined, and the flow regimes can be visualized at a given angular velocity.

Novelty of this work is:

1. We are introducing two-dimensional modelling to predict the average saturation during capillary centrifuge experiments to examine the uncertainty that potential heterogeneity could introduce to average saturation measurements.
2. Streamline simulation that considers capillary pressure numerically is being used for the first time to model capillary pressure centrifuge measurements.
3. The potential uncertainty of having heterogeneity in the core is considered and visualized by streamline distributions and its influence on average saturation is described by solving the transport equation along streamlines.
4. The accuracy of phase saturation prediction for the centrifuge simulation has been improved by taking core-scale heterogeneity into account.

The applicability of the new two-dimensional centrifuge simulation method for phase saturation predictions to model physical problems is validated by comparing the numerical results and the experimental results for centrifuge experiments. Several two-dimensional permeability distributions with realistic permeability contrasts are used to investigate the effects of core heterogeneities on the estimated capillary pressure curves. The new centrifuge simulation method has the potential to account for the effect of heterogeneities compared to the conventional centrifuge simulation methods.

1.7 Thesis outline

This thesis is organized in five chapters. **Chapter 1** includes the general background knowledge for capillary pressure measurements and modelling. It also outlines the objectives and motivation for this research thesis. **Chapter 2** provides some related literatures on data interpretation methods for centrifuge experiments, streamline simulation and Riemann problem. **Chapter 3** discusses the basic information used to construct a centrifuge simulation model and provides the methodologies for modelling the centrifuge experiments using the semi-analytical streamline simulation method that includes capillary pressure in two-dimensional systems. The transport problems have been solved by the Riemann approach so the average saturation value for each incremental rotational speed can be obtained. As for the centrifuge data reducing method used in this research thesis, fitting technique has been performed on the raw data and the Forbes-Splines method has been used to generate the capillary pressure curve. The effects of heterogeneities are reflected on the difference between numerical and experimental capillary pressure curves. **Chapter 4** demonstrates some applications of the centrifuge simulation model. Centrifuge simulations have been performed under several permeability distributions. Porosity is assumed to be isotropic and homogeneous throughout the thesis for simplicity, which means the porosity is set to be a constant in the simulations. These cases are described and discussed in this chapter based on their results. The significance and limitations of the research have been presented as well. **Chapter 5** gives a brief summary of the conclusions form this research thesis and provides the recommendations for future work.

2 Literature Review

2.1 Determine Capillary Pressure Curves from Centrifuge Experiments

The capillary pressure from centrifuge experiments is a function of the distance from the inlet face for a given angular velocity. Therefore, the capillary pressure is changing from the inlet face to the outlet face of the core at equilibrium. In practice, the capillary pressures at the inlet end of the core are usually calculated for capillary pressure curve calculation. However, the saturation measured from the volume of displaced fluid is equal to the average saturation. To use the capillary pressure at the inlet face, the corresponding saturation at the inlet face must be converted from the average saturation (Tiab and Donaldson, 2015). The capillary pressure curves can be obtained from centrifuge experiments in two different ways. This first way is to obtain capillary pressure curves by calculation (Section 2.1.1)and the other way is to obtain capillary pressure curves by phase saturation prediction (Section 2.1.2).

2.1.1 Calculating Phase Saturations from Centrifuge

This section introduces some experimental data point correlation methods that can be used to obtain capillary pressure curve expressions by calculating phase saturations from centrifuge experiments. These methods are divided into two types: the first type is to calculate phase saturation by correlating inlet phase saturation ($inletS_w$) with average phase saturation ($aveS_w$) so that the $inletS_w$ can be calculated based on $aveS_w$; the second type is to calculate phase saturation by using some fitting/interpolation techniques or using a given analytical form to describe the relationship between capillary pressures and saturations.

Instead of measuring the capillary pressure curves directly from centrifuge experiments, the

calculation and conversion techniques need to be implemented on the raw data (displaced volume at incremental speed, rotational speed). These techniques will be introduced in the following. Therefore, researchers (Hassler and Brunner,1945; van Domselaar, 1984; Rajan, 1986; and Ruth and Wong, 1991) have presented data conversion methods to transform average saturation to inlet face saturations. All these methods are approximations and Seth (2006) provides a good summary of 13 data interpretation techniques. The development of the tomography technique has improved the interpretation of centrifuge data (Wunderlich, 1985). This technique can be used to capture the saturation profiles, but for high permeable cores, the actual saturation profiles are hard to create since the redistribution of fluids are rapid.

Figure 11 shows the scheme of the centrifuge experiment. In this figure, r_1 is the distance from the center of rotation to the inner face of the core plug, r_2 is the distance from center of rotation to the outer face of the core plug, and ω is the angular velocity. P_{c_1} and P_{c_2} are capillary pressure at the inlet and outlet face, respectively.

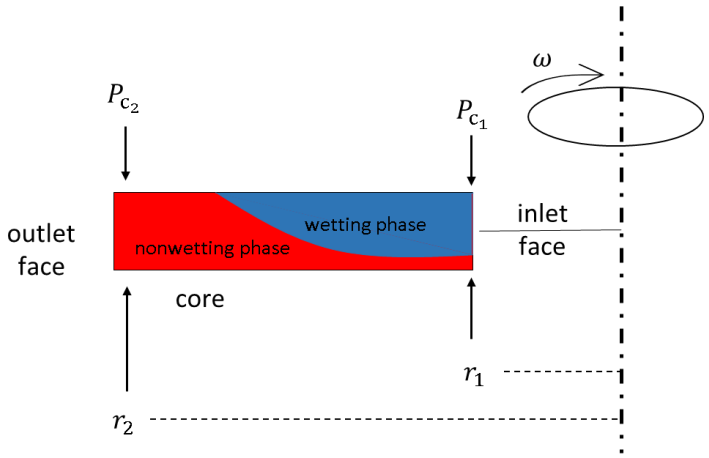

Figure 11 Scheme of the centrifuge experiment (after Forbes, 1991)

Before processing the experimental data from centrifuge experiments, several assumptions need to

be made for subsequent calculations. Assumptions include:

1. Hassler and Brunner (1945) assumed the boundary condition for most centrifuge data reported in the literature that the end face of the core remains 100% saturated with the wetting phase at all centrifugal speeds of the test. Thus, **the capillary pressure at the end face is equal to zero during the entire centrifugal process**. In the study of O' Meara et al. (1992), such condition is correct if there is a continuous film on the rubber pad surface to hold the core at the bottom, which is the most prevailing assumption. Meanwhile, the Bond number should be calculated to ascertain this critical boundary conditions for single-speed displacement experiments; however, no substantial deviations will occur in the calculations of capillary pressure curves even though this assumption breaks down.

2. **Cavitation is not present in the core sample** (Hirasaki et al., 1988). Cavitation is concerned with air-liquid capillary pressure measurements when the air pressure is one atmosphere and the capillary pressure exceeds one atmosphere. In this case, the liquid is in tension (under negative absolute pressure) and the bulk liquid is not stable when it is in tension, which may lead to larger entry capillary pressure or the discontinuity of liquid.

3. **The fluid system in the core has reached equilibrium when the produced wetting phase fluid is measured** (Christiansen and Cerise, 1992). Considerable amounts of fluid production are still found even after spinning the core constantly for 14 days; therefore, it is reasonable that many laboratory operators will record non-equilibrium data. Many scientists (Ward and Morrow, 1987; Omoregle, 1988; Slobod et al., 1951) have talked about effects of these errors. A method to avoid these errors by measuring relative permeability and capillary

pressure curves at the same time during centrifuge was introduced by O'Meara and Crump (1985). To simply this calibrating process, an easy way to estimate equilibrium saturations was proposed (O'Meara et al., 1992).

4. **There is no centrifugal force in the radial direction** (Christiansen and Cerise, 1992). Nevertheless, the centrifugal field in the core was proved to be radial and a dimensionless geometric factor accounting for the radial impact in centrifuge experiments was introduced. It was suggested that the geometric shape of the spinning plug should be considered in the data reduction process.

5. **The core plug is homogeneous.** Most reservoir core samples are heterogeneous, which may contribute to a level of inaccuracy in the calculated capillary pressure curve (Mannseth et al., 1998).

The average saturation can be derived from the liquid production using the sample pore volume and the negative sign becomes a positive for imbibition process:

$$aveS_w = aveS_{wi} - \frac{V_{displaced}}{V_p} \tag{2.1}$$

where is $aveS_w$ average saturation, $aveS_{wi}$ is initial average saturation (at start of test), V_p is pore volume (cc) and $V_{dispalced}$ is volume of displaced fluid (cc).

For drainage experiments, capillary pressure at a position of r is (McPhee et al., 2015):

$$P_c = \frac{1}{2}\Delta\rho\omega^2(r_2^2 - r^2) \tag{2.2}$$

where, $\Delta\rho$ is the density difference between the fluid phases (g/cm^3).

Converting the units, the capillary pressure at the inlet face can be calculated as:

$$P_{c_1} = 1.578 \times 10^{-1}(\Delta\rho)(r_1^2 - r_2^2) \cdot RPM^2 \quad (2.3)$$

where, RPM is revolutions per minute.

The saturation calculated in Equation (2.1) is average saturation for the core plug, but the capillary pressure calculated in Equation (2.3) is the value at the inlet face of the core. Therefore, the average phase saturation should be converted to inlet face saturation that is corresponding to inlet face capillary pressure. The previous derivations of capillary pressure and water saturation are not accurate solutions due to the geometrical shape of the core plug, the lengths of the centrifugal arm and core holder, and boundary conditions. The average saturations cannot be used directly to plot the capillary pressure curve since the corresponding average capillary pressure cannot be measured in the centrifuge experiment. According to Equation (2.2), the capillary pressure is varying along the core at a given angular velocity. Thus, the capillary pressure at the inlet face and the corresponding inlet face saturation are calculated to plot the resulting capillary pressure curve. All equations calculating the inlet face saturation are approximations since they cannot be solved explicitly and analytically. The interpretation process of experimental data points from centrifuge experiments is the main source for deviations and an appropriate solution of the centrifuge equation should be used to ensure an acceptable accuracy.

The methods for saturation calculation of first type are introduced as the followings.

This history of using the centrifuge experiment to measure capillary pressure can be traced back to 1940s (Slobod et al, 1951). Before data conversion techniques were widely applied, people used to measure water saturations by sectioning the core subject to one centrifugal force so that saturations of the entire core could be acquired (King, 1899). Once the level corresponding to the zero capillary

pressure is known, the capillary pressure curve can then be calculated. However, it is almost impossible to section such a small sample as rock cores from reservoirs and the longer column is required if capillary pressures at low water saturation areas need to be more accurately calculated. Therefore, Hassler and Brunner (1945) proposed a calculation process that uses average water saturation at each angular velocity and rotational speed to calculate capillary pressure curves. Since then, significant contributions were made by various scientists with increasing interest in the centrifuge experiment and its data processing method.

In the method proposed by **Hassler and Brunner (1945)**, average saturation $\overline{S}$ is related to S (inlet face saturation) by:

$$\overline{S} = \frac{1}{(r_2 - r_1)} \int_{r_1}^{r_2} S_{(r)}\, dr \tag{2.4}$$

Substituting P_c for r and replacing it by xP_{c_1}, where x is used as an integration variable (dimensionless), the equation above can be converted to:

$$\overline{S}(P_{c_1}) = \frac{1 + \sqrt{1 - B}}{2} \int_0^1 \frac{S(xP_{c_1})}{\sqrt{1 - Bx}}\, dx \tag{2.5}$$

where $B = 1 - (\frac{r_1}{r_2})^2$. For imbibition experiments, the same equations are obtained by exchanging r_1 for r_2 and P_{c_1} for P_{c_2}.

This equation is called the fundamental equation (centrifuge equation) because for both drainage and imbibition experiments, this equation needs to be inverted to obtain inlet face saturation value from average saturation value.

This first approximate method to convert the fundamental equation was proposed by Hassler and

Brunner (1945) and it successfully obtained the saturation at inlet face by assuming the core plug to be extremely short ($B \approx 0$). The resulting equation derived from it is:

$$\mathrm{S} = S_{HB} = \overline{S} + P_c \frac{d\overline{S}}{dP_{c_1}} \tag{2.6}$$

Based on this correlation the capillary pressure curve can be drawn from slopes of a curve of $P_c\bar{S}$ versus P_{c_1} by accelerating the core sample incrementally from which the specific P_{c_1} for each rotational speed can be attained and the average saturation $\bar{S}$ can be measured. Nevertheless, the derivation above does not take the geometric shape of the core into account and the acceleration across the core is assumed to be the same, which is not true. If the length of the core is considered, the following relations can be determined:

$$\int_0^{P_{c_1}} S(P_c)dP_c = P_{c_1}\bar{S} + \int_0^z [1 - \frac{(\cos\frac{1}{2}\theta)^2}{\sqrt{1 - \frac{P_c}{2}sin^2\theta}}]S(P_c)dP_c \tag{2.7}$$

where $\cos\theta = \frac{r_1}{r_2}$.

This equation can be solved numerically by successive approximation and the successive terms can be consecutively calculated using the following equation until results converge to accepted decimal places:

$$S_{k+1}(P_{c_1}) = \frac{d}{dP_{c_1}} \int_0^{P_{c_1}} [1 - \frac{(\cos\frac{1}{2}\theta)^2}{\sqrt{1 - \frac{P_c}{z}sin^2\theta}}]S_k(P_c)\, dP_c \tag{2.8}$$

Nonetheless, it has been shown that the solution of Hassler and Brunner always underestimates the true capillary pressure curve, but the solution by van Domselsaar often overestimates it (Forbes, 1994).

Hoffman (1963) introduced an analytical equation to account for the relationship between average water saturation and local water saturation and it also takes the length of the core into consideration. The equation is given as:

$$S(P_{c_1}) = \frac{2r_1}{r_1 + r_2}(\bar{S} + P_{c_1}\frac{d\bar{S}}{dP_{c_1}}) \tag{2.9}$$

He noted that this calculation method only applies to the situation when fluids inside the core reach hydrostatic equilibrium; thus, this condition will require a longer experimental period, which may make the benefits of using centrifuge experiments less attractive. To boost the efficiency of centrifuge experiments, the technique that allows the core to speed up consistently with a particular acceleration was introduced. For the centrifuge speed is a function of time, Equation (2.9) can be converted to:

$$S(t)_{r_1} = \frac{2r_1}{r_1 + r_2}[\bar{S}(t) + \frac{\omega(t)\bar{S}'}{2\omega'(t)}] \tag{2.10}$$

And the capillary pressure at the inlet face is also correlated to time elapsed:

$$P_{c_1}(t) = \frac{1}{2}\Delta\rho\omega^2(t)({r_2}^2 - {r_1}^2) \tag{2.11}$$

By determining capillary pressures and water saturations at different times, a capillary pressure curve can be derived without maintaining the core at balance states, which substantially reduces the experimental time. However, the derivation of this equation was later proved to be erroneous by **Luffel (1964)**.

Ayappa et al. (1986) improved the approximate solution derived by Rajan (1986) by replacing the partial differential part with the differential operator and a more appropriate equation to estimate

the inlet face saturation was derived:

$$S(P_{c_1}) = \bar{S}(P_{c_1}) + \frac{2r_1 P_{c_1}}{r_1 + r_2}\frac{d\bar{S}(P_{c_1})}{dP_{c_1}} + \frac{r_1}{r_2 B}\int_0^{P_{c_1}} \left[\frac{1-(1-BP_c/P_{c_1})^{1/2}}{(1-BP_c/P_{c_1})^{1/2}}\right]^2 \frac{d\bar{S}(P_{c_1})}{dP_c} dP_c \tag{2.12}$$

To broaden the valid range of approximate solutions proposed by Hassler-Brunner and van Domselaar (1984), a precise solution especially suitable for long core plugs was also introduced:

$$S(P_c) = \frac{1}{\pi}\frac{d}{dP_c}\int_0^{P_c} \frac{2\bar{S}(P_{c_1})\sqrt{P_{c_1}}}{\sqrt{P_c - P_{c_1}}} dP_{c_1} \tag{2.13}$$

This equation can be evaluated by use of a product integration method (Linz, 1985).

The parameter estimation technique proposed by Bentsen and Anli (1977) relies heavily on a capillary pressure displacement model that may not be able to describe the behavior of capillary pressure curve when water saturation reaches to unity, an interpretation method without parametric assumption of capillary pressure curves was presented (**Skuse et al., 1988**). This method also includes the integral part that was neglected in the centrifuge equation derived by Hoffman so that it greatly improves accuracy of the approximation. The estimated equation is:

$$S(P_{c_1}) \approx \frac{2R}{1+R}\frac{d}{dP_{c_1}}\left[P_{c_1}\bar{S}(P_{c_1})\right] + \frac{(1-R^2)}{2R^2}\bar{S}(P_{c_1}) - \frac{1}{2}(1 - R^2)\int_0^{P_{c_1}} \frac{P_c}{{P_{c_1}}^2}\bar{S}(P_c)\left\{\left[1-(1-R^2)\frac{x}{P_{c_1}}\right]^{3/2} + \frac{3}{2}(1-R^2)\frac{P_c}{P_{c_1}}\left[1-(1-R^2)\frac{P_c}{P_{c_1}}\right]^{-5/2}\right\} dP_c \tag{2.14}$$

where $R = \frac{r_1}{r_2}$.

Forbes (1994) thought that many approximations are precise within a limited range of B and they often require complex integration, which can only be evaluated by iterative procedures or forcing the data into a given mathematical correlation that may not be able to describe the full behavior of capillary pressure curves. These processes are tedious and can lead to some unpredictable errors because of the analytical form used to fit the data. Thus, he came up with a user-friendly data conversion method without any smoothing or fitting of the data, which can even be used to process noisy experimental data.

A summary of the reviewed saturation calculation approaches by interpreting $inletS_w$ from $aveS_w$ is presented in Table 2.

Table 2 Literature summary of phase saturation calculation method by interpreting $inletS_w$ from $aveS_w$

Year	Author(s)	Main Contributions
1945	Hassler and Brunner	Introduced the first centrifuge data interpretation method by ignoring the core length
1963	Hoffman	An analytical relationship between average and local water saturation that considers core length
1964	Luffel	Proved the constantly accelerated technique proposed by Hoffman was erroneous
1986	Ayappa et al.	Improved the accuracy of the partial differential part in fundamental equation by replacing it with the different operator. A more proper correlation between average saturation and inlet face saturation was derived
1988	Skruse et al.	Presented a centrifuge reducing method without parametric estimation of capillary pressure curves, which greatly improves the accuracy of inlet face saturation approximation in terms of average saturation
1994	Forbes	A rapid and simple phase saturation prediction method that allows conversion of sparse data (average saturation) into inlet face saturation without smoothing, averaging, fitting

The methods for saturation calculation of second type are introduced as the followings.

Bentsen and Anli (1977) assumed capillary pressures and wetting-phase saturation conform to the

capillary pressure model and then used the least-square method to find unknown parameters in the model. The capillary pressure model they used is:

$$P_c = -\sigma \ln S_n + P_{cd} \tag{2.15}$$

where $S_n = \frac{S_w - S_{wi}}{1 - S_{wi}}$, P_{cd} is the threshold capillary pressure when the wetting phase begins to be displaced, and σ is a normalizing factor.

From Equation (2.2), the capillary pressure at distance h from outlet face of the core is:

$$P_c = \Delta\rho\omega^2 \left(r_1 - \frac{r}{2}\right) r \tag{2.16}$$

Combining the two equations above and the average saturation across the core is then estimated as:

$$\bar{S}_w \cong S_{wi} + \frac{\sigma(1 - S_{wi})(2r_1 - L)}{(2r_1 - L - r^*)P_{c1}} \left[\frac{2r_1 - L - r^* P_{cd}}{2r_1 - r^*\sigma} + 1 - e^{-\frac{P_{c1} - P_{cd}}{\sigma}}\right] \tag{2.17}$$

with $r^* = r_1 - \sqrt{{r_1}^2 - \frac{2P_{cd}}{\Delta\rho\omega^2}}, \omega \geq \omega_c$.

where, L is the length of the core, ω_c is the critical value of angular velocity, below which no displacement begins, S_{wi} is the irreducible wetting phase saturation. Parameters P_{cd}, S_{wi}, σ can then be estimated by implementing the above equation and experimental average water saturation data in least-squares method by finding the minimum square difference between experimental measurements and estimated values (Marquardt, 1963). With estimated parameters, the capillary pressure curve can be plotted based on the capillary pressure model.

A linear interpolation method for capillary pressure curves was introduced by **Ruth and Wong (1991)** and they assumed that any unknown data point can be derived once the two neighboring data points are known:

$$S(Z) = S_{k-1} + \frac{S_k - S_{k-1}}{Z_k - Z_{k-1}}(Z - Z_{k-1}) \tag{2.18}$$

where $Z = P_{c1}$, and the subscript k means the experimentally derived value of Z and the corresponding calculated of S.

This method attempts to evaluate the integral proposed by Melrose by sequentially calculating the inlet face saturation and S_k provided the initial guess of the threshold capillary pressure and corresponding saturation, which can be easily estimated from the experimental data (Melrose, 1986).

Nordtvedt and Kolltvelt (1991) assumed the capillary pressure curve to be a piecewise spline function and solved an optimization problem to estimate coefficients in the spline function. The capillary pressure curve is assumed piecewise to be:

$$S_w(P_c) = a_{i,0} + a_{i,1}P_c + a_{i,2}P_c^2, i = 1,2 \dots n_I \tag{2.19}$$

where i is the number of interval and n_I is the total number of intervals. By varying the water saturation at each knot of spline function and threshold capillary pressure that can be regarded as an independent variable vector, the resulting average saturation can be calculated and compared to experimental average saturation. By minimizing the experimental and estimated data, an optimal set of water saturation at spline knots and displacement capillary pressure can be determined. Then by solving the equations constructed by known water saturations, threshold capillary pressure and continuity of the spline curve and its derivative, coefficients of spline function, thus capillary pressure curve can be determined. The determination of the spline function between capillary pressure and saturation relies on a regression method. A calculation method to determine

confidence intervals of capillary pressure curves from estimated mathematical functions was introduced for the purpose of quality check (Nordtvedt et al., 1993).

The methods that can be used to calculate phase saturation by fitting capillary centrifuge data are listed in Table 3.

Table 3 Literature summary of phase saturation calculation method by fitting centrifuge capillary data

Year	Author(s)	Main Contributions
1977	Bentsen and Anli	Interpreted the centrifuge data by forcing them into a given capillary pressure model. Capillary pressure can be calculated by implementing the model in least-squares method by finding the minimum square difference between experimental measurements and estimated values
1991	Ruth and Wong	Proposed a linear interpolation method for centrifuge data processing by assuming any unknown datapoint (capillary pressure versus inlet face saturation) can be derived based on two neighboring data points
1991	Nordtvedt and Kolltvelt	Assumed the capillary pressure curve to be a piecewise spline function and solved an optimization problem for coefficients approximations in the spline function

2.1.2 Phase Saturation Predictions from Centrifuge

This section introduces some capillary pressure curve prediction method that can be used to predict phase saturation at the inlet face by correlating it with average saturation or solving fluid flow equations in the centrifuge system. Compared to the methods introduced in Section 2.1.1, the methods introduced here can be used to obtain capillary pressure curves instead of fitting the centrifuge data. The fitting of the data can sometimes be questionable and leads to errors in resulting capillary pressure curves (Forbes, 1994). In this section, different methods to predict phase saturations are introduced and these methods can be generally divided into two types. The first type are correlations to fit the capillary pressure and equilibrium average saturation by appropriate simplifications of fluid flow equations in centrifuge system. This analytical model is

often be included in a commercial core flow simulator to predict equilibrium phase saturations for a given capillary pressure. The second type is to construct a mathematical relationship between capillary pressure and inlet face saturation (from average saturation) based on different mathematical functions, such as logarithmic function, exponential function or LET function (Skjaeveland et al., 2000; Lomeland and Ebeltoft, 2008). The phase saturation for a given capillary pressure can be obtained by inverting the correlations directly.

The phase saturation prediction methods of first type are introduced as the following.

Fleury et al. (2000) introduced a mathematical model that uses two exponential functions to predict equilibrium average saturation. This model is applicable to the multi-speed centrifuge experiments when the average saturation of the core is measured as a function of time with a constant rotational speed. The average saturation at equilibrium is predicted:

$$\bar{S}_w(t) = S_{wi} + \Delta S_{eq}[1 - (w \times \exp\left(-\frac{t}{T_1}\right) + (1 - w) \times \exp\left(-\frac{t}{T_1}\right)) \tag{2.20}$$

where ΔS_{eq} is the saturation variation during the considered speed step, T_1, T_2 are characteristic times of the exponential functions and w denotes the affected weight to the first exponential.

In the above equation, four parameters should be estimated to fit the experimental data to determine the saturation at infinite time.

Andersen et al. (2017) derived a mathematical model between rotation speed (capillary pressure) and equilibrium average saturation by simplifying the equations for Darcy's Law and conservation law of the centrifuge system. The inlet water saturation at equilibrium can be predicted by inverting

the mathematical correlation:

$$S_w^{eq}(x) = S_{wi} + \frac{1 - S_{wi}}{k}\left(\frac{a}{P_c^{eq}(x) - b} - 1\right), \quad P_c^{eq}(x) > P_{cd} \tag{2.21a}$$

$$S_w^{eq}(x) = 1, \quad else \tag{2.21b}$$

where S_w^{eq}, P_c^{eq} are water saturation and capillary pressure at equilibrium, parameter a, b are set according to the end points of the capillary pressure curve and parameter k controls the steepness of the curve near S_{wi}.

A summary of the reviewed phase saturation prediction approaches by solving general flow equations in the centrifuge system is presented in Table 4.

Table 4 Literature summary of phase saturation prediction method by solving flow equations

Year	Author(s)	Main Contributions
2000	Fleury et al.	Proposed a mathematical model that uses a bi-exponential function to correlate average saturation with time when the system is at equilibrium. The average saturation can be predicted by estimating 4 parameters in the function
2017	Andersen et al.	A mathematical model that allows phase average saturation prediction for each rotation speed by simplifying general fluid flow equations of the centrifuge system

The phase saturation prediction methods of second type are introduced as the following.

Skjaeveland et al. (2000) presented a capillary pressure correlation and an associated hysteresis loop scheme for mixed-wet reservoir since no comprehensive and widely accepted correlation is available for reservoirs at wettability conditions other than completely water-wet. The correlation that consists of oil and water branches is:

$$P_c = \frac{c_w}{(\frac{S_w - S_{wi}}{1 - S_{wi}})^{a_w}} + \frac{c_o}{(\frac{S_o - S_{or}}{1 - S_{or}})^{a_o}} \tag{2.22}$$

where S_{or} is residual oil saturation, $a's, c's$ are constants and there are different sets for imbibition and drainage processes, respectively.

The inlet face saturation can be predicted by converting above equation for a given capillary pressure. The capillary pressure curve that is drawn from this correlation contains a positive water branch with an asymptote at water residual saturation and a negative oil branch with an asymptote at residual oil saturation. This correlation is validated by fitting data from porous plate and centrifuge experiments on cores and can be used to generate representative capillary pressure curves for reservoir simulations.

LET - Lomeland and Ebeltoft (2008) developed an analytical capillary pressure correlation that uses the mathematical LET function as a basic element to model a branch or a feature of a capillary pressure curve naturally. The structure of the LET function is:

$$F(S_{wn}) = \frac{S_{wn}^{L}}{S_{wn}^{L} + E(1 - S_{wn})^{T}} \tag{2.23}$$

where S_{wn} is normalized water saturation, parameter L describes the lower part of the curve, parameter T describes the top part of the curve and parameter E describes the position of the slope of the curve.

The inlet face saturations can be predicted by using the capillary pressure versus inlet saturation correlation based on LET function to solve the flow equations in centrifuge system. The input parameters are capillary pressure (rotational speed), core length, diameter, permeability and porosity, etc. The outputs of the simulator are inlet face saturation for a given capillary pressure and then an interpreted capillary pressure curve.

There are three options available in CYDAR to calculate capillary pressure curves from centrifuge experiments. This first option is called Hassler-Brunner method, which is a historic method described by Hassler and Brunner (1945). The equations that are used in the Hassler-Brunner method are Equation (2.4) to Equation (2.8) in Section 2.1.1. The second option is called Forbes method using Equation (3.5) to (3.22) in Section 3.2.2. The final option is called Forbes-Splines method using Equation (3.5) to (3.33) in Section 3.2.2 , which is widely used to process capillary centrifuge data in the core analysis. A summary of the reviewed phase saturation prediction approaches by correlating $inletS_w$ with $aveS_w$ in the centrifuge system is presented in Table 5.

Table 5 Literature summary of phase saturation prediction by using correlation

Year	Author(s)	Main Contributions
2000	Skjaeveland et al.	Presented a capillary pressure correlation and an associated hysteresis loop scheme for mixed-wet reservoir. The inlet face saturation can be predicted by using the correlation that consists of oil and water branches
2008	LET - Lomeland and Ebeltoft	An analytical capillary pressure correlation that uses the mathematical LET function as a building block. The phase saturation can be predicted by using the correlation to solve fluid flow equations in the centrifuge system
2021	CYDAR group	Presented three methods for capillary pressure curve calculations from experimental data: Hassler-Brunner method, Forbes method, Forbes-Splines method.

As mentioned before, the methods for predicting inlet phase saturations are divided into two types. In this thesis, the Forbes-Splines method of second type is used to process capillary centrifuge data. Unlike the traditional Forbes method, the calculations of Forbes-Splines method are performed on the analytical fit of the capillary pressure versus average saturation data and thus, the results are more accurate. Additionally, spline fit or interpolation is used to minimize the differences between $P_c(aveS_w)_{original}$ curve (from the fitted data points) and the $P_c(aveS_w)_{recalculated}$ curve from the

experimental $P_c(inletS_w)$ curve. Constraints on the spline function can be implemented to have a monotonic capillary pressure curve. Therefore, Forbes-Splines method, an advanced centrifuge data interpretation technique combining the Forbes method and the spline interpolation technique in CYDAR (a software for special core analysis laboratory), has been used to calculate capillary pressure curves from centrifuge experiments or simulations. This technique for centrifuge data interpretation used in this thesis can also be applied to other capillary pressure correlations.

2.2 Numerical Simulation using Streamline Methods

Streamline simulation has been proved to be an effective approach for predicting the fluid flow and solving the flow problems in fine-scale geology models. Therefore, the two-dimensional centrifuge simulation method introduced in this thesis is based on streamline tracing methods. The phase saturations throughout the core at equilibrium are predicted by solving the flow problems considering capillary pressure along streamlines, which can be achieved by using the MATLAB toolbox named as MRST (MATLAB Reservoir Simulation Toolbox). The streamline tracing method in MRST is based on Pollock's method introduced in Section 3.3.6 so that the two-dimensional flow problem during centrifuge can be solved semi-analytically using streamlines. By assuming capillary pressure to be constant at each angular velocity/time step, the streamlines tracing method can be used to visualize the flow regimes and to predict the phase saturations. The streamline tracing method used in this thesis considers capillary pressure numerically when solving for the pressure distribution at a given time step. A capillary pressure module in MRST (Equation (3.1) in Section 3.1) can be used to include the capillary pressure when tracing streamlines in the centrifuge system. The fluid densities used in the numerical simulations are the same as the values

used in the lab-scale centrifuge experiments because the effects of the heterogeneity distributions on fluid flow are of interest.

All centrifuge interpretation methods require the assumption of a homogeneous rock sample, which may lead to deviations in phase saturations that are measured from experiments (Christiansen and Cerise, 1992). Therefore, the modelling of centrifuge experiments is necessary for it can describe and quantify the effects core heterogeneity on fluid flow. To simulate the fluid displacement process in a core sample during the centrifuge experiment for measuring capillary pressure curves, a streamline simulator can be applied effectively. In a centrifuge experiment, streamline modelling can be used to understand the flow process of wetting and non-wetting phases in the rotated core plug. It can be used to improve the accuracy of capillary pressure curve measurements by calibrating average wetting phase saturations.

A thorough understanding of dynamic physical movement of fluids in a reservoir is crucial to the production in oil fields. Over the years, the streamline simulation method has become a satisfactory replacement for the conventional finite-difference simulation method due to its high computational speed (Datta-Gupta and King, 2007). Streamline simulation is also a useful tool for modelling visualization experiments, history matching and reservoir management. It is robust in solving fluid flow problems in homogeneous and heterogeneous systems. Streamline simulation is not applicable in displacing processes that include cross-streamline problems, since no fluid can flow across different streamlines (Datta-Gupta and King, 1995). Streamlines are instantaneous curves that are everywhere tangential to the velocity field (Bear, 2013). A stream tube is a spatial region bundled by streamlines as shown in Figure 12. No flux can cross the stream tube boundaries, which

means that the calculation along a stream tube is decoupled from other stream tubes. In this research thesis, streamlines are traced in steady state flow in which the fluids in the core have reached equilibrium at each rotational speed. The fluid movement with time can be described by use of streamlines, the density of which shows the magnitude of the flow velocity. The denser distribution of streamlines indicates a high flow region in the flow field; in contrast, spare streamlines represent a slow fluid flow. Time-of-flight (TOF) is the time that a neutral particle takes to travel along a streamline (Pollock, 1988). Given the instantaneous velocity field, streamlines can be computed in the core. Since only one velocity vector exists in any location of the field, streamlines can never cross.

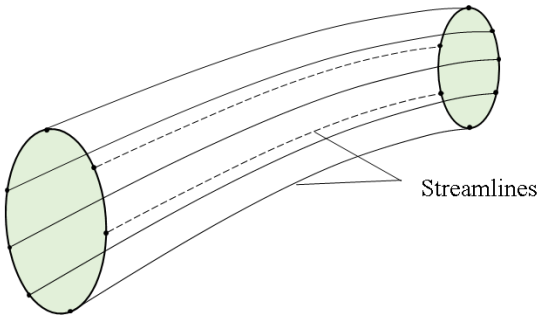

Figure 12 Schematic of a stream tube

The general steps for streamline simulation can be summarized as: i) the pressure equations are solved based on known parameters of rock and fluid so the pressure fluid can be calculated; ii) velocity field is calculated by virtue of Darcy's Law and streamlines; and iii) Riemann approach is used as a proper way to solve the transport problem (Zhang et al., 2012). In this project, streamline simulations have been conducted to model the fluid flow in a core thus assessing the impact of core heterogeneity. Table 6 lists the summary of the major developments in streamline tracing methods.

Table 6 Literature summary of streamline tracing methods

Year	Author(s)	Main Contributions
1781	Lagrange	Introduced the concept of streamline
1934	Muskat and Wyckoff	First application of streamline simulation in reservoir engineering problems
1937	Muskat and Wyckoff	Presented the governing analytical solution of stream function
1951	Fay and Pratts	Proposed the two-dimensional semi-analytical streamline tracing method
1971	LeBlanc and Caudle	Introduced a stream tube model with changing mobility ratios
1988	Pollock	Presented a three-dimensional semi-analytical streamline simulation method
1992	Cordes and Kinzelbach	Introduced a post-processing method that reconstructs the flow rate at cell interfaces
1995	Datta-Gupta and King	Approximated streamlines as a hyperbolic function in each grid block
2001	Prevost et al.	Streamline tracing in unstructured girds
2006	Matringe et al.	Applied the mixed finite element scheme in two-dimensional streamline tracing method
2010	Johansen	Proposed a semi-analytical streamline tracing approach by approximating pressure functions
2012	Zhang et al.	Proposed a comprehensive study of streamline tracing methods based on velocity approximations

Lagrange (1781) was the first to derive stream functions for two-dimensional streamline generation. Muskat and Wyckoff (1934) first introduced the idea of using streamlines to solve the artificial flooding problems in man-made typical flooding networks from which the pressure distribution can be obtained. They also compared efficiency and conductivity of each individual flooding pattern and concluded that the spatial arrangement of wells is perhaps of limited significance in flood efficiency. Their paper was the first application of streamline simulation in petroleum engineering under reasonable assumptions. In 1938, they derived the governing solutions of the stream function analytically and presented the potential function for the two-dimensional displacement problem by assuming fluids are incompressible (Muskat, 1938).

Prats (1951) extended the application of stream tube simulation to petroleum engineering in a two-

dimensional homogeneous system containing two wells. Streamlines were calculated numerically in different stages by use of a semi-analytical method so that the shifting streamlines can be traced. Their approach can also be used to estimate the breakthrough time with some degrees of uncertainties.

To describe the two-phase displacement problem in a two-dimensional reservoir with heterogeneity, LeBlanc and Caudle (1971) presented a stream tube simulation approach such that the flux along each streamline was integrated for velocity calculation. This method significantly increased the simulation efficiency and was commonly used in two-phase fluid flow.

As one of the most frequently used streamline tracing methods in commercial simulators is Pollock's method (1988) that adopts a finite-difference method to calculate the pressure field from which the velocity field can then be determined. Its calculation is grid-block based along with two assumptions, which means the location of streamline and the time that a particle takes to travel along the streamline (time-of-flight) are obtained analytically in each cell. The computing speed of this method boosts remarkably as compared to the Runge-Kutta approach used by Shafer (1987). Nonetheless, Pollock's method can only be applied to Cartesian coordinate system. To satisfy the need to model more complex geological reservoirs, Prevost et al. (2002) extended the streamline simulation to unstructured grids, such as curvilinear corner-point geometry grids and unstructured triangular grids. The critical essence of tracing streamlines in unstructured grid blocks is to perform the tracing algorithm of structured grid in a unit cube transformed from the irregular grid block.

To overcome the disadvantages in traditional particle tracing method in field tracer tests, such as numerical deviations or low computational efficiency for the solution of the velocity equation, low

resolution of the tracer front, Datta-Gupta and King (1995) proposed a semi-analytical approach as an alternative in which volumetric flow rate are approximated piecewise with continuity. Therefore, streamlines can be approximated as a hyperbolic function in each block to trace streamlines analytically.

The limitation of Pollock's method is that it assumes each streamline will only go through the cell face once without coming back, which means only one velocity is presented in each grid block face. This hypothesis seems untenable when it comes to the modelling of geologically complicated reservoirs where a streamline can come back and go through a cell more than once (Thiele, 2001). For these situations, finite element and finite volume methods are needed to improve the accuracy of streamlines.

The use of triangular and polygonal grids in the finite element method makes it a better representation of the structurally complex stratum. It also assumes the pressure field to be a piecewise polynomial, the partial derivative of which can then be used to calculate the velocity distribution (Zhang, 2017; Zhang et al., 2021). As the calculated velocity field contains certain degrees of discontinuities along cell boundaries in traditional finite element method, Cordes and Kinzelbach (1992) introduced a method that can recalculate the flow rate at interfaces of sub-quadrilaterals by mass conservation law, which contributes to a continuous velocity field. The mixed finite element method can also give results of flow rate at grid faces. Matringe et al. (2006) presented a new streamline tracing approach that makes it possible to trace streamlines in irregular girds consisted of triangles or quadrilaterals with consideration of heterogeneities. This method was based on the idea of mixed finite element methods and gave rise to a velocity approximation

function that is reasonable for streamline computations. They concluded that high-order tracing can produce smaller deviations in the computation of time-of-flight whereas it is restricted to two-dimensional problems. As for the finite volume method, the main advantage of it is that it can be used to both structured and unstructured grids. Zhang et al. (2012) did a systematic study of the velocity interpolation methods in polygonal grid blocks, which are generally implemented as postprocessing after calculating the fluxes at the grid block interfaces for numerical scheme without calculating the velocity field directly. They highly recommended a lower-order locally conservative method rather than higher-order interpolation for streamline tracing because it gives analytic solution and increase the efficiency of implementation.

Johansen (2010) proposed a new semi-analytical streamline tracing technique in that streamline and the time for a particle to travel through a streamline are calculated by a closed formula in each grid block. This method can be used in both Cartesian and Polar coordinate systems by using a different way to treat the anisotropy in near well regions. The researcher assumed a bilinear pressure function for two-dimensional problems and a trilinear pressure function for three-dimensional problems so that the pressure is continuously distributed in the field. The mathematical expressions for the calculations of streamlines and time-of-flight can then be obtained by Darcy's Law.

The streamline simulations can be applied in the modelling of centrifuge experiments because it is capable of describing the flow state of fluids in the core and showing the stagnant areas caused by heterogeneities. The streamline distribution in a heterogeneous core is of course different from that in a homogeneous core; therefore, the effects of heterogeneities can be investigated by use of

streamlines.

In this thesis, Pollock's method is applied for semi-analytical tracing of streamlines in the modelling of centrifuge experiments because it is proved to a sophisticated streamline tracing method with high efficiency. Additionally, a digital model with a highly heterogeneous permeability field, generated by a Gaussian random field approach, is built and used for centrifuge simulations. We address the wetting phase saturations by mapping the transport problems onto one-dimensional streamlines; therefore, an analytical saturation distribution and numerical average saturations can be obtained. In this thesis, a two-dimensional fluid system has been considered in the modelling of centrifuge experiments and the streamline simulation has been incorporated in the centrifuge simulation to visualize the heterogeneities in the core during the displacement.

2.3 Two Phase Flow in Porous Media

The transport problem along each streamline or stream tube in streamline tracing methods needs to be solved by mapping one-dimensional solutions of mass conservation equations. Solving the mass conservation equations for the two-phase immiscible displacement process under certain boundary conditions is called a Riemann problem. Buckley and Leverett (1942) proposed an analytical solution for the two-phase immiscible displacement front in one spatial dimension under constant flow rate condition. This theory assumes the constant flow rates of wells and uniform initial reservoir conditions. The mapping of the one-dimensional Riemann equations to the streamline or stream tube is the Riemann approach (Thiele, 1995).

Higgins and Leighton (1962a, 1962b, 1964) were the first to use the Riemann solution from one-dimensional displacement under constant flow rate (Buckley-Leverett theory) to simulate nonlinear

displacement for regular well patterns in a homogeneous areal field. Streamlines were bundled to form stream tubes to deal with the structurally complex reservoir and the fluid saturation was calculated in each streamtube. The flow resistance in each streamtube was recalculated at each time step even though the tube bundles were fixed during the displacement process. The volume of injected fluid in each streamtube was then distributed proportionally to the ratio of the flow resistance of each streamtube to the total resistance of the whole system. The results of Higgins and Leighton showed good agreement with the experimental data obtained from Dyes et al (1954). for viscosity ratios ranging from 0.1 to 1000.

Martin et al. (1973) found that the results of streamline method for favorable mobility ratios are not as good as for unfavorable mobility ratios, which can probably be attributed to the fundamental assumption of fixed streamlines when the mobility ratio is less than unity. Additionally, he also argued that calculated streamlines in the water drainage region are almost independent of the upswept area but most of the pressure drop occurs in this region. Updating the stream tubes at the end of each time step as the fluid progresses may be a better solution for this problem.

To explain the chemical reactions and physical diffusion in the main direction of flow, Bommer and Schechter (1979) found the solutions of the mass conservation equations for multi-phase flow in each streamline by virtue of a finite difference method. Martin and Wegner (1979) concluded that the conventional streamtube simulation method is suitable for most of the two-phase flow problems at lower computational cost compared to variable tube approaches. A new numerical streamline simulation method was proposed in the paper as well.

Glimm et al. (1981) developed a solution of Riemann problem in that a local flow direction is

determined based on a pressure equation. The hyperbolic equations to tracing the shock front without numerical and physical dispersion for both homogeneous and heterogeneous reservoirs were introduced, which are applicable to immiscible flooding with changing mobility ratios.

Bratvedt et al. (1992) proposed a new front tracking method with the consideration of gravity. The hyperbolic conservation equations were solved at each time step by a gravity driven computation method and a new way to calculate the saturation was also presented. The pressure equation was solved implicitly whereas the saturation equation was solved explicitly by a block based numerical streamline approach as the font progresses. Their method concentrated on the front tracking of discontinuous surface that was regarded as a separated object and can be used for any stream tube with various geometry.

Thiele et al. (1996) solved the complicated nonlinear multiphase flow problems rapidly by the streamline simulation. They changed the stream tube geometries with time and solved the transport problem by Riemann approach instead of calculating tube resistances. This approach can precisely estimate the water breakthrough time for highly nonlinear displacements and relatively large time steps can be taken to capture the nonlinearities of the displacement since the trajectories of the stream tubes were almost unchanged. The main assumption for mapping analytical solutions to recalculated paths is that the paths of stream tubes do not vary a lot in each incremental time step.

Glimm et al. (1999) presented an advanced algorithm for the interaction of an untracked shack wave with a tracked contact discontinuity and described the micro topology of the interface based on interface crossings with cell block edges.

Nilsen and Lie (2009) used the Riemann approach in three-dimensional models for streamline

simulation, the results of which showed that streamline tracing and front tracking methods can be used to model compressible flow efficiently.

Buckley and Leverett theory is only suitable for cases under constant flow rate boundary conditions but not constant pressure boundary conditions. The analytical Riemann solutions under constant pressure boundary conditions were proposed by Johansen et al. (2017) and they presented an algorithm for the explicit calculation of the total velocity. An analytical solution for the displacement front location, the breakthrough time at the outlet and saturation profiles after frontal breakthrough were given in this paper. Johansen and Liu (2017) solved the three-dimensional Riemann problem analytically in stream tubes with given cross sectional area, which has substantially extended the applications of Riemann approach along stream tubes.

In this research thesis, Riemann approach along streamlines in oil displacement process under constant pressure boundaries is used to determine the flow rate as a function of simulation time, average water saturation and saturation profiles along streamlines in terms of time-of-flight. The major advantage of the semi-analytical method over the traditional numerical approach is that it produces less numerical error and substantially reduces the computational time.

3 Methodology for the Modelling of Centrifuge Experiments

3.1 Overall Workflow for Modelling of Centrifuge Experiments

In this section, the major procedures for the modelling of centrifuge experiments are summarized. When the centrifuge system is at equilibrium, the capillary pressure is equal to the pressure difference across the core (provided by the angular velocity). As the angular velocity is increased incrementally during centrifuge, different capillary pressures and pressure differences can be obtained. The capillary pressure is interpreted in each angular velocity (time step) using streamline tracing method.

This thesis aims to study the influences of heterogeneity by using a two-dimensional centrifuge simulation method for phase saturation predictions proposed as shown in Figure 13. It is noted that **Step 6** to **14** need to be done iteratively for each angular velocity from centrifuge experiments in the laboratory. When the rotational system becomes stable at the given angular velocity, the capillary pressure is a constant and equal to the pressure difference across the core. Thus, the numerical boundary condition for each iteration depends on the experimental value of capillary pressure. The two-dimensional centrifuge simulations in this thesis are conducted by using the streamline tracing method considering capillary pressure numerically in MRST. This section introduces the syntax and equations that are used in each step of the two-dimensional centrifuge simulation for phase saturation prediction.

To visualize the flow regimes and predict phase saturation in the two-dimensional centrifuge simulation, the capillary pressure needs to be included in the streamline simulation at each angular velocity/time step. The built-in capillary pressure module in MRST can be used to include the

capillary pressure in the streamline simulations. The following syntax can be used to activate this capillary pressure module. In **Step 4**, the capillary numerical model (fluid model considering capillary pressure) is constructed by using:

$$fluid = initSimpleFluidPc('pn1', pv1, \dots) \tag{3.1}$$

where 'pn'/pv - List of 'key'/value pairs defining specific fluid characteristics.

The detailed equations used in this step are introduced in Section **Error! Reference source not found.**.

In **Step 5**, the permeability distribution is plotted by using:

$$plotCellData(G, K) \tag{3.2}$$

where K is the permeability for each grid block of the digital model.

In **Step 6**, the boundary conditions are imposed using:

$$bc = pside(bc, G, side, p); \tag{3.3}$$

where $side$ is the end face of the digital model, p is the pressure difference.

The densities of fluids are not updated in each iteration and the equations used in other steps are also introduced in Figure 13.

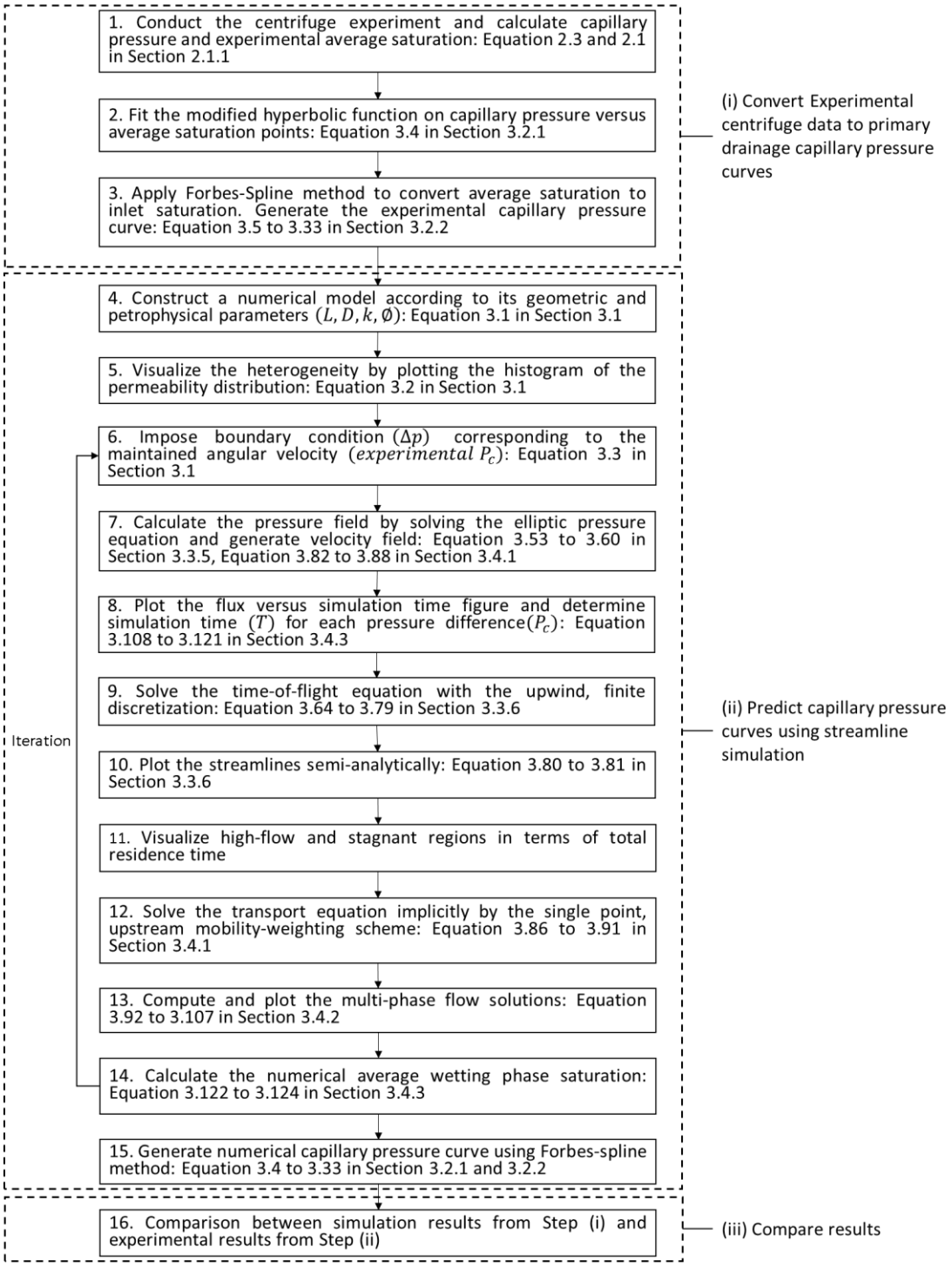

Figure 13 Flow chart for the two-dimensional centrifuge simulation

3.2 Conversion of Experimental Centrifuge Data into Primary Drainage Capillary Pressure Curves

The section introduces the details of converting experimental centrifuge data into drainage capillary

pressure curve as shown in **Step (i)** of Figure 13. The modified hyperbolic function is first used to fit the capillary pressure versus average saturation points since the shape of this function can represent the most of the typical capillary pressure curves. The Forbes-Spline method is then applied to convert capillary pressure versus average saturation curve to capillary pressure versus inlet face saturation curve (capillary pressure curve).

3.2.1 The Fitting of Modified Hyperbolic Function on Experimental Data

In this thesis, the modified hyperbolic function is first used to fit the average wetting phase saturation versus capillary pressure data points and then the average wetting phase saturation curve can be obtained. The traditional Forbes method for estimating the local wetting phase saturation is a simple finite difference method and the value of $inletS_w$ is estimated based on the value of $inletS_w$ and $aveS_w$ in the previous step. Here, the initial value of $inletS_w$ can be taken as a unity if the core plug is fully saturated with brine. Nevertheless, the number of iterations is constrained to the number of the experimental data points in this method. For example, if only six data points are available in the average wetting phase saturation versus capillary pressure curve, the calculation in this differencing scheme will only be done with six points, the resulting capillary pressure curve of which may not be smooth or precise. To improve the accuracy of this scheme when data points are sparse or noisy, an approximated function, for example, a modified hyperbolic function, can be first used to fit capillary pressure versus average wetting phase saturation data points. The fitting average wetting phase saturation curve is a solid foundation for performing the centrifuge data reducing method when the number of experimental data points is small, since enough number of capillary pressure versus average saturation data points can be found on the fitting curve as required.

If the modified hyperbolic function does not give a good fit, the splines can be used. The modified hyperbolic function can be expressed as,

$$c = |P_c - a|^{\alpha}(aveS_w - b), \alpha > 0 \tag{3.4}$$

where c, a, b, α are coefficients in the function.

The capillary pressure versus average saturation curve from modified hyperbolic fit can then be used as an input for the Forbes-Splines method.

3.2.2 Forbes-Splines Method for the Calculation of Capillary Pressure Curves

In the Forbes-Splines method, the data interpretation method developed by Forbes (1994) is applied to convert the average wetting phase saturations to the inlet face wetting phase saturations. The equations that are used in the Forbes-Splines scheme are Equation (3.5) to (3.22) in Section 3.2.2. The spline fit or interpolation technique is used to perform the calculation since the constraints on the spline function can be implemented to have a monotonic capillary pressure curve. Using spline fit to conduct the Forbes-Splines method can also obtain the best fit between the recalculated and the original capillary pressure versus average saturation curves. After the treatment of raw data from centrifuge experiments, an experimental capillary pressure curve can be obtained.

Converting average saturation to inlet face saturation is necessary before the plotting of capillary pressure curve. In the literature review section, several reducing methods were discussed and they all have their limitations. For example, methods that are easy to be implemented without smoothing, fitting or averaging tend to significantly reduce the accuracy of the capillary pressure curve (Forbes, 1994). Conversely, methods that require complicated differentiation and integration may be tedious and will force the data in an estimated mathematical form, which might produce unknown errors

(Hassler and Brunner. 1945; Bentsen and Anli, 1977; Nordtvedt et al., 1993). Thus, a conversion incorporating the Forbes method and spline interpolation technique, known as Forbes-Splines method, is used to convert the centrifuge data into drainage capillary pressure curves. The details about the derivation of Forbes method are given as the followings. The range of the exact value of inlet face saturation is limited into,

$$\bar{S} + P_c \frac{d\bar{S}}{dP_{c_1}} \leq S \leq \bar{S} + \frac{2\sqrt{1-B}}{1+\sqrt{1-B}} P_c \frac{d\bar{S}}{dP_{c_1}} \tag{3.5}$$

In integration form, it is expressed as,

$$\int_0^1 S(xP_{c_1})\, dx \geq \bar{S} \geq (1 + \frac{1-\sqrt{1-B}}{2\sqrt{1-B}}) \int_0^1 x^{\frac{1-\sqrt{1-B}}{2\sqrt{1-B}}} S(xP_{c_1}) dx \tag{3.6}$$

where x is regarded as a dimensionless integration variable, $\bar{S}$ is the average saturation across the core, P_{c_1} is the capillary pressure at inlet face.

For drainage experiments, B is calculated as,

$$B = 1 - \left(\frac{r_1}{r_2}\right)^2, 0 \leq B \leq 1 \tag{3.7}$$

where r_1 is the distance from center of rotation to outer face of the core plug and r_2 is the distance from center of rotation to inner face of the core plug.

The Equation (2.5) (fundamental equation) can then be estimated within this interval as,

$$\bar{S}(P_{c_1}) \approx (1+a) \int_0^1 x^a\, S(xP_{c_1}) dx \tag{3.8}$$

where $0 \leq a \leq \frac{1-\sqrt{1-B}}{2\sqrt{1-B}}$.

To have good agreement between Equation (3.8) and the Equation (2.5) (fundamental equation),

the value of a can be taken as $\frac{1-\sqrt{1-B}}{1+2\sqrt{1-B}}$.

The solution S_a can then be taken as a good approximation of S,

$$\bar{S}(P_{c_1}) = (1+a)\int_0^1 x^a\, S_a(xP_{c_1})dx \tag{3.9}$$

Rearranging Equation (3.9) by differentiation,

$$\mathrm{S}(P_c) \approx S_a(P_c) = \bar{S}(P_c) + \frac{P_c}{1+a}\frac{d\bar{S}}{dP_{c_1}}(P_c) \tag{3.10}$$

However, S_a approximation is only accurate when B is no more than 0.7. To make a better estimation of the inlet face saturation when B is larger than 0.7, S_b solution is proposed and can be obtained by solving the following equation,

$$\bar{S}(P_{c_1}) = \int_0^1 (S_b(xP_{c_1}) + \frac{xP_{c_1}}{1+b}\frac{dS_b}{dP_c}(xP_{c_1}))dx \tag{3.11}$$

To make Equation (3.11) a reasonable approximation of the Equation (2.5) (fundamental equation), the value of b can be taken as $\frac{1+2\sqrt{1-B}}{1-\sqrt{1-B}}$.

Then the solution of S_β can be expressed as,

$$\mathrm{S}(P_c) \approx S_b(P_c) = (1+b)\int_0^1 x^b S_{HB}(xP_c)dx \tag{3.12}$$

Hence, a solution combining the solution of S_a and S_b can be written as,

$$\mathrm{S}(P_c) \approx S_{ab} = \frac{B}{2}S_b + (1-\frac{B}{2})S_a \tag{3.13}$$

To solve this equation containing both integration and differentiation, the $S_\alpha(P_c)$ can be rewritten as:

$$S_a(P_c) = \frac{d\bar{S}{P_{c1}}^{1+a}}{d{P_{c1}}^{1+a}} \tag{3.14}$$

$S_\beta(P_c)$ can be related to S_{HB}:

$$S_{HB} = \frac{dP_{c1}\bar{S}}{dP_{c1}} = \frac{d{P_{c1}}^{1+b}S_b}{d{P_{c1}}^{1+b}} \tag{3.15}$$

Defining $\{\overline{S_\iota}, P_i\}$ and $\{\bar{S}_{i-1}, P_{i-1}\}$ as the end points in each small area in the curve and $P_{i-1} < P_i$. Subscripts $\mathrm{i} - \mu$ denote the function value within the pressure region (P_{i-1}, P_i) at pressure $P_i - \mu$. The Equation (3.14) and Equation (3.15) are converted to:

$$S_{ai-1/2} = \frac{P_i^{1+a}\bar{S}_i - P_{i-1}^{1+a}\bar{S}_{i-1}}{P_i^{1+a} - P_{i-1}^{1+a}} \tag{3.16}$$

$$\frac{P_i\bar{S}_i - P_{i-1}\bar{S}_{i-1}}{P_i - P_{i-1}} = \frac{P_i^{1+b}\bar{S}_{bi} - P_{i-1}^{1+b}\bar{S}_{bi-1}}{P_i^{1+b} - P_{i-1}^{1+b}} \tag{3.17}$$

Equations above can be reorganized, and the solution is obtained as:

$$S_{ai-1/2} = \frac{\bar{S}_i - (\frac{P_{i-1}}{P_i})^{1+\alpha}\bar{S}_{i-1}}{1 - (\frac{P_{i-1}}{P_i})^{1+\alpha}} \tag{3.18}$$

$$S_{bi} = (\frac{P_{i-1}}{P_i})^{1+b}S_{bi-1} + \frac{1 - (\frac{P_{i-1}}{P_i})^{1+b}}{1 - (\frac{P_{i-1}}{P_i})}[\bar{S}_i - (\frac{P_{i-1}}{P_i})\bar{S}_{i-1}] \tag{3.19}$$

$$S_{i-\frac{1}{2}+B/4} \approx S_{abi-\frac{1}{2}+\frac{B}{4}} = \left(1 - \frac{B}{2}\right)S_{ai-\frac{1}{2}} + \frac{B}{2}S_{bi} \tag{3.20}$$

$$0 \le \mathrm{B} \le 1, \mathrm{B} = 1 - (\frac{r_1}{r_2})^2 \tag{3.21}$$

$$\alpha = \frac{1 - \sqrt{1-B}}{1 + 2\sqrt{1-B}} = \frac{r_2 - r_1}{r_2 + 2r_1}, b = \frac{2}{a}; drainage \tag{3.22}$$

The discrete capillary pressure versus inlet face saturation points can be obtained once the

conversion process has been done. Then the spline interpolation technique can be used to fit these discrete points to a smooth capillary pressure curve. Instead of fitting a single polynomial to all the data points at once, spline fitting technique divides the values into continuous interpolation intervals where low degree polynomials are used to fit the values (Schoenberg, 1988). The spline interpolation technique is preferable than other fitting techniques for it significantly reduces the interpolation errors. For spline interpolation, one low degree polynomial $y = f_i(x)$ for the values within in (x_{i-1}, y_{i-1}) and (x_i, y_i), where $i = 1,2, \dots, n$. Therefore, there will be n polynomials for $n + 1$ knots. The first and the second derivatives of the successive polynomial functions should have same values at the connecting knots.

In the interpretation process of centrifuge experiments, we can consider a polynomial function $P_c(S_w)$ that can interpolate the values from (S_{w1}, P_{c1}) to (S_{w2}, P_{c2}) and we have,

$$P_c(S_w) = \big(1 - \alpha(S_w)\big)P_{c1} + \alpha(S_w)P_{c2} + \alpha(S_w)\big(1 - \alpha(S_w)\big)[\big(1 - \alpha(S_w)\big)A + \alpha(S_w)B] \tag{3.23}$$

where $\alpha(S_w) = \frac{S_w - S_{w1}}{S_{w2} - S_{w1}}$, $A = k_1(S_{w2} - S_{w1}) - (P_{c2} - P_{c1})$, $B = -k_2(S_{w2} - S_{w1}) + (P_{c2} - P_{c1})$, k_1, k_2 are slopes for point (S_{w1}, P_{c1}) and (S_{w2}, P_{c2}) respectively.

Differentiating Equation (3.23) twice for the first and second derivatives,

$$P_c{}' = \frac{P_{c2} - P_{c1}}{S_{w2} - S_{w1}} + (1 - 2\alpha)\frac{A(1 - \alpha) + B\alpha}{S_{w2} - S_{w1}} + \alpha(1 - \alpha)\frac{B - A}{S_{w2} - S_{w1}} \tag{3.24}$$

$$P_c{}'' = 2\frac{B - 2A + (A - B)3\alpha}{(S_{w2} - S_{w1})^2} \tag{3.25}$$

Substituting the value of α when $S_w = S_{w1}, S_{w2}$, the Equation (3.25) reduces to,

$$P_c''(x_1) = 2\frac{B-2A}{(S_{w2}-S_{w1})^2} \tag{3.26}$$

$$P_c''(x_2) = 2\frac{B-2A}{(S_{w2}-S_{w1})^2} \tag{3.27}$$

So now consider (S_{wi}, P_{ci}) when $i = 1,2,\dots,n$,

$$P_{ci} = (1-\alpha)P_{c(i-1)} + \alpha P_{ci} + \alpha(1-\alpha)[(1-\alpha)A_i + \alpha B_i] \tag{3.28}$$

where $\alpha = \frac{S_w - S_{w(i-1)}}{S_{wi} - S_{w(i-1)}}$.

The parameters for Equation (3.28) can be expressed as,

$$A_i = k_{i-1}\left(S_{wi} - S_{w(i-1)}\right) - \left(P_{ci} - P_{c(i-1)}\right) \tag{3.29}$$

$$B_i = -k_i\left(S_{wi} - S_{w(i-1)}\right) + \left(P_{ci} - P_{c(i-1)}\right) \tag{3.30}$$

where $k_0 = P'_{c1}(S_{w0}), k_i = P'_{ci}(S_{wi}) = P'_{c(i+1)}(S_{wi})$

Therefore, the relationship between the slopes and the coordinates can be expressed as,

$$\begin{aligned}\frac{k_{i-1}}{S_{wi} - S_{w(i-1)}} + \left(\frac{1}{S_{wi} - S_{w(i-1)}} + \frac{1}{S_{w(i+1)} - S_{wi}}\right)2k_i + \frac{k_{i+1}}{S_{w(i+1)} - S_{wi}} \\ = 3\left(\frac{P_{ci} - P_{c(i-1)}}{\left(S_{wi} - S_{w(i-1)}\right)^2} + \frac{P_{c(i+1)} - P_{ci}}{\left(S_{w(i+1)} - S_{wi}\right)^2}\right)\end{aligned} \tag{3.31}$$

$$\frac{2}{S_{w1} - S_{w0}}k_0 + \frac{1}{S_{w1} - S_{wo}}k_1 = 3\frac{P_{c1} - P_{c0}}{(S_{w1} - S_{wo})^2} \tag{3.32}$$

$$\frac{1}{S_{wn} - S_{w(n-1)}}k_{n-1} + \frac{2}{S_{wn} - S_{w(n-1)}}k_n = 3\frac{P_{cn} - P_{c(n-1)}}{(S_{wn} - S_{w(n-1)})^2} \tag{3.33}$$

Equation (3.31) to (3.33) can form $n+1$ linear equations that defines $k_0, k_1, \dots, k_n$.

After the spline interpolation process, a capillary pressure curve from the discrete data points $(S_{wi}, P_{ci}),\ i = 1,2,\dots,n$ is obtained. The data process technique introduced in this section can be used to interpret the numerical generated and experimental P_c versus $aveS_w$ data points, by which

the deviations between numerical and experimental data can be measured.

3.3 Prediction of Capillary Pressure Curves Using Streamline Simulation

3.3.1 Capillary Pressure Numerical Model Geometry and Boundary Conditions

The digital model for streamline simulations is illustrated in Figure 14. A brine-saturated core plug is placed in a rotational system on an axis termed x. This is a two-dimensional flow system allowing fluid flow in the direction normal to the x axis. The inner boundary where $x = r_1$ is exposed to non-wetting phase, which submerges the core plug in the core holder. The core is exposed to the wetting phase at $x = r_2$. The pressure of the nonwetting phase is continuous in the space outside the core, whereas the non-wetting phase only has pressure continuity inside the core at $x = r_1$. In here, we only consider the drainage process. When the system begins to rotate, non-wetting phase enters at r_1 and wetting phase is displaced out of the core at r_2. Accelerating the rotational speed further reduces the wetting phase saturation of the core.

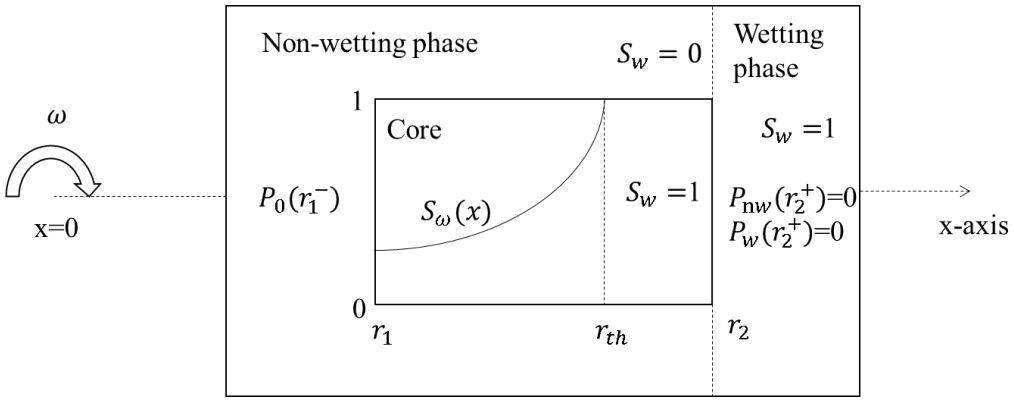

Figure 14 The geometry of a centrifuge core holder

It is assumed that the capillary pressure at $x = r_2$ is zero (Forbes, 2000). Therefore, both wetting phase and non-wetting phase pressures are zero:

$$P_{nw}(r_2^+, t) = 0, P_w(r_2^+, t) = 0, P_c(r_2^+, t) = 0, \tag{3.34}$$

where the superscripts $+, -$ denote the right and left side of the boundary respectively, subscripts

nw, w denote non-wetting and wetting phase respectively, t means rotational time.

It is known that the pressure of the wetting phase is continuous and mobile at r_2.

$$P_w(r_2^+, t) = P_w(r_2^-, t) = 0, f_w(x = r_2, t) = 1 \tag{3.35}$$

where f_w is the water fractional flow function.

The non-wetting phase pressure at r_1 can be obtained by integrating the pressure from r_2 to r_1 and the pressure inside the core decreases hydrostatically across the core:

$$P_{nw}(r_1^+, t) = \int_{r_2}^{r_1} P_{nw} dx = \int_{r_2}^{r_1} \rho_{nw}\omega^2 x dx = \frac{1}{2}\rho_{nw}\omega^2(r_1^2 - r_2^2) \tag{3.36}$$

The non-wetting phase has pressure continuity at r_1:

$$P_{nw}(r_1^+, t) = P_{nw}(r_1^-, t) = -\frac{1}{2}\rho_{nw}\omega^2(r_2^2 - r_1^2), f_w(x = r_1, t) = 0 \tag{3.37}$$

The wetting phase pressure is determined based the capillary relationship between two phases:

$$P_w(r_1^+, t) = P_{nw}(r_1^+, t) - P_c\big(S_w(r_1^+, t)\big) = -\frac{1}{2}\rho_{nw}\omega^2(r_2^2 - r_1^2) - P_c\big(S_w(r_1^+, t)\big) \tag{3.38}$$

When no more wetting phase is displaced from the core, a balance between capillary pressure and centrifugal force has been established at r_1 :

$$[\frac{\partial P_c}{\partial x} + \Delta\rho\omega^2 x]_{x=r_1} = 0 \tag{3.39}$$

where $\Delta\rho$ is the density difference between two phases.

Therefore, the pressure difference across the core is equal to the capillary pressure between two phases at equilibrium:

$$\Delta P = P_c(t) = \frac{1}{2}\Delta\rho\omega^2(r_2^2 - r_1^2) \tag{3.40}$$

3.3.2 Capillary Pressure Numerical Model Assumptions

As previously discussed in Section 2.1.1, some assumptions need to be made in the streamline simulation. In this research thesis, the streamline simulation is performed by assuming constant pressure boundary conditions. Accordingly, the fluids in the system are in steady state flow when it reaches equilibrium. Waterfront tracking calculations are under the same boundary conditions. Additionally, there are assumptions relating to the data processing of centrifuge experiments. Considering the assumptions of streamline simulations and centrifuge experiments, following assumptions for the two-dimensional centrifuge simulation can be made:

- Incompressible rock and fluids
- Diffusive effects are neglected
- Gravity is negligible
- Capillary pressure is zero at the end face of the core
- Cavitation is not present in the core
- The fluids in the core have reached equilibrium when the displaced wetting phase is measured at each incremental rotational speed. Therefore, this fluid flow in the rotational system has become stable.

In centrifuge experiments, oil and water can be assumed to be incompressible and diffusion free. Since the core is rotated at an ultra-high angular speed, the core is mainly subject to centrifugal acceleration so that gravity plays a minor role in the displacement process. Homogeneity of the core is not assumed allowing the effects of heterogeneity to be studied. Additionally, the fluid flow in the core is not restricted to one dimension.

3.3.3 Averaging Method for Permeability

The permeabilities generated using a Gaussian field are distributed randomly in the digital model. It is essential to calculate the upscaled/average permeability of the whole model so that a digital model with a randomly distributed permeability field can have the same average permeability as the homogeneous model. Therefore, the predicted phase saturations calculated in a heterogeneous case can be compared to the values calculated in a homogeneous case by keeping the average permeability unchanged.

The harmonic average permeability is calculated as:

$$K^* = (\frac{1}{L}\int_0^L \frac{1}{K(x)}\,dx)^{-1} \tag{3.41}$$

where L is the length of the core.

The arithmetic average permeability can be calculated as:

$$K^* = \frac{1}{LH}\int_0^H \int_0^L K(x,y)dxdy \tag{3.42}$$

The above two equations can be combined to calculate the average permeability:

$$\boldsymbol{K}^* = \begin{bmatrix} A_{-1}(K) & 0 \\ 0 & A_1(K) \end{bmatrix} \tag{3.43}$$

This average permeability is sometimes called harmonic-arithmetic average permeability.

3.3.4 Introduction of Streamline Tracing Method

It is widely accepted that streamline simulation receives increased attention in field/core scale simulation for petroleum engineering because it can efficiently visualize and describe the fluid flow. The three-dimensional transport problem is converted to one-dimensional transport problem along each streamline during the simulation. This conversion process decouples a three-dimensional

problem to a one-dimensional problem and makes solving transport equations along streamlines tractable. The elliptic pressure equation is solved under constant boundary conditions, so that the velocity field can be generated according to Darcy's Law. The constant pressure boundary condition is maintained when no more fluid is displaced out of the rotated core during centrifuge. Then the streamlines are calculated accordingly. Therefore, the accuracy of a streamline simulator relies heavily on pressure solutions and streamline trajectories. Datta-Gupta and King (2007) summarized the main procedures for most of the streamline simulation:

1. Calculate the pressure field by solving the elliptic pressure equation under given boundary conditions by following **Step 7** of Figure 13.
2. Generate the velocity field according to Darcy's Law by following **Step 7** of Figure 13.
3. Compute time-of-flight along streamlines by following **Step 9** of Figure 13.
4. Plot streamlines according to mobility ratios and well conditions by following **Step 10** of Figure 13.
5. Solve the transport equation in the streamlines for a proper time interval by following **Step 12** of Figure 13.
6. Obtain saturation profile using streamline by following **Step 13** of Figure 13.

In the Pollock-based streamline simulation, the velocity functions are approximated and the pressure in each grid block is assumed to be constant.

In centrifuge experiments, fluids in the core are assumed to be at equilibrium at each incremental rotational speed; therefore, streamlines in the centrifuge simulation were traced in steady state flow in which the flow characteristics are independent of time. The streamline is shown in

Figure 15 and defined as:

$$\boldsymbol{v} \times d\boldsymbol{\xi} = 0 \tag{3.44}$$

where $\times$ is the cross product; $\boldsymbol{v}$ is the flow velocity vector, $\boldsymbol{v} = (v_x, v_y, v_z)$; $d\boldsymbol{\xi}$ is the infinitesimal arc-length of the streamline, $d\boldsymbol{\xi} = (d_x, d_y, d_z)$.

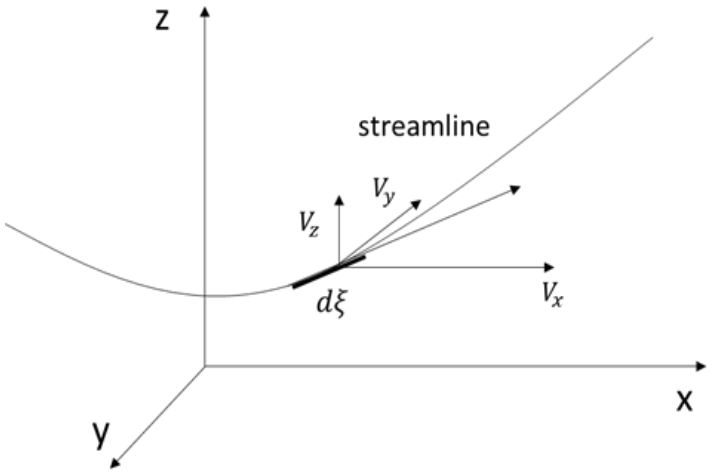

Figure 15 Streamline and the velocity vector

This results in the definition of a streamline as,

$$\frac{dx}{v_x} = \frac{dy}{v_y} = \frac{dz}{v_z} \tag{3.45}$$

In the $x - y$ plane, the above equation reduces to,

$$\frac{dx}{v_x} = \frac{dy}{v_y} \quad \text{or} \quad v_y dx - v_x dy = 0 \tag{3.46}$$

The instantaneous geometrical characteristic of the streamline can be described as,

$$\psi(x, y) = constant \tag{3.47}$$

where $\psi(x, y)$ is the stream function, the value of which is constant along a streamline (Lagrange, 1781).

Differentiating the stream function along a certain streamline and we have,

$$d\psi = \frac{\partial \psi}{\partial x} dx + \frac{\partial \psi}{\partial y} dy = 0 \tag{3.48}$$

Combining Equation (3.46) and Equation (3.48) results in:

$$\frac{\partial \psi}{\partial x} dx + \frac{\partial \psi}{\partial y} dy = v_y dx - v_x dy \tag{3.49}$$

The mathematical relationships between the stream function and the directional components of the flow velocity vector can be derived as,

$$v_y = \frac{\partial \psi}{\partial x};\ v_x = -\frac{\partial \psi}{\partial y} \tag{3.50}$$

Thus, the algebraic expression for the stream function can be derived by replacing the partial differentials of the stream function with the directional components of the velocity vector,

$$\psi = \int v_y dx - \int v_x dy \tag{3.51}$$

In the centrifuge simulation of this thesis, a particle is released at the launching point at the inlet face of the core and travels through the porous media and lands at the exit point at the outlet face. The (forward) time-of-flight τ is defined as the time that a particle takes to travel form its starting point (x_0, y_0, z_0) to a particular point (x, y, z) on the streamline. The time-of-flight can then be defined in terms of x, y, z,

$$\tau = \int_{x_0}^{x} \frac{dx}{v_x} = \int_{y_0}^{y} \frac{dy}{v_y} = \int_{z_0}^{z} \frac{dz}{v_z} \tag{3.52}$$

A parameter $(x, y\ or\ z)$ that is monotonically changing along the streamline will be selected as a directional parameter when the time-of-flight is calculated. The directional velocity will become zero as the denominator if the chosen directional parameter is not monotonic, which will introduce

large deviations in time-of-flight calculations. The particle will stop at a point where all directional velocities become zero. To represent the spatial coordinate of a point on a streamline with the time-of-flight and the Cartesian coordinates, time-of-flight should be used as a spatial coordinate during streamline simulation.

3.3.5 Solution of the Pressure Distribution

In the streamline tracing method used in this research thesis, the pressure values at grid blocks need to be obtained so that the pressure and velocity field can be approximated accordingly. A finite difference method for solving the pressure equations in centrifuge experiments was used. The assumption of the governing equations for the fluid flow in the porous media is the fluid and the porous media are incompressible, gravity is negligible, and the fluid flow is under steady-state condition. By assuming the capillary pressure to be constant at each time step, the capillary pressure is included in the calculation of pressure distribution when the centrifuge system is at equilibrium. These assumptions are valid when no more wetting phase fluid is produced at the graduated tube (Andersen et al., 2017).

The mass conservation equation is.

$$\nabla \cdot (A\boldsymbol{u}) = q \tag{3.53}$$

where, A is area, $\boldsymbol{u}$ is Darcy velocity**,** q is the volumetric outflow/inflow rate.

The modelling of the centrifuge experiment using MRST is dynamic and unstable; however, the rotated system in the lab-scale experiment is stable at the time of measurement. Thus, the flow rate for a given angular velocity in the lab-scale experiment can be measured and then it can be used to find the corresponding stable moment in the dynamic modelling of the centrifuge experiment.

The fluids in the porous media comply to Darcy's Law,

$$\boldsymbol{u} = -\lambda \nabla P \tag{3.54}$$

where $\boldsymbol{u}$ is Darcy velocity, λ is the mobility and P is pressure.

Combining the Equation (3.53) and Equation (3.54) together produces the Laplace equation,

$$\nabla \cdot (A\lambda \nabla P) = q \tag{3.55}$$

The Laplace equation is also called the pressure equation that should be solved. The pressure at the centered node of the gird block can then be calculated.

As shown in Figure 16, the pressure gradient $\frac{\partial P}{\partial x}$ from the grid block (i) to $(i+1)$ in the finite difference method is replaced with,

$$\frac{\partial P}{\partial x} = \frac{2(P_{i+1} - P_i)}{\Delta x_i + \Delta x_{i+1}} \tag{3.56}$$

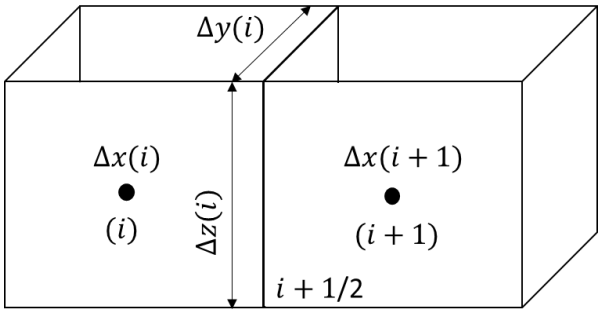

Figure 16 Finite difference method in pressure calculation

The λ on the interface $(i+1/2)$ can be determined by the harmonic mean,

$$\lambda_{i+1/2} = (\Delta x_i + \Delta x_{i+1})\left(\frac{\Delta x_i}{\lambda_i} + \frac{\Delta x_{i+1}}{\lambda_{i+1}}\right)^{-1} \tag{3.57}$$

Therefore, the out normal flux from the grid block (i) to $(i+1)$ is,

$$v_{i+1/2} = \frac{u_{i+1/2}}{\emptyset} = \frac{2(P_{i+1} - P_i)}{\emptyset(\frac{\Delta x_i}{\lambda_i} + \frac{\Delta x_{i+1}}{\lambda_{i+1}})} \tag{3.58}$$

An approximation to the $A\boldsymbol{u}$ in the mass conservation equation can be obtained by summing all interfaces to the specific grid block. To simplify the expressions, the transmissibility in the interface $(i + 1/2)$ is estimated,

$$T_{i+1/2} = 2\Delta y_i \Delta x_i (\frac{\Delta x_i}{\lambda_i} + \frac{\Delta x_{i+1}}{\lambda_{i+1}})^{-1} \tag{3.59}$$

Substituting the expression of transmissibility into Equation (3.58), the relationship of the grid block wise constant pressure $P_{i.j.k}$ can be derived,

$$\begin{aligned} &T_{i+\frac{1}{2},j,k}\left(P_{i,j,k} - P_{i+1,j,k}\right) + T_{i-\frac{1}{2},j,k}\left(P_{i,j,k} - P_{i-1,j,k}\right) + T_{i,j+1,k}\left(P_{i,j,k} - P_{i,j+1,k}\right) \\ &\quad + T_{i,j-1,k}\left(P_{i,j,k} - P_{i,j-1,k}\right) + T_{i,j,k+\frac{1}{2}}\left(P_{i,j,k} - P_{i,j,k+1}\right) \\ &\quad + T_{i,j,k-\frac{1}{2}}\left(P_{i,j,k} - P_{i,j,k-1}\right) = q_{i,j,k}; \end{aligned} \tag{3.60}$$

where the k index is the z coordinate direction, the j index is the y coordinate direction, and the i index is the x coordinate direction.

It is noted the derivation of the pressure distribution is based on a three-dimensional system but it is also applicable to two-dimensional system by ignoring the z coordinate. After implementing this method, the pressure at each grid block can be calculated, which is the fundamental for tracing streamlines in a grid.

3.3.6 Semi-Analytical Generation of Streamlines

In the streamline tracing process, the particle is traced by calculating the incremental changes of the particle's coordinate, which can be obtained by multiplying velocity components by a finite

time step. The above process should be repeated iteratively until the particle reaches outer boundary or the locations are at intermediate times required. From here, it is noted that the approximation of velocity field in the fluid flow is essential for tracing a streamline explicitly. The velocity vector and pressure at every point in the computation filed should be known for analytical tracing of streamlines, which is difficult to be realized. Therefore, the streamline tracing method used in this thesis is a semi-analytical particle tracking method with velocities calculated from a block centered finite-difference pressure solution (Pollock, 1988). There are three major ways to interpolate the velocity vector from the interface flux from a finite-difference model and some other interpolation schemes may also be reasonable: step function interpolation, linear interpolation and multilinear interpolation. The centrifuge simulation applies the linear interpolation by assuming that the principal velocity components vary linearly with respect to their own coordinate direction instead of all three principal directions in a grid block. The main advantage of implementing this interpolation scheme is that all the velocity component functions can be integrated directly in each individual grid block for an explicit solution of a streamline segments. Thus, the additional numerical deviations and constraints of time step are excluded because explicit computation are not necessary. In the beginning of the drainage centrifuge simulation, the core with the wetting phase fluid inside is submerged by the nonwetting phase fluid. When core begins to rotate, the nonwetting fluid will start to enter the core and this can be considered as the injection for all grids. In the meantime, the wetting phase will be displaced out of the core, which can be considered as the production for all grids. Therefore, the following equations can be derived.

The mass conservation equation in a steady-state flow system is,

$$\frac{\delta(\emptyset v_x)}{\delta x} + \frac{\delta(\emptyset v_y)}{\delta y} + \frac{\delta(\emptyset v_z)}{\delta z} = W \tag{3.61}$$

where v_x, v_y, v_z are the principal components of the average linear velocity vector, $\emptyset$ is porosity and W is the volume rate of water produced or injected by internal sources and sinks per unit volume of aquifer.

Figure 17 indicates a finite-sized cell of the flow field and the velocity components of inflow and outflow across six faces.

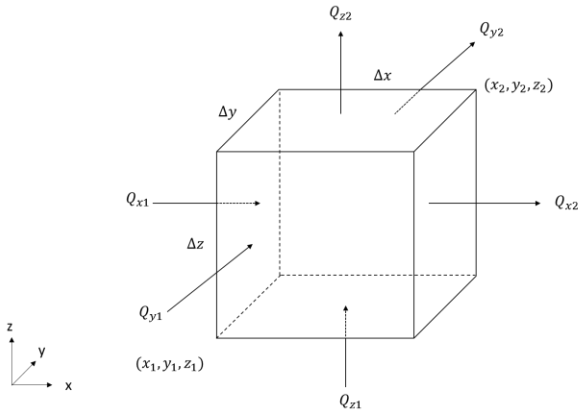

Figure 17 Finite-difference cell and definition of cell face flows

The six faces in this cube are $x_1, x_2, y_1, y_2, z_1, z_2$. Face x_1 is the face perpendicular to the x direction at $x = x_1$ and the other five faces are defined in the same principles. The intercell average velocity component can be calculated as,

$$v_{x1} = Q_{x1}/(n\Delta y\Delta z) \tag{3.62a}$$

$$v_{x2} = Q_{x2}/(n\Delta y\Delta z) \tag{3.62b}$$

$$v_{y1} = Q_{y1}/(n\Delta x\Delta z) \tag{3.62c}$$

$$v_{y2} = Q_{y2}/(n\Delta x\Delta z) \tag{3.62d}$$

$$v_{z1} = Q_{z1}/(n\Delta x\Delta z) \tag{3.62e}$$

$$v_{z2} = Q_{z2}/(n\Delta x\Delta z) \tag{3.62f}$$

where Q is a volume flow rate across a cell face, $\Delta x, \Delta y, \Delta z$ are the infinitesimal cell dimensions in the respective coordinate directions. Given the internal sources or sinks within the cell, the mass conservation equation can be written as,

$$\frac{(\emptyset v_{x2} - \emptyset v_{x1})}{\Delta x} + \frac{(\emptyset v_{y2} - \emptyset v_{y1})}{\Delta y} + \frac{(\emptyset v_{z2} - \emptyset v_{z1})}{\Delta z} = \frac{Q_s}{\Delta x\Delta y\Delta z} \tag{3.63}$$

where Q_s are the sources or sinks in the grid block.

The pressure at the central node of the grid block can be calculated by substituting Darcy's Law for each of the flow terms in the mass conservation equation (McDonald and Harbaugh, 1988). The solution of the resulting algebraic expressions can produce the pressure at the center of the calculated grid block. The other pressure values at six neighboring cells can be obtained with feasible approximation of the transmissibility between cells. Once all the pressure values have been computed, the intercell flow rates in Equation (3.62) can be calculated by use of Darcy's Law.

The next step is to calculate the velocity vector at every point of the flow filed based on the flow rates between cells, which can be easily achieved using the linear interpolation scheme. A continuous or piece-wise continuous function is used to interpolate the velocity components in a grid block,

$$v_x = A_x(x - x_1) + v_{x1} \tag{3.64a}$$

$$v_y = A_y(y - y_1) + v_{y1} \tag{3.64b}$$

$$v_z = A_z(z - z_1) + v_{z1} \tag{3.64c}$$

where A_x, A_y, A_z are the velocity component gradients within the cell and can be expressed as,

$$A_x = (v_{x2} - v_{x1})/\Delta x \tag{3.65a}$$

$$A_y = (v_{y2} - v_{y1})/\Delta y \tag{3.65b}$$

$$A_z = (v_{z2} - v_{z1})/\Delta z \tag{3.65c}$$

The velocity vector field computed from Equation (3.64) to (3.65) are continuous and satisfies the mass conservation equation at every point in the grid block, which is significant because it ensures that distributions of streamlines will be dependent on the movement of water through the core. Given the velocity distribution, a particle in the system can now be traced and the corresponding path line can be generated. The x-component of the particle's velocity changes with the rate as,

$$(\frac{dv_x}{dt})_p = (\frac{dv_x}{dx})(\frac{dx}{dt})_p \tag{3.66}$$

where the subscript p means the travelling particle.

The x-component of particle's velocity can be expressed as,

$$v_{xp} = (dx/dt)_p \tag{3.67}$$

Differentiating Equation (3.64a) with respect to x we have,

$$\frac{dv_x}{dx} = A_x \tag{3.68}$$

Substituting Equation (3.67) and (3.68) in Equation 3.66,

$$(\frac{dv_x}{dt})_p = A_x v_{xp} \tag{3.69}$$

Equations in the other coordinate direction can be obtained following the same derivation method,

$$(\frac{dv_y}{dt})_p = A_y v_{yp} \tag{3.70}$$

$$(\frac{dv_z}{dt})_p = A_z v_{zp} \tag{3.71}$$

Equation (3.69) to (3.71) can be rearranged and integrated between t_1 and t_2 $(t_2 > t_1)$,

$$\ln\left[\frac{v_{xp}(t_2)}{v_{xp}(t_1)}\right] = A_x \Delta t \tag{3.72}$$

$$\ln\left[\frac{v_{yp}(t_2)}{v_{yp}(t_1)}\right] = A_y \Delta t \tag{3.73}$$

$$\ln\left[\frac{v_{zp}(t_2)}{v_{zp}(t_1)}\right] = A_z \Delta t \tag{3.74}$$

The x, y, z-coordinate functions with respect to time t_2 can be obtained by substituting Equation (3.64) in the above equations,

$$x_p(t_2) = x_1 + \left(\frac{1}{A_x}\right)[v_{xp}(t_1)\exp(A_x \Delta t) - v_{x1}] \tag{3.75}$$

$$y_p(t_2) = y_1 + \left(\frac{1}{A_y}\right)[v_{yp}(t_1)\exp(A_y \Delta t) - v_{y1}] \tag{3.76}$$

$$z_p(t_2) = z_1 + \left(\frac{1}{A_z}\right)[v_{zp}(t_1)\exp(A_z \Delta t) - v_{z1}] \tag{3.77}$$

$v_{xp}(t_1), v_{yp}(t_1), v_{zp}(t_1)$ are known functions of the coordinates so that the coordinates of the particle at time t_2 can be calculated from Equation (3.72) to (3.74).

Figure 18 shows a two-dimensional streamline in an orthogonal grid block.

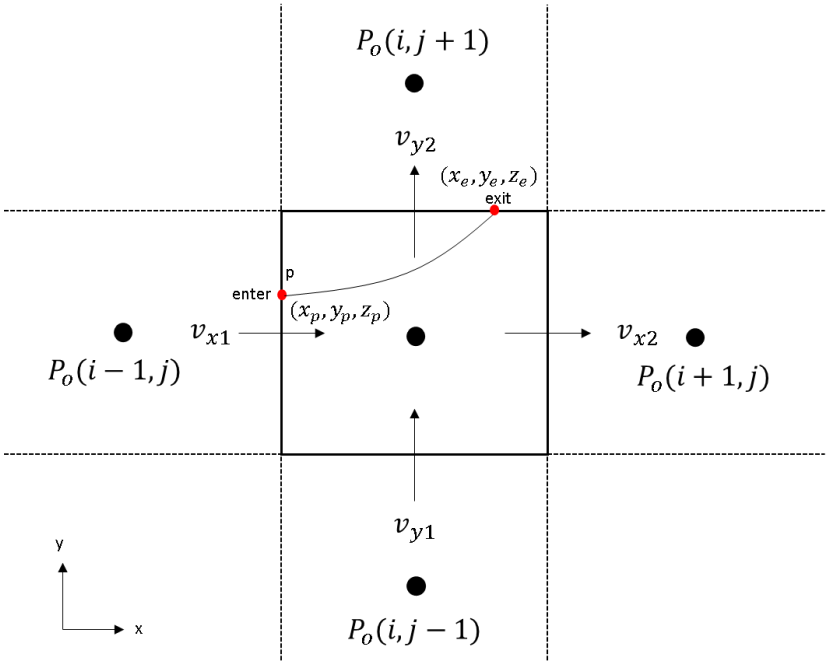

Figure 18 Schematic of a streamline through an orthogonal grid block in 2D

For the present example, the particle enters in P and velocity components at the four faces require that the particle exits in either face y_2 or face x_2. The key to find out the actual exiting face is comparing the travel time that the particle takes to arrive at face y_2 and face x_2, which can be calculated from Equation (3.72) and (3.73),

$$\Delta t_x = (1/A_x)\ln\left(v_{x2}/v_{xp}\right) \tag{3.78}$$

$$\Delta t_y = (1/A_y)\ln\left(v_{y2}/v_{yp}\right) \tag{3.79}$$

The smaller value of Δt_x and Δt_y is the actual incremental travel time, known as Δt_e and the corresponding exiting coordinates can be computed. However, if Δt_x is the same as Δt_y, the particle will leave the cell at the corner point. The exiting coordinates of the particle can then be calculated as,

$$x_e = x_1 + \left(\frac{1}{A_x}\right)\left[v_{xp}(t_p)\exp(A_x\Delta t_e) - v_{x1}\right] \tag{3.80}$$

$$y_e = y_1 + \left(\frac{1}{A_y}\right)\left[v_{yp}(t_p)\exp(A_y \Delta t_e) - v_{y1}\right] \tag{3.81}$$

The time that a particle takes to leave the cell is: $t_e = t_p + \Delta t_e$, which is called as time-of-flight. This step is repeated until the particle reaches the boundary so that the entire streamline tracking the particle through the whole system can be generated.

3.4 Two-phase Displacement Considering Capillary Pressures

In centrifuge simulation based on streamline methods, two-dimensional transport problems need to be decoupled to one-dimensional problems along streamlines that can be solved by the Riemann approach. Buckley and Leverett (1942) presented analytical Riemann solutions in one-dimensional two-phase problems under constant flow rate boundary conditions, whereas the solutions under constant pressure boundary conditions were proposed by Johansen and James (2016). To obtain the average water saturation in centrifuge experiments, a Riemann solution under constant pressure boundary conditions is needed. In this section, the basic flow equations for immiscible two-phase displacement during centrifuge are introduced. Then the analytical Riemann solutions for the constant flow rate boundary condition and constant pressure boundary condition are given.

3.4.1 Flow Equations in Two-phase Flow Problems

In the centrifuge experiments, there are two phases (wetting and non-wetting phases) existing in the core plug under rotation. A certain volume of the wetting phase fluid is produced in the graduated tube at each incremental rotational speed, and it is assumed that fluids in the core are immiscible and incompressible. Therefore, this is an immiscible, incompressible two-phase flow problem.

For two-phase flow in the core, the mass conservation equation for phase α can be written as,

$$\frac{\partial}{\partial t}(\emptyset\rho_w S_w) + \nabla\cdot(\rho_w\vec{v}_w) = \rho_w q_w \tag{3.82}$$

$$\frac{\partial}{\partial t}(\emptyset\rho_n S_n) + \nabla\cdot(\rho_n\vec{v}_n) = \rho_n q_n \tag{3.83}$$

where $\emptyset$ is the rock porosity, ρ is the density of the fluid, S is the saturation, $\vec{v}$ is the macroscopic Darcy velocity, q denotes fluid sources and sinks, subscript w, n denotes wetting phase and nonwetting phase respectively.

Considering nonwetting phase pressure p_n and wetting phase saturation S_w as primary variables, Equation (3.82) and (3.83) become,

$$\frac{\partial}{\partial t}(\emptyset\rho_w S_w) + \nabla\cdot\left(\frac{\rho_w \boldsymbol{K} k_{rw}}{\mu_w}(\nabla p_n - \nabla P_c(S_w) - \rho_w g\nabla \mathrm{z})\right) = \rho_w q_w \tag{3.84}$$

$$\frac{\partial}{\partial t}(\emptyset\rho_n(1-S_w)) + \nabla\cdot\left(\frac{\rho_n \boldsymbol{K} k_{rn}}{\mu_n}(\nabla p_n - \rho_n g\nabla \mathrm{z})\right) = \rho_n q_n \tag{3.85}$$

where $\boldsymbol{K}$ is the main permeability, k_{rw}, k_{rn} are relative permeability of wetting and non-wetting phase respectively, z is the vertical coordinate, g is the gravitational acceleration.

It is assumed that porosity and fluid densities are constant in the incompressible flow, so the mass conversation equations reduce to,

$$\emptyset\frac{\partial S_w}{\partial t} + \nabla\cdot(\vec{v}_w) = q_w \tag{3.86}$$

$$\emptyset\frac{\partial S_n}{\partial t} + \nabla\cdot(\vec{v}_n) = q_n \tag{3.87}$$

The total Darcy velocity in terms of the pressure for the nonwetting phase is,

$$\begin{aligned}\vec{v} = \vec{v}_n + \vec{v}_w &= -\boldsymbol{\lambda_n}\nabla p_n - \boldsymbol{\lambda_w}\nabla p_w + (\boldsymbol{\lambda_n}\rho_n + \boldsymbol{\lambda_w}\rho_w) \\ &= -(\boldsymbol{\lambda}_n + \boldsymbol{\lambda_w})\nabla p_n + \boldsymbol{\lambda_w}\nabla p_c + (\boldsymbol{\lambda_n}\rho_n + \boldsymbol{\lambda_w}\rho_w) g\nabla z\end{aligned} \tag{3.88}$$

where $\boldsymbol{\lambda}_n$, $\boldsymbol{\lambda}_w$ are mobilities of nonwetting phase and wetting phase respectively.

Rearranging the above equation and we have,

$$-\nabla \cdot (\lambda \mathbf{K} \nabla p_n) = \mathrm{q} - \nabla[\boldsymbol{\lambda}_{\boldsymbol{w}} \nabla p_c + (\boldsymbol{\lambda}_{\boldsymbol{n}} \rho_n + \boldsymbol{\lambda}_{\boldsymbol{w}} \rho_w) g \nabla z] \tag{3.89}$$

where total mobility $\boldsymbol{\lambda} = \boldsymbol{\lambda}_{\boldsymbol{n}} + \boldsymbol{\lambda}_{\boldsymbol{w}} = \lambda \mathbf{K}$ and total source $q = q_n + q_w$.

This is the pressure equation governing incompressible two-phase flow, which has an elliptic character.

The expression of $\vec{v}_w$ can be solved by multiplying phase velocity by the other phase's mobility and subtracting the results,

$$\begin{aligned} \lambda_n \vec{v}_w - \lambda_w \vec{v}_n &= \lambda \vec{v}_w - \lambda_w \vec{v} \\ &= -\lambda_n \lambda_w \mathbf{K}(\nabla p_w - \rho_w \mathrm{g} \nabla z) + \lambda_n \lambda_w \mathbf{K}(\nabla p_n - \rho_n \mathrm{g} \nabla z) \\ &= \lambda_n \lambda_w \mathbf{K}[\nabla p_c + (p_w - \rho_w) \mathrm{g} \nabla z] \end{aligned} \tag{3.90}$$

Inserting Equation (3.90) into Equation (3.89), the saturation equation (transport equation) can be written as,

$$\emptyset \frac{\partial S_w}{\partial t} + \nabla \cdot [f_w \vec{v} + f_w \lambda_n \boldsymbol{K} \Delta \rho g \nabla z] = q_w - \nabla \cdot (f_w \lambda_n \boldsymbol{K} P_c' \nabla S_w) \tag{3.91}$$

where $\Delta \rho = \rho_w - \rho_n$, fractional flow function $f_w = \frac{\lambda_w}{\lambda_w + \lambda_n}$.

The capillary pressure term on the right-hand side denotes the saturation equation has a parabolic character.

3.4.2 The Buckley-Leverett Displacement Theory

In the streamline simulation, two-dimensional transport problems in grid blocks can be decoupled to a series of one-dimensional problems along streamlines, in which analytical solutions can be applied. Thus, the Riemann problem for a one-dimensional system can be solved. Buckley and

Leverett developed an analytical Riemann solution for a two-phase immiscible displacement in a one-dimensional porous media system, as shown in Figure 19. The system is assumed to have an inclination of α with the horizontal plane and the fluids and rock are incompressible.

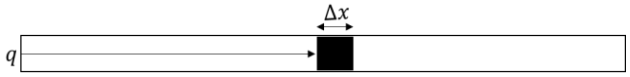

Figure 19 Flow system in Buckley-Leverett theory

The Darcy's Law for oil and water can be written as,

$$q_w = -A\lambda_w(\frac{\partial p_w}{\partial x}) \tag{3.92}$$

$$q_o = -A\lambda_o(\frac{\partial p_o}{\partial x}) \tag{3.93}$$

where A is the cross-sectional area of the flow system, λ_w, λ_o are the mobility ratio of the water and oil, respectively.

The total flow rate q is,

$$q_t = q_o + q_w \tag{3.94}$$

The capillary pressure between two phases is given by,

$$p_o - p_w = P_c \tag{3.95}$$

Combining above equations, the fractional flow function of water can be expressed as,

$$f = \frac{\lambda_w}{\lambda} + \frac{\lambda_w A}{q\lambda}\frac{dP_c(S_w)}{dS_w}\frac{\partial S_w}{\partial x} \tag{3.96}$$

where λ is the total mobility ratio, $\Delta\rho$ is the density different between water and oil.

Consider a horizontal medium in the absence of capillary forces, the expression for functional flow function reduces to,

$$f = \frac{\lambda_w}{\lambda} \tag{3.97}$$

The mass conservation equation of water in a control volume of length Δx in the flow system for a time step of Δt can be expressed as,

$$[(q_w\rho_w)_x - (q_w\rho_w)_{x+\Delta x}]\Delta t = [(S_w\rho_w)^{t+\Delta t} - (S_w\rho_w)^t]A\Delta x\emptyset \tag{3.98}$$

When Δx and Δt are getting close to zero, differentiating the above equation partially,

$$A\emptyset\frac{\partial(S_w\rho_w)}{\partial x} + \frac{\partial(q_w\rho_w)}{\partial x} = 0 \tag{3.99}$$

The density of water is a constant because fluids are incompressible, the above equation has become,

$$A\emptyset\frac{\partial(S_w)}{\partial x} + \frac{\partial(q_w)}{\partial x} = 0 \tag{3.100}$$

Combining the fractional flow function and above equation yields,

$$\frac{\partial S_w}{\partial t} + \frac{q}{A\emptyset}\frac{\partial f}{\partial x} = 0 \tag{3.101}$$

Rewriting the above equation,

$$\frac{\partial(S_w)}{\partial t} + \frac{q}{A\emptyset}\frac{\partial f}{\partial S_w}\frac{dS_w}{dx} = 0 \tag{3.102}$$

Equation (3.102) is called as Buckley-Leverett equation that gives an analytical Riemann solution. The water saturation profile is a function of both of x and t, and the derivative of water saturation can be written as,

$$dS_w = \frac{\partial S_w}{\partial x}dx + \frac{\partial S_w}{\partial t}dt \tag{3.103}$$

The propagation of saturation profile can be tracked by setting the total derivative of the water saturation to be zero,

$$dS_w = 0 = \frac{\partial S_w}{\partial x} dx + \frac{\partial S_w}{\partial t} dt \tag{3.104}$$

Substituting the above equation into the Buckley-Leverett equation,

$$\frac{dx}{dt} = \frac{q}{\emptyset A} \frac{df}{dS_w} \tag{3.105}$$

Integrating the above equation and the expression of the fluid front location can be derived,

$$\int dx = \int \frac{q}{\emptyset A} \frac{df}{dS_w} \tag{3.106}$$

$$x = \frac{qt}{A\emptyset} \frac{df}{dS_w} \tag{3.107}$$

where x is the front location of the fluid.

Equation (3.107) can be used to plot the saturation profile and the typical results in Lie (2019) are shown in Figure 20, which is unphysical because there are two saturation values corresponding to one location. This multivalued solution can be avoided by adding a discontinuity in the front. The two shaded areas before and after should have the same size following the mass conservation law. In centrifuge experiments, the average water saturation in the core can be obtained based on the saturation profile when the system reaches equilibrium.

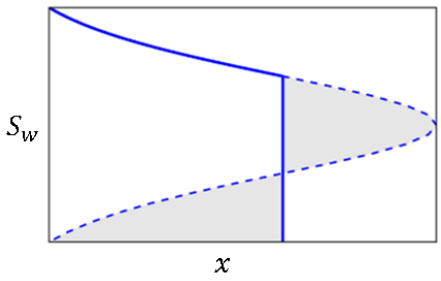

Figure 20 The saturation profile with a discontinuity (from Lie, 2019)

3.4.3 A semi-analytical Riemann Solution in Centrifuge Experiments

The flow problems with two or three dimensions are usually solved by the following steps: first,

decouple the multi-dimensional flow problems into one-dimensional transport problem along streamlines; second, solve the one-dimensional transport problem along each streamline; third, integrate the solutions from all streamlines.

Darcy's Law along streamlines can be written as,

$$q = -\lambda A(\xi)\frac{\partial P}{\partial \xi} \tag{3.108}$$

where ξ is the arc length of streamline, A is the cross sectional area of stream tube,

The Riemann problem under constant pressure difference along a one-dimensional streamline is described as Equation (3.109) and (3.110),

$$\frac{\partial s}{\partial t} + \frac{q}{\emptyset A}\frac{\partial f}{\partial \xi} = 0 \tag{3.109}$$

$$q(t) = -\lambda(\xi, s)A(\xi)\frac{\partial P}{\partial \xi} \tag{3.110}$$

with constant condition,

$$s(\xi, 0) = s_R, for\ \xi \in [0, L] \tag{3.111}$$

$$s(0, T) = s_l, for\ t \geq 0 \tag{3.112}$$

$$\Delta P(t) = P_i(t) - P_o(t) = constant, for\ t \geq 0 \tag{3.113}$$

In the above equations, the cross section independent of time can be estimated as,

$$A(\xi) = \frac{q_r}{\emptyset v(\xi)} \tag{3.114}$$

where $v(\xi)$ is the total velocity along streamlines, q_r is the reference flow rate along streamlines. The capillary pressure is included in the calculation using Equation (3.1) in Section 3.1. Therefore, the ΔP in Equation (3.113) is equal to zero when the centrifuge system is at equilibrium since the

capillary pressure is the same as the differential pressure provided by angular velocity.

The total flow rate along a particular streamline can be written as,

$$q(t) = -\lambda(\xi, s)A(\xi)\frac{\partial P}{\partial \tau}\frac{\partial \tau}{\partial \xi} \tag{3.115}$$

The time-of-flight can be expressed as,

$$\tau = \int \frac{1}{v} d\xi \tag{3.116}$$

Differentiating the above equation yields,

$$\frac{\partial \tau}{\partial \xi} = \frac{d\tau}{d\xi} = \frac{1}{v(\xi)} \tag{3.117}$$

Substituting Equation (3.116) and (3.117) into Equation (3.115),

$$q(t) = -\frac{\lambda(\xi, s)q_r}{\emptyset(\xi)v(\xi)^2}\frac{dP}{d\tau} \tag{3.118}$$

Integrating the above equation along streamline yields,

$$q(t)\int_0^{\tau^R} \frac{\emptyset(\xi)v(\xi)^2}{\lambda(\xi, s)} d\tau = -q_r \int_{P_i}^{P_o} dP \tag{3.119}$$

Combing the above two equations gives,

$$q(t) = \frac{q_r \Delta P}{\int_0^{\tau^R} \frac{\emptyset(\xi)v(\xi)^2}{\lambda(\xi, s)} d\tau} = \frac{q_r \Delta P}{R(t)} \tag{3.120}$$

where ΔP is the total pressure difference along the streamline and τ^R is the time-of-flight at the outlet of the streamline.

The denominator in the above equation is the total flow resistance of the streamline,

$$R(t) = \int_0^{\tau^R} \frac{\emptyset(\xi)v(\xi)^2}{\lambda(\xi, s)} d\tau \tag{3.121}$$

The total flow resistant is defined as the differential pressure required for keeping the flow rate at the reference value.

The propagation velocity of the fluids with a certain saturation is,

$$\left.\frac{d\xi}{dt}\right|_s = \frac{q(t)}{\emptyset(\xi)A(\xi)} f'(s) \tag{3.122}$$

Integrating the mass conservation equation by applying the boundary conditions, we have:

$$\frac{\partial S_w^{eq}}{\partial t} = -\frac{1}{\emptyset(r_2 - r_1)} u_T \tag{3.123}$$

where S_w^{eq} represents water saturation at equilibrium, u_T is the total Darcy velocity/drainage rate. It is assumed that the uniform mobility value $\lambda_w^*, \lambda_{nw}^*$ can be used to represent two-phase flow region resulting in total mobility $\lambda_T^* = \lambda_w^*, +\lambda_{nw}^*$ and fractional flow function $f_w^* = \lambda_w^*/\lambda_T^*$. The drainage rate can be expressed as:

$$\begin{aligned} u_T = \frac{K f_w^*}{\frac{(r_{th} - r_1)}{\lambda_T^*} + \frac{(r_2 - r_{th})}{\mu_w^{-1}}} \Big(\frac{1}{2}\Delta\rho\omega^2(r_2^2 - r_1^2) - P_{c_1} \\ + \frac{(1 - f_w^*)}{f_w^*}\frac{1}{2}\Delta\rho\omega^2\Big(\left[r_2^2 - \frac{P_{cd}}{\frac{1}{2}\Delta\rho\omega^2}\right] - r_{th}^2\Big)\Big) \end{aligned} \tag{3.124}$$

where r_{th} is the location of threshold capillary pressure.

3.5 Comparison between Numerical and Experimental Results

Numerical average water saturations calculated from two-dimensional centrifuge simulations are compared with experimental average water saturations measured from centrifuge experiments. Sum of squared error (SSE) and mean squared error (MSE) were used to describe the deviations between the simulated and the experimental data. SSE is the sum of the squared differences

between each observation and its group's mean, which can be used as a measure of variation within a cluster (Mood, 1950). If all cases within a cluster are identical the SSE would then be equal to 0. The formula for SSE is:

$$SSE = \sum_{i=1}^{n} (X_i - \bar{X})^2 \tag{3.125}$$

where n is the number of observations, X_i is the value of i^{th} observation and $\bar{X}$ is the mean of all observations.

MSE is the average difference between the estimated and the actual values (Pishro-Nik, 2016). The formula for MSE is:

$$MSE = \frac{1}{n} \sum_{i=1}^{n} (X_i - \bar{X})^2 \tag{3.126}$$

If the MSE are no more than 0.002, the numerical data generated from centrifuge simulations are within the acceptable range of deviation from experimental data (Ruth, 1997); therefore, the centrifuge simulator used in this thesis will be considered to be reliable.

The way to compare the results of centrifuge experiments with the results of two-dimensional centrifuge simulation is shown in Figure 21. The experimental average wetting phase saturation ($experimental\ ave S_w$) in Step (A) is calculated from the centrifuge experiment in the laboratory, whereas the corresponding numerical average wetting phase ($numerical\ ave S_w$) in Step (a) is predicted from the two-dimensional centrifuge simulation. Capillary pressure (P_c) was calculated based on the incremental rotational speeds during centrifuge. The inlet face saturation

($inletS_w$) is converted from $aveS_w$ by using Forbes-Splines method and then the capillary pressure curve is plotted. $P_c(aveS_w)$ denotes the capillary pressure versus average wetting phase saturation curve and $P_c(inletS_w)$ means the capillary pressure versus inlet face wetting phase saturation curve (capillary pressure curve). The reason for fitting data points in Step (A) to a curve in Step (B) is introduced in Section 3.2.1. In this thesis, experimental results from Step (A), (B) and (C) are compared to numerical results from Step (a), (b) and (c), respectively.

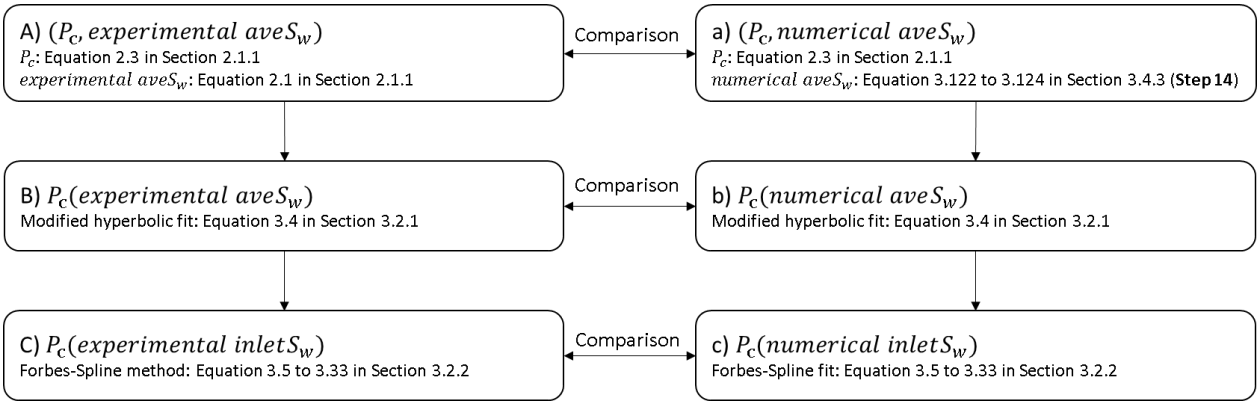

Figure 21 Logic of comparing experimental results from centrifuge experiment with numerical results from centrifuge simulation, Step (A) to (C) are results from Step (i) of Figure 13, Step (a) to (c) are results from Step (ii) of Figure 13

The typical capillary pressure versus average water saturation data points in Step (A), ($P_c, aveS_w$), are shown in Table 7. The typical capillary pressure versus average water saturation curve known as average water saturation curve, $P_c(aveS_w)$, and local capillary pressure curve, $P_c(inletS_w)$, are shown in Figure 22 from the manual book of CYDAR. The red data points in the figure are plotted according to the data in Table 7.

Table 7 Typical capillary pressure versus experimental average water saturation data points from centrifuge

Pc (bar)	experimental aveSw (frac.)

4.116	0.304
3.251	0.350
2.489	0.400
1.830	0.451
1.270	0.705
0.811	0.811
0.427	0.908
0.204	0.965
0.051	1.000

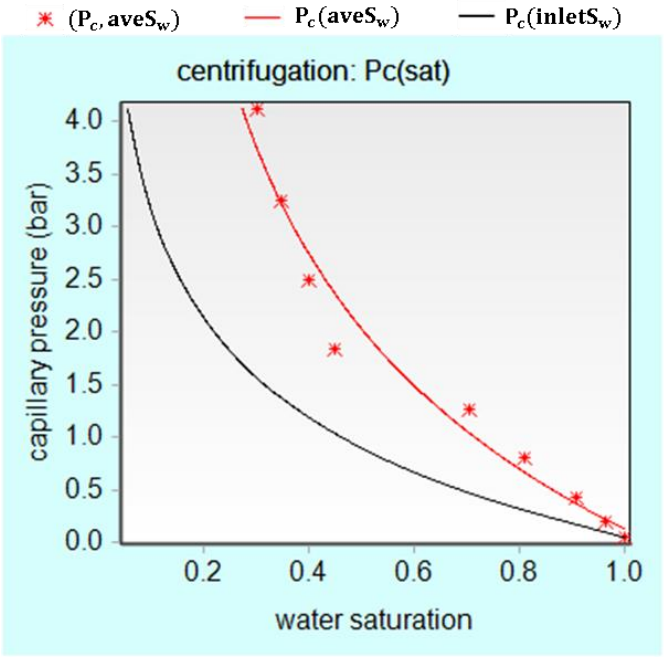

Figure 22 Typical average water saturation curve and local capillary pressure curve from centrifuge experiments (from CYDAR User Manual, 2021)

3.6 Simulating Centrifuge Experiment Process

The detailed procedures for each step of the centrifuge simulation are listed as the follows:

1. Conduct the centrifuge experiment and calculate capillary pressure and experimental average saturation using Equation (2.3) and (2.1) from the Section 2.1.1.

Conduct the high-speed centrifuge experiment in the laboratory and record the volume of displaced fluid in each angular velocity. Calculate the capillary pressure based on the angular velocity and calculate the experimental average saturation based on the volume of displaced fluid.

2. Fit the modified hyperbolic function on capillary pressure versus average saturation points using Equation (3.4) from the Section 3.2.1.

Use the modified hyperbolic function to fit the experimental data. When the modified hyperbolic function cannot give acceptable results, spline function can be used.

3. Apply Forbes-Splines method to convert average saturation to inlet saturation. Generate the experimental capillary pressure curve using Equation (3.5) to (3.33) from the Section 3.2.2.

Use the Forbes-Splines method in MRST to convert average wetting phase saturations to inlet wetting phase. The resulting capillary pressure curve can then be plotted.

4. Construct a numerical model according to its geometric and petrophysical parameters (L, D, k, $\varnothing$) using Equation (3.1) from the Section 3.1.

Grid is a network of lines that cross each other to form a tessellation of planar or volumetric object. Structured grid only allows the use of a basic shape and then it will be repeated under some regular pattern so that the spatial topology of the grid remain unchanged during the process. Quadrilaterals and hexahedrons are typically used in two- and three-dimensional grids respectively, but other general shapes can also be applied to construct grids. In our cases, finite Cartesian grids that consist of a finite number of cells within the range of boundary domain are considered because the streamline simulations in MRST only accept regular Cartesian grids. It is almost impossible to solve storage and transport problems in real-size rock bodies as such enormous models are beyond digital calculations; therefore, a continuum hypothesis and volume averaging are both incorporated to introduce macroscopic petrophysical properties, which can be considered as input to flow simulators. The simulation can be more accurate if the grid size becomes smaller. Nonetheless, the

time that takes to reach equilibrium also increases. To keep a balance between efficiency and accuracy, the number of radial grid blocks is no more than 100 and the number of axial grid blocks should not exceed 200. The grid size can be determined by dividing the core length by the number of grid blocks. The petrophysical properties of the simulated rock are designated as constant values in each individual cell or as values attached to cell faces. The ratio of the void space to the bulk volume is defined as porosity, which means $0 < \emptyset < 1$. Thus, fraction occupied by rock matrix is defined as $1 - \emptyset$. Only interconnected pore space, effective porosity, is of interest for streamline simulations. The ability to transmit a fluid when the void space of a core is fully filled with this fluid is called permeability. In the MRST, only one column is needed for an isotropic permeability, and two or three columns for a diagonal permeability. In our cases, anisotropy is not considered.

The capillary relation between two phases from the experimental capillary pressure curve is taken as an input to the centrifuge digital model. In MRST, Fluid objects that can evaluate the petrophysical properties of rock and fluid, such as viscosity, fluid density and fluid compressibility, are applied, which consist of several preset properties and function handles. Therefore, the fluid properties of two immiscible fluids should be input, which can be determined by experimental measurements

5. Visualize the heterogeneity by plotting the histogram of the permeability distribution using Equation (3.2) from the Section 3.1.

It is often assumed that the porous media is homogeneous in the modelling of centrifuge experiments. Nonetheless, permeability and porosity may vary spatially within a core plug. Therefore, it is essential to understand rock heterogeneities by showing permeability distributions.

6. Impose boundary condition (Δp) corresponding to the maintained angular velocity ($experimental\ P_c$) using Equation (3.3) from the Section 3.1.

Boundary conditions cannot be given on the internal faces of cells, which may contribute to unreasonable results, and because the fluid flow through the core sample is set to be incompressible, the net boundary fluxes must equal to zero. In our cases, the system is assumed under constant pressure boundary conditions at equilibrium. The pressure difference is fixed and equal to the capillary pressure between two immiscible phases at each incremental rotational speed.

7. Calculate the pressure field by solving the elliptic pressure equation and generate velocity field using Equation (3.53) to (3.60) from the Section 3.3.5, Equation (3.82) to (3.88) from the Section 3.4.1.

Discretization methods, such as finite-difference, finite-volume and finite-element method, are needed for the solving Laplace/Poisson equation. For our cases, the two-point flux-approximation scheme will be implemented to solve the Laplace/Poisson equation as its pressure approximations are monotonous. This discretization scheme is also easy to be converted even though it would introduce numerical mistakes and not provide reasonable solutions for some types of grids. The pressure distribution can be obtained by solving the pressure equation using two-point flux-approximation scheme. The velocity field can be calculated according to Darcy's Law.

8. Plot the flux versus simulation time figure and determine simulation time (T) for each pressure difference(P_c) using Equation (3.108) to (3.121) from the Section 3.4.3.

The estimated capillary pressure mathematical model can be taken as an input to the centrifuge simulation describing the capillary relationship between two phases during the displacement.

However, the displacement process is dynamic so the flux in the core is a function of simulation time. Therefore, the simulation time for each capillary pressure needs to be determined according to the recorded experimental flux when the fluid system reaches to equilibrium. The flux can be considered as a bridge connecting a static state of the unsteady state flow to the steady state fluid flow. The system is at equilibrium when the no more wetting phase is displaced from the core and the corresponding flow rate can be calculated by dividing the cumulative volume of produced fluid by the rotational time interval. For one pressure difference (rotational speed), there is one corresponding flow rate. The simulation time can then be determined according to the flux versus simulation time figure.

9. Solve the time-of-flight equation with the upwind, finite discretization using Equation (3.64) to (3.79) from the Section 3.3.6.

After solving for the pressure and saturation equations, Darcy's velocities in each grid block can be computed and time-of-flight for streamlines can be obtained by integration method.

10. Plot the streamlines semi-analytically using Equation (3.80) to (3.81) from the Section 3.3.6.

In the semi-analytical streamline tracing method, the velocity functions are approximated with the pressure in each grid block is constant. There are generally three steps in a streamline tracking method (Zhang et al., 2012): Firstly, using a numerical method for solving the pressure at the centre of each discrete grid block; secondly, estimating the velocity field in each grid block and finally, calculating the time-of-flight and integrating streamlines based on the calculated velocity field at each grid block.

11. Visualize high-flow and stagnant regions in terms of total residence time.

Backward time-of-flight is the time a neutral particle takes to travel from a given point in the core to the outlet boundary. The equation for calculating backward time-of-flight is the same as that for calculating forward time-flight (Equation (3.74) in Section 3.3.4) but with different launching and exit points. The sum of the forward and backward time-of-flights give the total travel time in the core, which can be used to visualize the high-flow and stagnant regions. The sum of the forward and backward time-of-flights is denoted as $\sum TOF$. To account for core heterogeneities during centrifuge, high-flow and stagnant regions can be visualized, which can be achieved by computing the total residence time for each streamline. The streamlines are hindered if the low heterogeneous area appears in the displacement.

12. Solve the transport equation implicitly by the single point, upstream mobility-weighting scheme using Equation (3.86) to (3.91) from the Section 3.4.1.

It is common to write the system as a pressure equation and one or more transport equations; a specialized discretization scheme is stilled necessary for transport equations. In streamline tracing methods, two or three-dimensional transport problems are decoupled to one-dimensional problems along streamlines. This one-dimensional transport problem can be solved by the Riemann approach.

13. Compute and plot the multi-phase flow solutions using Equation (3.92) to (3.107) from the Section 3.4.2.

In this step, saturation distribution can be obtained by solving the multi-phase fluid flow problems during centrifuge. The transport problem is solved by mapping the one-dimensional solution for mass conservation equations along each streamline, which is called the Riemann approach (Thiele,

1995). The saturation profile is used to understand the effects of heterogeneities on saturation distribution and the corresponding average saturation value.

14. Calculate the numerical average wetting phase saturation using Equation (3.122) to (3.124) from the Section 3.4.3.

The numerical average wetting phase saturation is the average value of the wetting phase saturations in all grid blocks. The average wetting phase saturation is related to the simulation time, capillary pressure between two phases and permeability distribution at equilibrium; therefore, the influences of heterogeneity can be reflected on this data.

15. Generate numerical capillary pressure curve using Forbes-Splines method using Equation (3.4) to (3.33) from the Section 3.2.1 and 3.2.2.

The detailed steps are introduced in Section 3.5.

16. Comparison between simulation results from Step (i) and experimental results from Step (ii).

Compare experimental results from the centrifuge experiment and numerical results from the two-dimensional centrifuge simulation in this step.

4 Applications and Case Studies of Centrifuge Simulations

In this section, five centrifuge modelling cases have been completed. The Table 8 shows the comparisons between different cases. K_{avg} denotes the average permeability of the model and K_{heter} denotes permeability of the heterogeneous area. In Case 1, three centrifuge simulations have been done on three different homogeneous cores with varying porosity, permeability, and fluid properties. The results of all three centrifuge simulations were compared against experimental results to determine applicability of the new centrifuge simulation method for other imaginary cases. In Case 2, the objective is to determine if a core with a randomly distributed permeability but with the same average permeability as the homogenous core in Case 1.1. In Case 3, three simulations have been conducted on heterogeneous cores with three different lengths of heterogeneous areas. The results of these three simulations were compared to the results of Case 2 to determine the effects of the lengths of heterogeneous areas on the fluid flow and resulting capillary pressure curves during centrifuge. In Case 4, two simulations have been done on heterogeneous cores with a low permeability area (5 mm). The simulated results were then compared to the results of the randomly distributed Case 2 to study the effects of low permeability in the heterogeneous area. In Case 5, two simulations have been conducted on heterogeneous cores with a high permeability area (5 mm). The simulated results of Case 5 were then compared to the results of the randomly distributed Case 2 to investigate the effects of high permeability in the heterogeneous area.

Table 8 Comparisons of different cases

No. of cases		Objective	Core length (cm)	Heterogeneity length (mm)	K_{avg} (mD)	K_{heter} (mD)
Homogeneous Case 1	**Case 1.1**	Compare predicted and experimental results	5.2		360	
	Case 1.2		4.94		440	
	Case 1.3		5.96		76	
Randomly Distributed Case 2		Determine effect of permeability distribution	5.2		360	[322 400]
Heterogeneous Case 3 with different lengths of heterogeneous areas	**Case 3.1**	Examine the impact of the size of the low permeability areas on average saturation.	5.2	1	360	10
	Case 3.2		5.2	5	360	10
	Case 3.3		5.2	10	360	10
Heterogeneous Case 4 with a low permeability area	**Case 4.1**	Examine the impact of the permeability of the low permeability area.	5.2	5	360	200
	Case 4.2		5.2	5	360	100
Heterogeneous Case 5 with a high permeability area	**Case 5.1**	Examine the impact of the permeability of the high permeability area.	5.2	5	360	500
	Case 5.2		5.2	5	360	700

4.1 Case Studies for the Modelling of Centrifuge Experiments

4.1.1 Homogeneous Case 1: 2D homogeneous case

The objective of Homogeneous Case 1 is to show that the new two-dimensional centrifuge simulation method is able to predict average phase saturation values and thus capillary pressure curves when the system reaches equilibrium.

In a homogeneous core, the permeability throughout the core is constant. To validate the numerical data generated from the centrifuge simulation with experimental data, three Homogeneous Cases are presented here matching the petrophysical properties of three different cores used in centrifuge experiments. The core plugs used in this case are shown in Figure 23. The cores used in Homogeneous Case 1.1 and Case 1.2 are both from Bay du Nord, offshore Newfoundland, Canada

and the core in Homogeneous Case 1.3 is a Berea core from the U.S. All three core plugs are homogeneous. The length and permeability of the digital models were determined as the same as that of the cores in centrifuge experiments. The wetting phase in the centrifuge simulation was set as water and the nonwetting phase was set as oil. The densities and viscosities of the fluids used in the simulation were measured in the laboratory. The pressure differences between inlet and outlet faces of the core are set to the same as the experimental capillary pressures from the centrifuge experiment.

Figure 23 Cores that are used for centrifuge experiments in Homogeneous Case 1

To demonstrate the application of the two-dimensional centrifuge simulation method for phase saturation prediction, three different digital core models with varying lengths, porosities and permeabilities were used in the simulations. Meanwhile, the properties of oil and brine were changed to show that this two-dimensional centrifuge simulation method is suitable for the displacements with fluids of different properties. The details of the parameters used in three Cases are shown in Table 9. In Homogeneous Case 1.1, to model a core plug with a diameter of 3.79 cm and a length of 5.2 cm. The two-dimensional digital model used in the simulation is the cross section of a cube and it is parallel to the fluid flow; however, the core plug is a cylinder in three

dimensions. Therefore, to keep the cross sectional of the simulated cube the same as that of a cylinder in direction that is perpendicular to the fluid flow, the length of the digital model in axial direction was set to be 5.2 cm and the length in radial direction was set to be 3.36 cm making them have the same cross-sectional areas. The permeability is isotropic and homogeneous and equal to 360 mD. In Homogeneous Case 1.2, the length of the digital model in axial direction was 4.94 cm and the length in radial direction was 3.20 cm. The permeability is equal to 440 mD. In Homogeneous Case 1.3, the length of the digital model in axial direction was 5.96 cm and the length in radial direction was 3.36 cm. The permeability is also isotropic and homogeneous that equals to 76 mD.

Table 9 Parameters for Homogeneous Case 1

Parameters	**Units**	**Values**		
		Case 1.1 (360mD)	**Case 1.2 (440mD)**	**Case 1.3 (76mD)**
Length	cm	5.200	4.940	5.960
Diameter	cm	3.790	3.620	3.790
Porosity	%	28.280	28.100	18.240
K	mD	360	440	76
Bulk Density	g/ml	2.001	1.892	2.051
Skeletal density	g/ml	2.605	2.631	2.585
Swir	frac.	0.058	0.028	0.400
Oil Viscosity	cP	5.900	5.900	6.000
Oil density	kg/m^3	858	858	878
brine viscosity	cP	1.010	1.010	1.100
brine density	kg/m^3	1040	1040	1010
Re	cm	22.100+length		
Ri	cm	22.100		
Radial Blocks		100	100	100
Axial Blocks		155	154	178
Block size	cm	0.034	0.032	0.034

Figure 24 shows the pressure distribution for a homogeneous core in the Homogeneous Case 1.1

when the pressure difference of the core is 4.116 bar. The pressure distribution was calculated by solving Equation 3.53 to 3.60 in Section 3.3.5 **(Step 7)** and the pressure decreases gradually from the inlet face (left side) to the outlet face (right side) of the core in the figure. The result makes sense because the constant pressure boundary condition was imposed on the digital model and the pressure at the inlet face is larger than the outlet face. Equation (3.64) to (3.79) in Section 3.3.6 **(Step 9)** were used to calculate corresponding time-of-flights for Homogeneous Case 1.1 as shown in Figure 25. The time-of-flights for fluid particles in grid blocks increase from the inlet face to the outlet face, which is reasonable because the time that a particle takes to travel along a streamline increases as the distance from the launching point becomes larger. Equation (3.80) and (3.81) in Section 3.3.6 **(Step 10)** were sued to plot the streamlines for Homogeneous Case 1.1 during centrifuge as shown in Figure 26. The streamlines are going straightly from the inlet face to the outlet face since no barrier (heterogeneous area) is present in the model. It is assumed that the core is homogeneous, so the streamlines only have one-dimensional flow, which is an ideal situation. Figure 27 shows the centrifuge displacement front and the saturation profile for a particular capillary pressure ($4.116\ bar$) for Homogeneous Case 1.1 by using Equation (3.92) to (3.107) in Section 3.4.2 (**Step 13**). In Figure (a), saturation value in each grid block was calculated and the average saturation for the digital model was obtained by dividing the summation of the saturation values for all grid blocks by the number of grid block. The black arrow in the figure represents the displacement direction during centrifuge. The nonwetting phase (red part) is displacing the wetting phase (blue part) out of the core, which is reasonable for this is a drainage process in the centrifuge experiment. In Figure (b), the water (wetting phase) saturations in the oil (nonwetting phase) zone

is much smaller than that in the water zone since water is displaced by oil and no displaceable water is left before the displacement front.

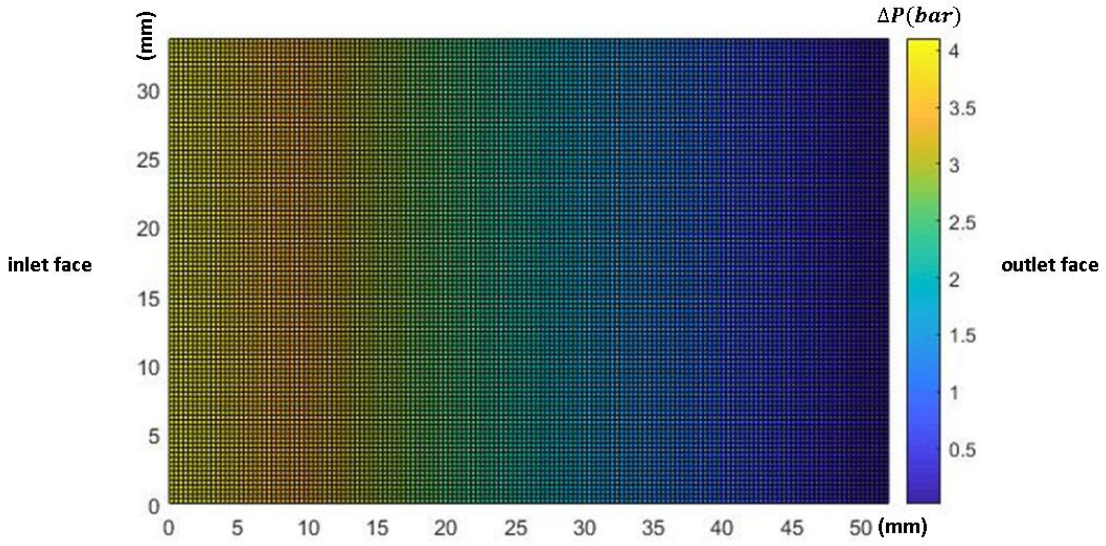

Figure 24 Pressure field for Homogeneous Case 1.1, a core with homogeneous permeability of 360mD from Bay du Nord

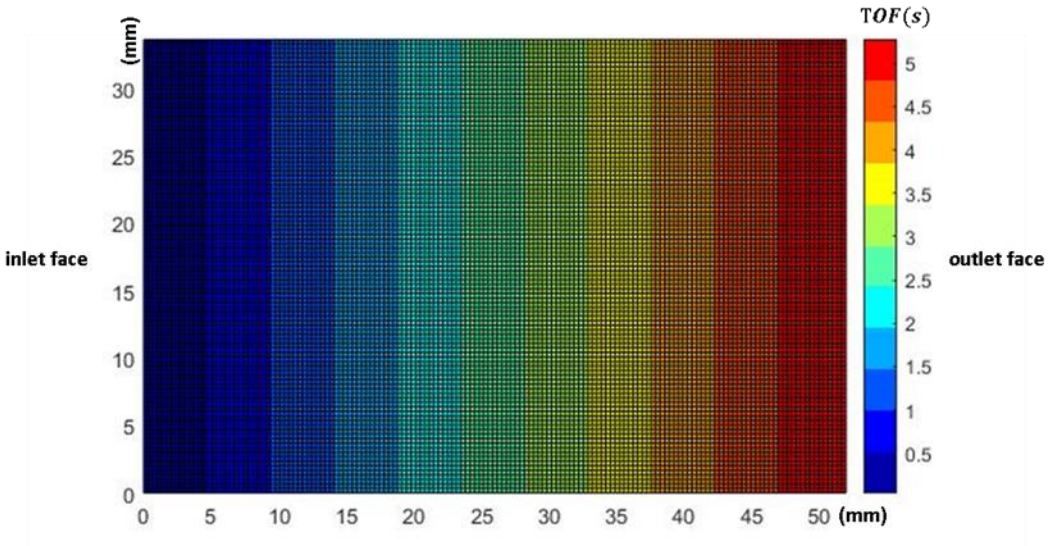

Figure 25 Time-of-flight for Homogeneous Case 1.1, a core with homogeneous permeability of 360mD from Bay du Nord

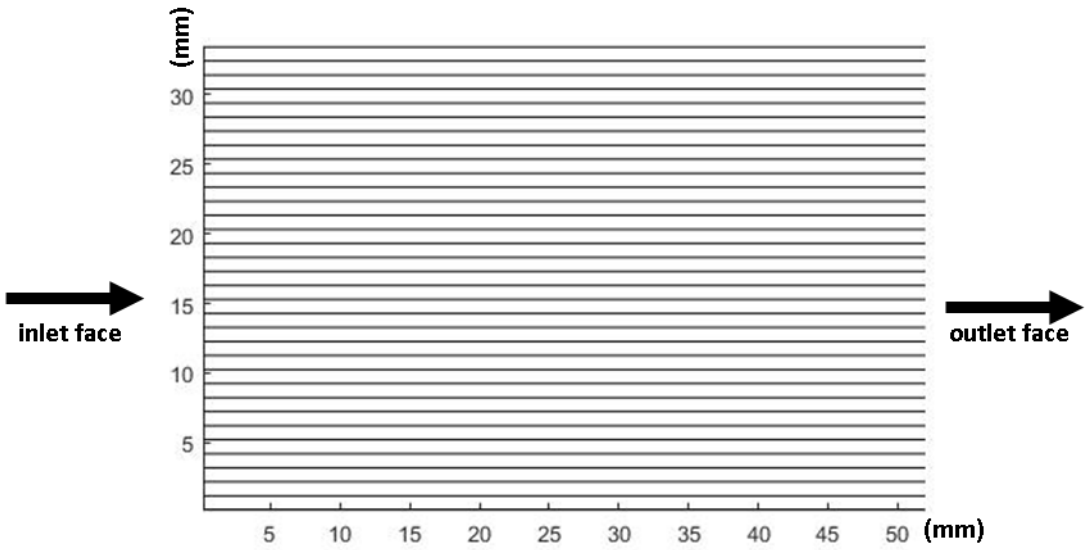

Figure 26 Streamlines for Homogeneous Case 1.1, a core with homogeneous permeability of 360mD from Bay du Nord

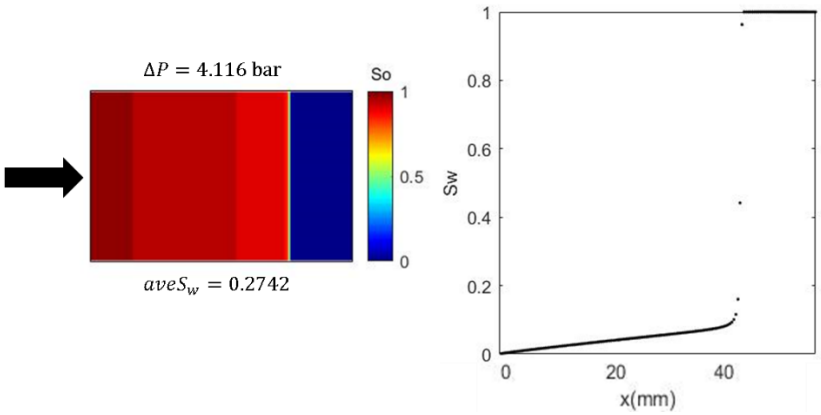

(a) (b)

Figure 27 Homogeneous Case 1.1when capillary pressure is 4.116 bar (a) two-phase displacement front, (b) water saturation distribution

To demonstrate the application of the two-dimensional centrifuge simulation method for phase saturation prediction, the numerical and experimental $aveS_w$ for Homogeneous Cases 1.1, 1.2 and 1.3 (three homogeneous digital models with varying properties) are shown in Table 10, 11 and 12, respectively. Pc was calculated based on the incremental rotational speed during centrifuge by using Equation (2.3) in Section 2.1.1. Experimental $aveS_w$ can be calculated based on the

displaced wetting phase volume measured from experiment by using Equation (2.1) in Section 2.1.1. Numerical $aveS_w$ can be predicted in the two-dimensional centrifuge simulation by using Equation (3.122) to (3.124) in Section 3.4.3 (**Step 14**). To validate the capability of the centrifuge simulation method to predict average phase saturations, the numerical $aveS_w$ were compared to the experimental values measured in the laboratory. The deviation of the simulated results is denoted as σ. The MSEs of all three simulations are no more than 6×10^{-4}, which is within an acceptable error range (Ruth, 1997). Among the three different core plugs, the Berea core from Case 1.3 has the best results with SSE equal to 0.0022 and MSE equal to 0.0003.

Table 10 Results of centrifuge simulation for Homogeneous Case 1.1, a core with homogeneous permeability of 360mD from Bay du Nord

Capillary pressure (bar)	**Flow rate (m^3/s)**	**Experimental aveSw (frac.)**	**Numerical aveSw (frac.)**	σ	σ^2
4.116	2.128E-07	0.304	0.274	0.030	0.0009
3.251	1.783E-07	0.350	0.326	0.024	0.0006
2.489	1.449E-07	0.400	0.383	0.018	0.0003
1.830	1.122E-07	0.451	0.438	0.013	0.0002
1.270	1.162E-07	0.705	0.671	0.034	0.0012
0.811	9.360E-08	0.811	0.791	0.020	0.0004
0.427	6.289E-08	0.908	0.876	0.032	0.0010
0.204	3.687E-08	0.965	0.935	0.030	0.0009
0.051	1.281E-08	1.000	1.000	0.000	0.0000
SSE: 0.0055					
MSE: 0.0006					

Table 11 Results of centrifuge simulation for Homogeneous Case 1.2, a core with homogeneous permeability of 440mD from Bay du Nord

Capillary pressure (bar)	**Flow rate (m^3/s)**	**Experimental aveSw (frac.)**	**Numerical aveSw (frac.)**	σ	σ^2
0.229	6.428E-07	0.123	0.103	0.020	0.0004
0.181	5.883E-07	0.131	0.117	0.014	0.0002

0.138	5.561E-07	0.191	0.168	0.023	0.0005
0.102	4.122E-07	0.449	0.428	0.021	0.0004
0.071	2.547E-07	0.654	0.622	0.032	0.0010
0.045	9.41E-08	0.809	0.782	0.028	0.0008
0.024	7.287E-08	0.914	0.887	0.027	0.0008
0.011	3.511E-08	0.961	0.942	0.019	0.0004
0.003	1.461E-08	1.000	1.000	0.000	0.0000
SSE: 0.0045					
MSE: 0.0005					

Table 12 Results of centrifuge simulation for Homogeneous Case 1.3, a Berea core with homogeneous permeability of 76mD

Capillary pressure (bar)	**Flow rate (m^3/s)**	**Experimental aveSw (frac.)**	**Numerical aveSw (frac.)**	σ	σ^2
1.848	4.528E-08	0.394	0.375	0.019	0.0003
1.357	3.288E-08	0.493	0.479	0.014	0.0002
0.944	1.329E-08	0.545	0.527	0.018	0.0003
0.603	9.46E-09	0.621	0.603	0.018	0.0003
0.340	5.217E-09	0.686	0.662	0.024	0.0006
0.152	2.876E-09	0.846	0.824	0.022	0.0005
0.038	1.582E-09	0.998	0.995	0.003	0.0000
SSE: 0.0022					
MSE: 0.0003					

Figure 28, 29 and 30 show the capillary pressure versus average saturation curves, $P_c(aveS_w)$ curves, and $P_c(inletS_w)$ curves for Homogeneous Cases 1.1, 1.2 and 1.3, respectively. Details for calculations are shown in Section 3.5. Experimental and numerical $P_c(aveS_w)$ curves were both obtained by fitting a modified hyperbolic function (Equation (3.4) in Section 3.2.1) on the P_c vs $experimenal/numerical\ aveS_w$ data points. Experimental and numerical $P_c(inletS_w)$ curves, known as capillary pressure curve, were obtained using Forbes-Splines method (Equation (3.5) to (3.33) in Section 3.2.2). The numerical $aveS_w$ points are at the same Pc as the experimental $aveS_w$ points since the experimental Pc points are considered as the inputs for the two-dimensional

centrifuge simulation. The experimental and numerical $P_c(inletS_w)$ curves converge at both saturation ends because they have the same irreducible water saturation value. It can be observed that there is deviation between numerical and experimental curves ($P_c(aveS_w)$ curves and $P_c(inletS_w)$ curves) in the middle saturations. This is reasonable because there may be some experimental deviations in the centrifuge experiments. For example, the measurements of spin rate and produced volumes of fluids, core porosity and dimensions and fluid densities may not be accurate. An operator may also have a false estimation of the time that the system takes to reach equilibrium. The numerical curves are close to the experimental curves and they successfully model the trends and characteristics of the experimental curves. Thus, it is reasonable to use the two-dimensional centrifuge simulation method introduced in this thesis to model centrifuge experiments for capillary pressure measurements. The numerical $aveS_w$ computed during the simulation are in a good agreement with the experimental $aveS_w$. The numerical $P_c(inletS_w)$ curves plotted from the Forbes-Splines method also indicate a good reliability of forecast for capillary pressures.

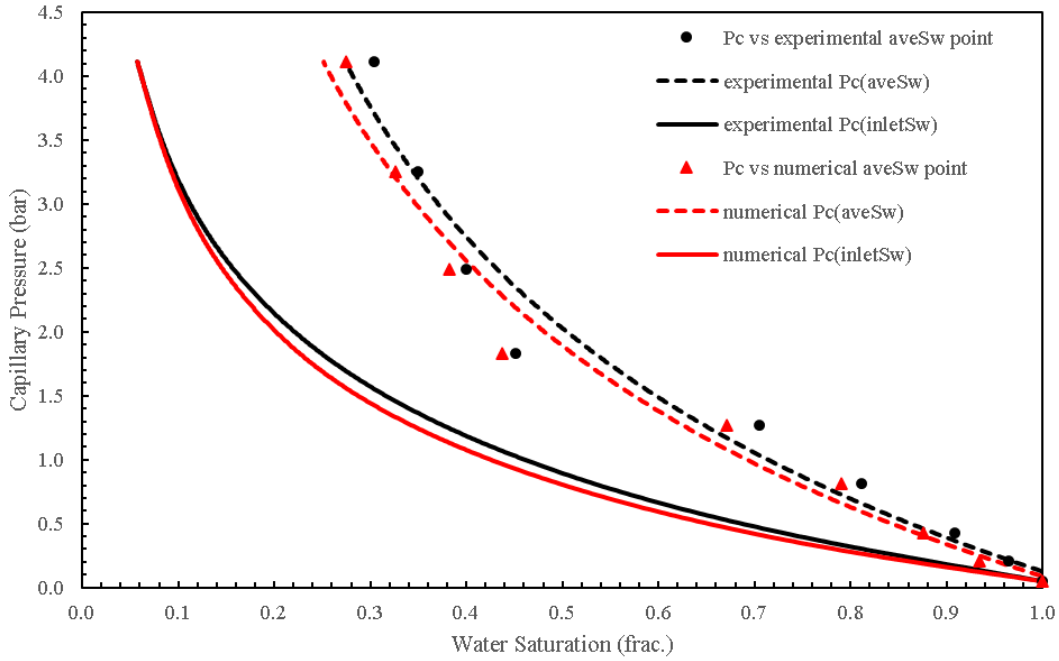

Figure 28 Numerical and experimental curves for Homogeneous Case 1.1, a core with homogeneous permeability of 360mD from Bay du Nord

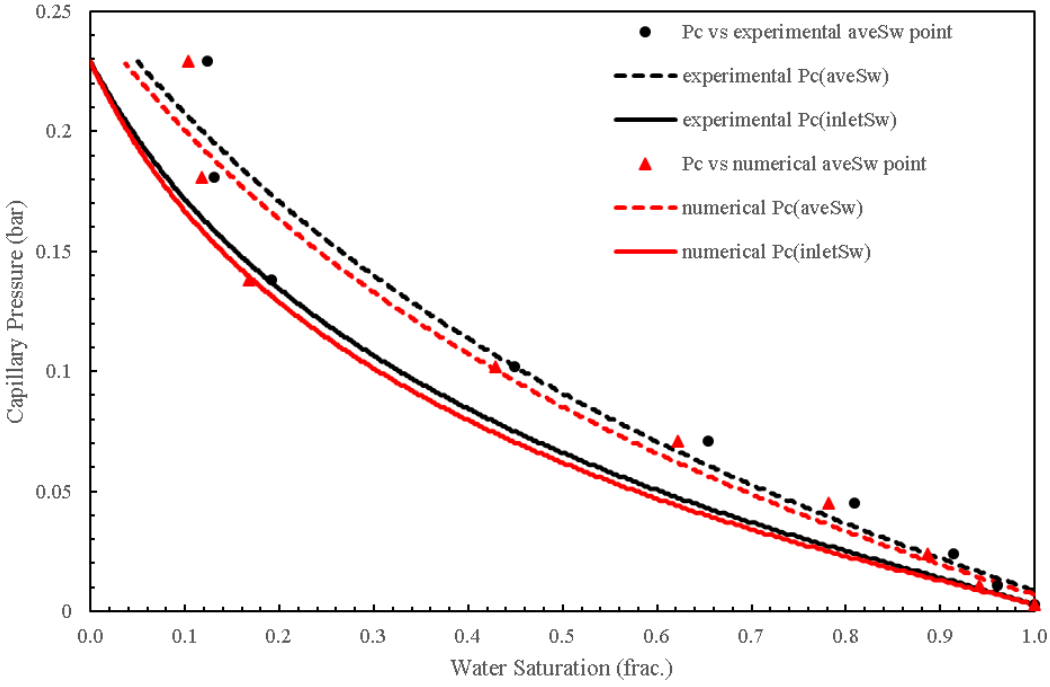

Figure 29 Numerical and experimental curves for Homogeneous Case 1.2, a core with homogeneous permeability of 440mD from Bay du Nord

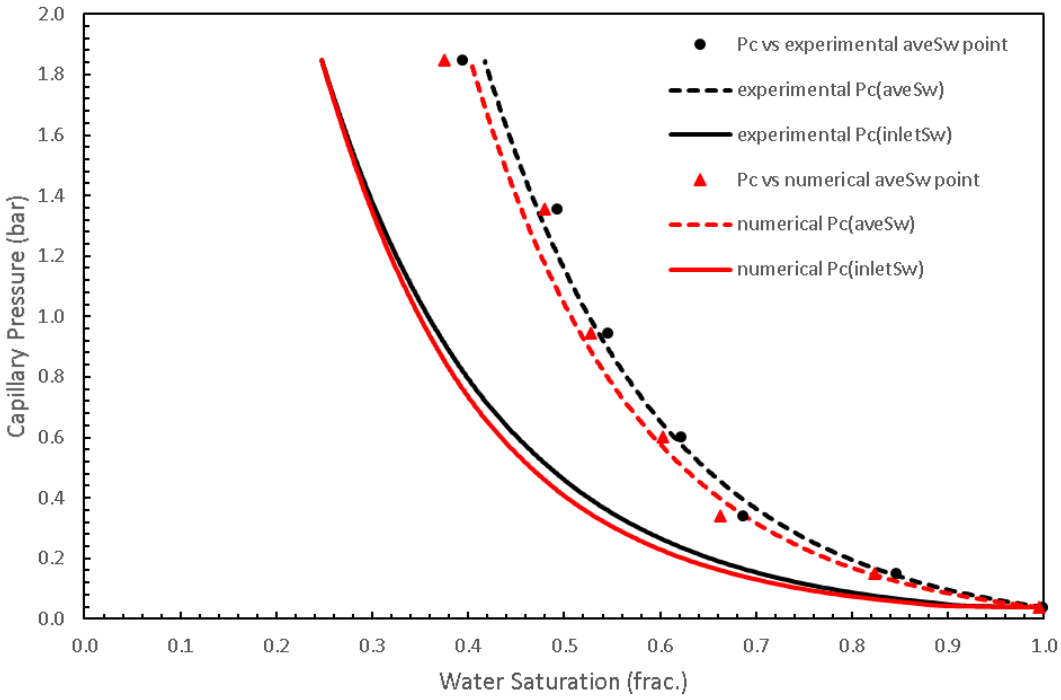

Figure 30 Numerical and experimental curves for Homogeneous Case 1.3, a Berea core with homogeneous permeability of 76mD

4.1.2 Randomly Distribute Case 2: 2D case with a randomly distributed permeability field

The objective of this case is to study the effects of heterogeneity generated by a Gaussian random field on fluid flow, phase saturations and capillary pressure curves.

In this case, the permeability distribution is as depicted in Figure 31 and 32. The mean permeability for a permeability field generated by a Gaussian random field can be determined by using Equation (3.41) to (3.43) in Section 3.3.3. The permeability is normally distributed ranging from 322 mD to 400 mD, while mean permeability is kept as the same as the homogeneous Case 1.1 (360 mD). All the other parameters have been kept as the same as the homogeneous Case 1.1. The pressure differences depend on the measured rotational speed (capillary pressure) from the centrifuge experiment.

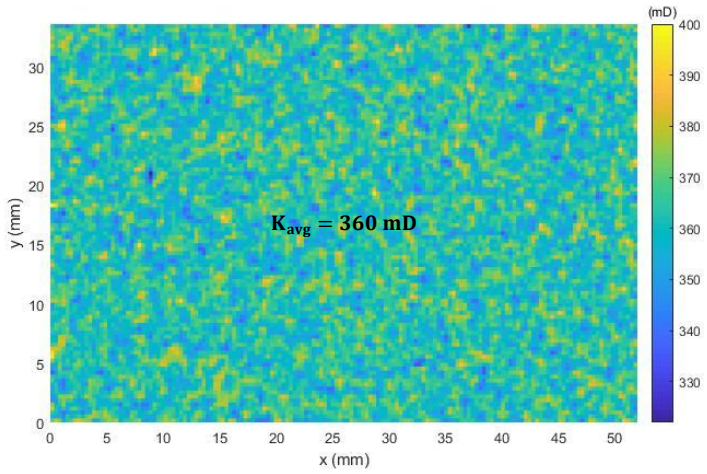

Figure 31 Permeability distribution for Randomly Distributed Case 2

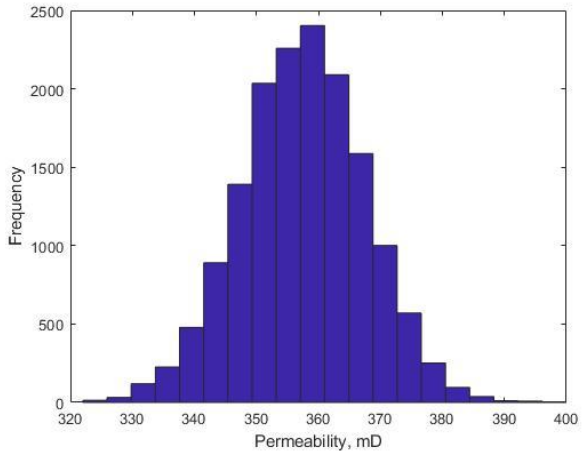

Figure 32 The histogram of the permeability distribution for Randomly Distributed Case 2

Figure 33 shows the time-of-flights calculated by Equation (3.64) and (3.79) in Section 3.3.6 (**Step 9**). The time-of-flights decrease from the inlet face to the outlet face even with some heterogeneity in the digital model. This is reasonable since the time that a particle takes to travel along a streamline has a positive correlation with the distance from the launching point. The calculated time-of-flights have the similar distributing pattern as the Homogeneous Case 1.1 since the standard deviation of the Gaussian flied is small and distribution of permeability can be regarded as homogeneous. Figure 34 shows the streamlines in the core calculated by Equation (3.80) and

(3.81) in Section 3.3.6 (**Step 10)** for Randomly Distributed Case 2. Even though the streamlines fluctuate in some regions, the overall movement of the fluids can be considered as a one-dimension flow under constant differential pressure boundary condition. This is because the influences of randomly distributed permeabilities on streamlines are not significant. Figure 35 shows the high flow and stagnant regions for Randomly Distributed Case 2 calculated in **Step 11**. It can be seen that the movement of the fluid particle may be deterred in the vertical direction other than the horizontal direction. It indicates that the fluid flow under the randomly distributed permeability field can also be considered as the steady state flow as compared to the fully homogeneous permeability field. Based on the above results, the heterogeneity in the radial direction can be ignored because it does not influence the fluid in axial direction. Part (a) of Figure 36 shows the centrifuge displacement front and part (b) shows the saturation profile calculated by Equation (3.92) to (3.107) in Section 3.4.2 (**Step 13**) when the capillary pressure is 4.116 bar for Randomly Distributed Case 2. The results of Figure 36 are almost identical to the results of Figure 27. Thus, the effects of randomly distributed permeability field on the fluid flow are negligible since the permeability distribution can be considered as homogeneous.

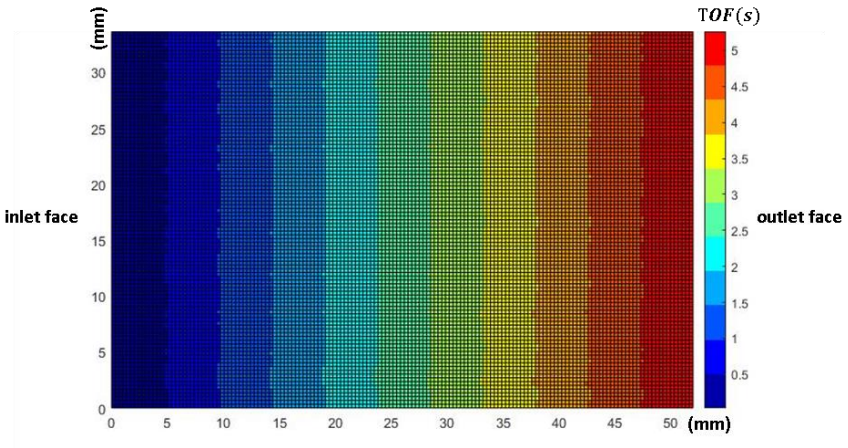

Figure 33 Time-of-flight for Randomly Distributed Case 2

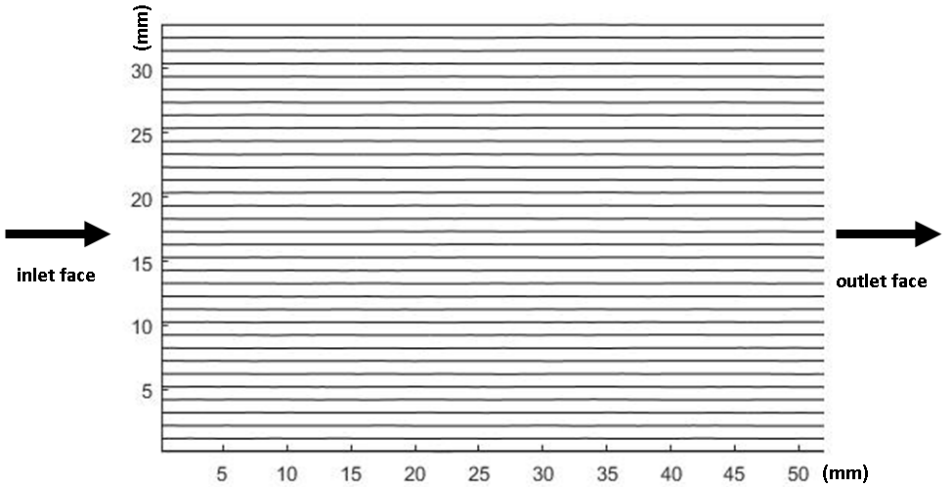

Figure 34 Streamlines for Randomly Distributed Case 2

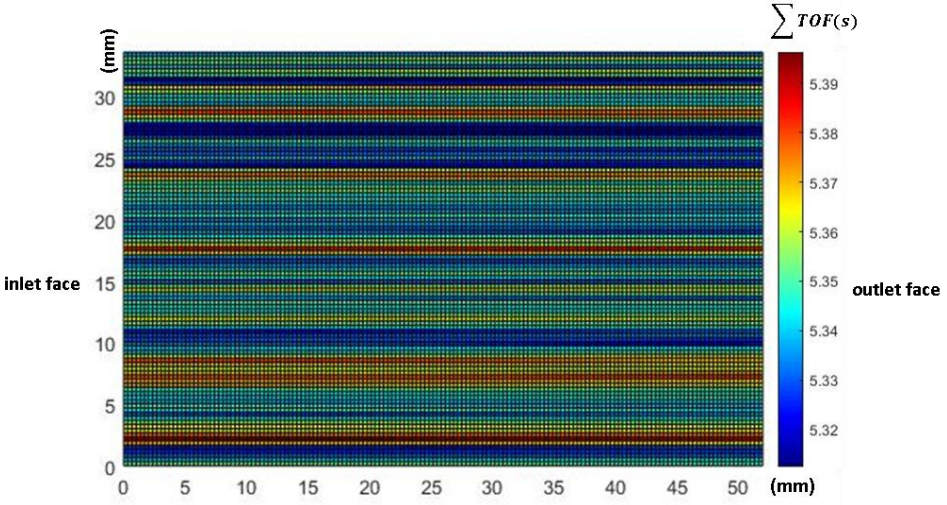

Figure 35 High flow and stagnant regions for Randomly Distributed Case 2

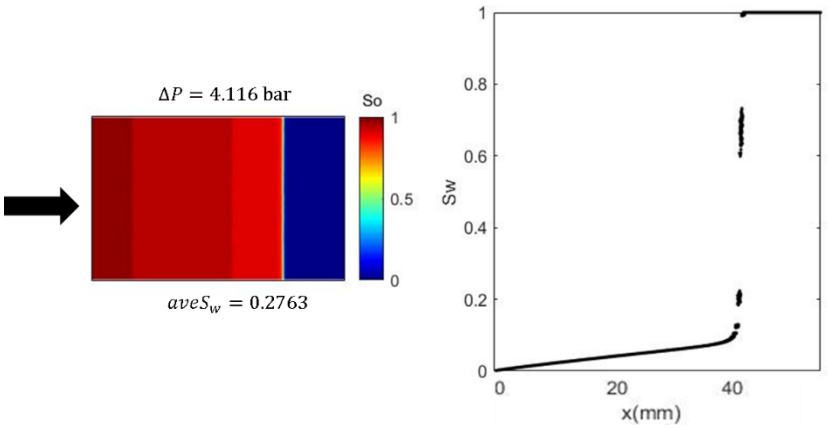

(a) (b)

Figure 36 Randomly Distributed Case 2 when capillary pressure is 4.116 bar (a) two-phase displacement front, (b) water saturation distribution

Table 13 gives a comparison of simulation results between Randomly Distributed Case 2 and Homogeneous Case 1.1 calculated in **Step 14**. Equations that were used to calculate the phase saturations and capillary pressures are introduced in Section 4.1.1. The SSE and MSE are rather small, which means the differences between the numerical average water saturations under the Gaussian random permeability field and the average water saturations under the homogeneous permeability field are marginal. This is due to the fact that the influences of the heterogeneity generated from the Gaussian random field on average phase saturations can be ignored. It is known that extracted cores from reservoirs are mostly heterogeneous in permeability distributions; therefore, it is more practical and realistic to use geostatistical methods to make realizations of permeability in simulations (Lie, 2019). In this case, a Gaussian random field is superior to a homogeneous field in the representation of the permeability field in the modelling of centrifuge experiments (Shikhov and Arns, 2015). The average permeability of the randomly distributed field

has been set to be the same as the homogeneous field. In the following cases, the randomly distributed permeability fields have been applied in the matrices of the cores except for the heterogeneous areas.

Table 13 Comparisons of simulation results for Homogeneous Case 1.1 and Randomly Distributed Case 2

Capillary pressure (bar)	**aveSw for Homogeneous Case 1.1 (frac.)**	**aveSw for Randomly Distributed Case 2 (frac.)**	σ	σ^2
4.116	0.274	0.272	2.40E-03	5.76E-06
3.251	0.326	0.324	2.00E-03	4.00E-06
2.489	0.383	0.381	1.30E-03	1.69E-06
1.83	0.438	0.436	2.30E-03	5.29E-06
1.27	0.671	0.671	-3.00E-04	9.00E-08
0.811	0.791	0.790	8.00E-04	6.40E-07
0.427	0.876	0.875	6.00E-04	3.60E-07
0.204	0.935	0.934	3.00E-04	9.00E-08
0.051	1.000	1.000	0	0
SSE: 1.79E-05				
MSE: 1.99E-06				

Figure 37 shows $P_c(aveS_w)$ curves and $P_c(inletS_w)$ curves for Homogeneous Case 1.1 and Randomly Distributed Case 2. The equations that were used to calculate numerical $aveS_w$ curves and Pc curves are introduced in Section 4.1.1. It is noted that the curves, $P_c(aveS_w)$ curves and $P_c(inletS_w)$ curves, for Randomly Distributed Case 2 overlap the curves for Homogeneous Case 1.1 owing to the fact that the effects of the heterogeneity produced from the Gaussian random field on average phase saturations are marginal. Thus, it is proved that the Randomly Distributed Case 2 can produce equivalent $P_c(aveS_w)$ and $P_c(inletS_w)$ curves as the Homogeneous Case 1.1.

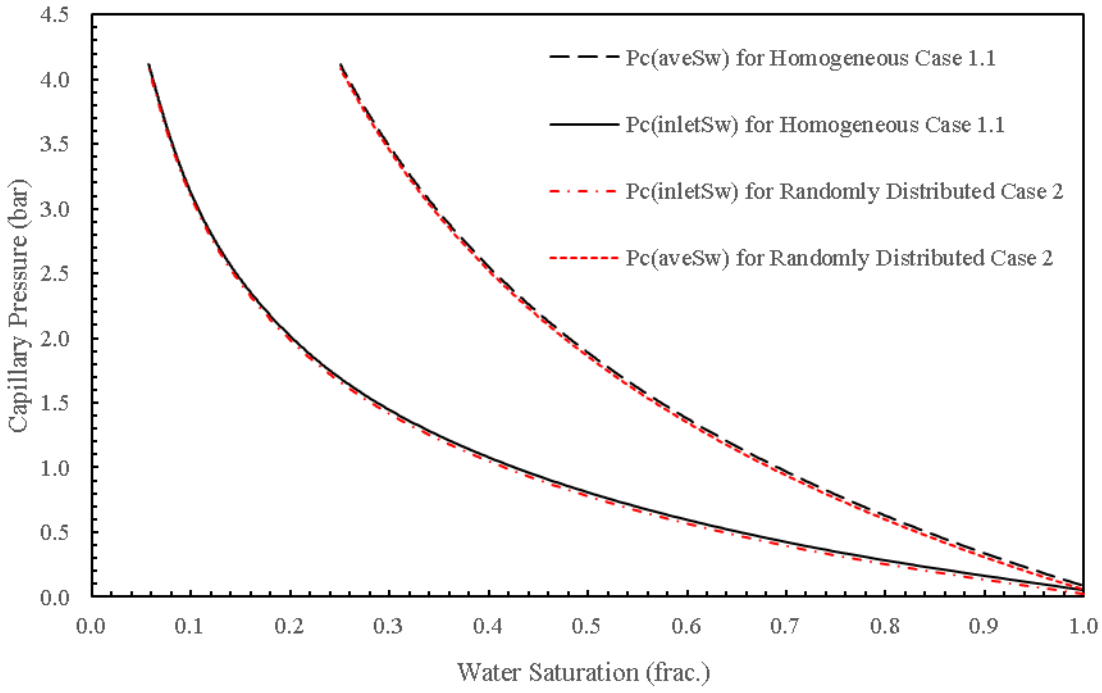

Figure 37 Pc ($aveS_w$) curves and Pc ($inletS_w$) curves for Homogeneous Case 1.1 and Randomly Distributed Case 2, the average permeability of the core is 360mD

4.1.3 Heterogeneous Case 3: 2D heterogeneous case with different lengths of heterogeneous areas

The objective of this case is to investigate the effects of the lengths of heterogeneous areas on fluid flow, phase saturations and capillary pressure curves from centrifuge.

Three Cases are shown here with different values of the lengths of heterogeneous areas. The heterogeneous area is considered as a square with four sides of equal length. The lengths of the heterogeneous areas in three Cases have been set to be $1, 5, 10$ mm respectively. The detailed parameters of the heterogeneous areas are shown in Table 14 and the other parameters in the simulation, such as the length and the diameter of the core, viscosities and densities of the fluids, are the same as that of the Randomly Distributed Case 2. As shown previously in Table 9, 155 grid

blocks are used in axial direction and 100 grid blocks are used in radial direction for simulation. These grid blocks are then numbered accordingly, and the heterogeneous area is placed in the center of the digital model both in axial and radial direction. The permeability distributions for three Cases are shown in Figure 38, 39 and 40, respectively. The permeability of the heterogeneity in the core plug is 10 mD and the mean permeability of the core plug still ranges from 322 mD to 400 mD. The equations that were used to calculate mean permeability of a heterogeneous model are introduced in Section 4.1.2.

Table 14 Parameters for the heterogeneous areas used in Heterogeneous Case 3

No. of case	**Length of heterogeneous area (mm)**	**Number of grid blocks**	**Radial Blocks with Low Permeability**	**Axial Blocks with Low Permeability**	**Permeability of heterogeneous area （mD)**
3.1	1	30	49-52	76-79	10
3.2	5	149	43-58	70-85	10
3.3	10	298	35-65	63-93	10

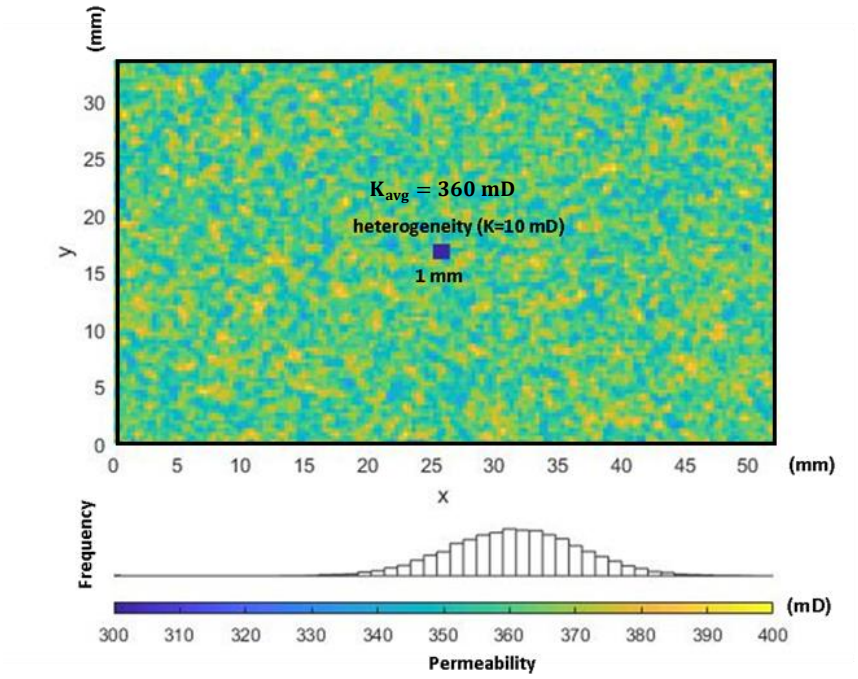

Figure 38 Permeability distribution for Case 3.1 with a heterogeneous area (1mm)

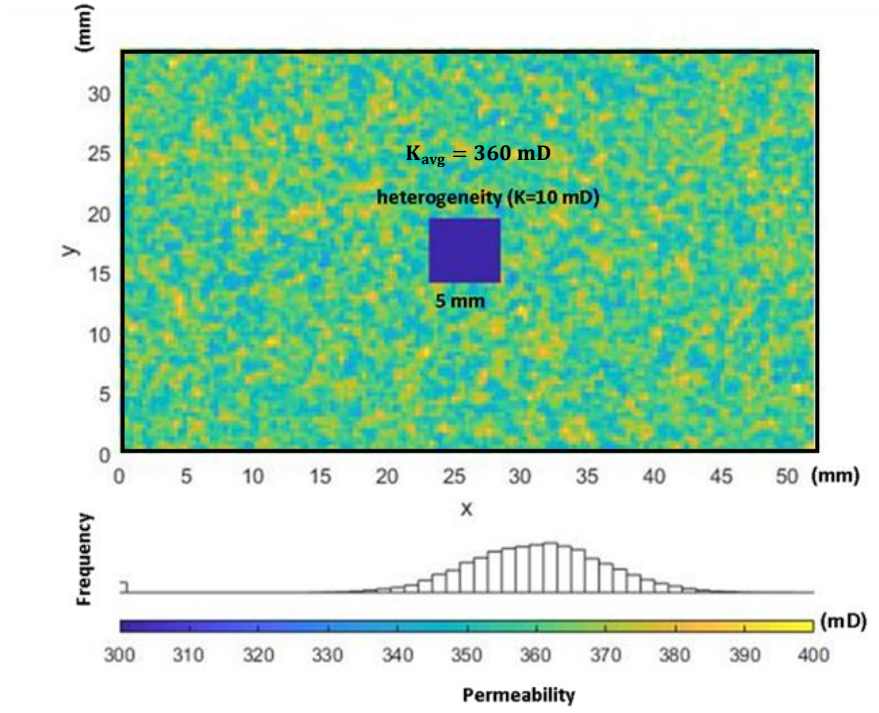

Figure 39 Permeability distribution for Case 3.2 with a heterogeneous area (5mm)

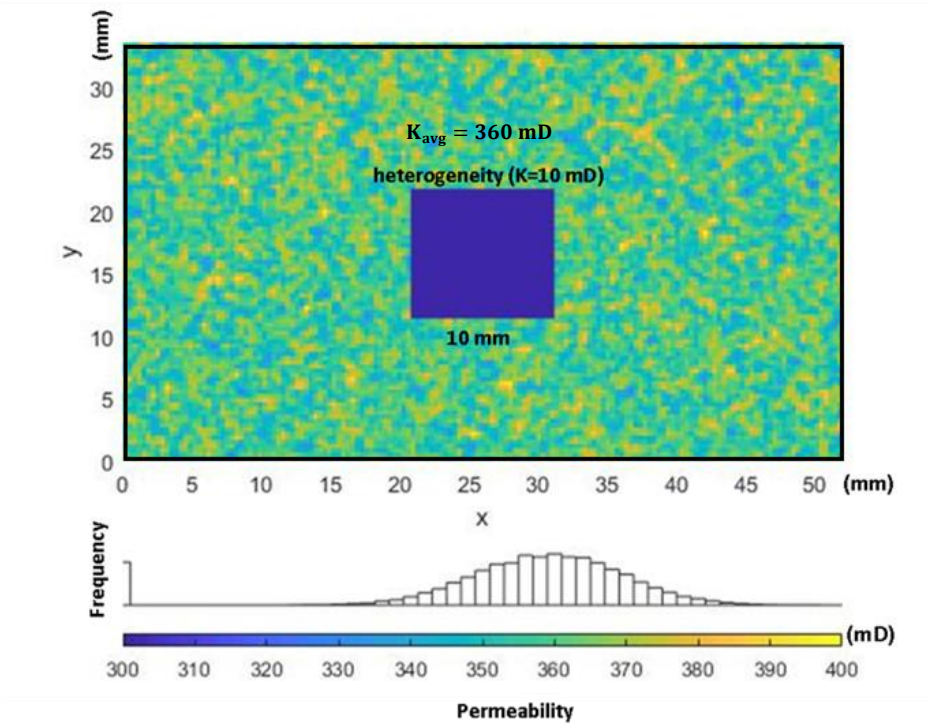

Figure 40 Permeability distribution for Case 3.3 with a heterogeneous area (10mm)

Figure 41 displays calculated time-of-flights for three Cases with different lengths of the heterogeneous areas by using Equation (3.64) and (3.79) in Section 3.3.6 (**Step 9**). The time-of-flights increase dramatically in the heterogeneous area because the movements of fluid particles are deterred in the area with low permeability value. As the heterogeneous area grows bigger, the area with larger time-of-flights becomes bigger since a grid block with low permeability makes the travel time of a fluid particle become longer. Figure 42 shows the corresponding streamlines by using Equation (3.80) and (3.81) in Section 3.3.6 (**Step 10**). From part (a) to part (c) of the figure, streamlines that are hindered in the center increase since the no flow area decreases. Streamlines around the larger stagnant region tend to have more displacement in radial direction, which is a two-dimensional fluid flow. Figure 43 shows the high flow and stagnant regions for three Cases by calculating $\sum TOF$ in **Step 11**. The corresponding stagnant regions will grow larger when it comes

to bigger heterogeneous areas. Apparently, larger heterogeneous area will have much more impact on the fluid flow.

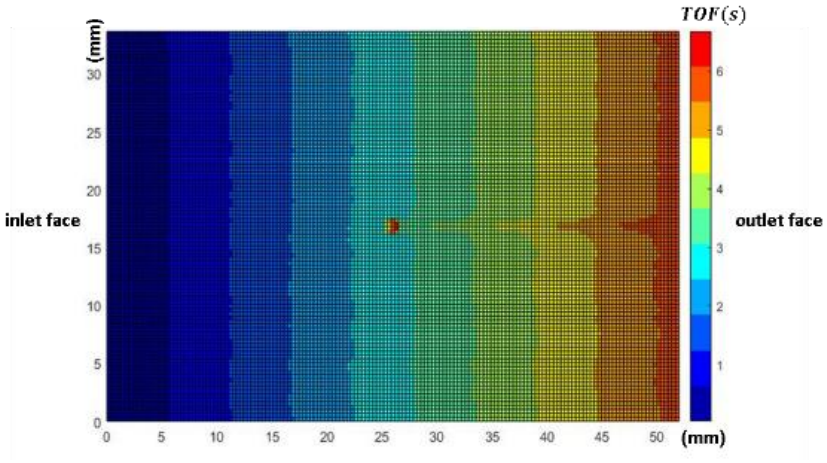

(a)

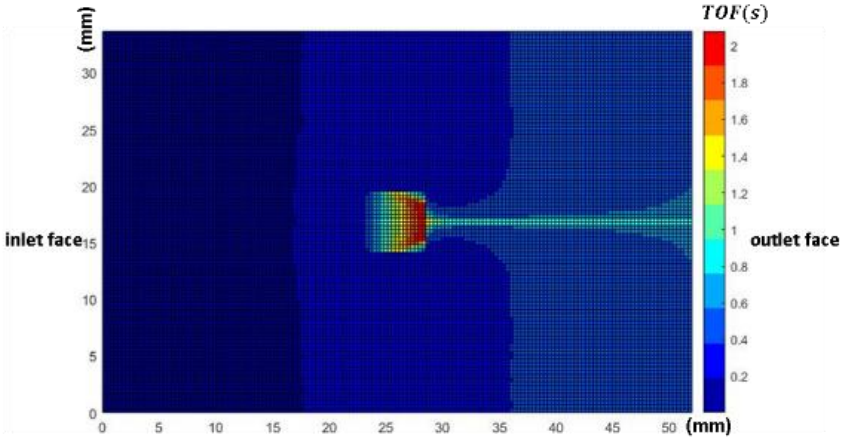

(b)

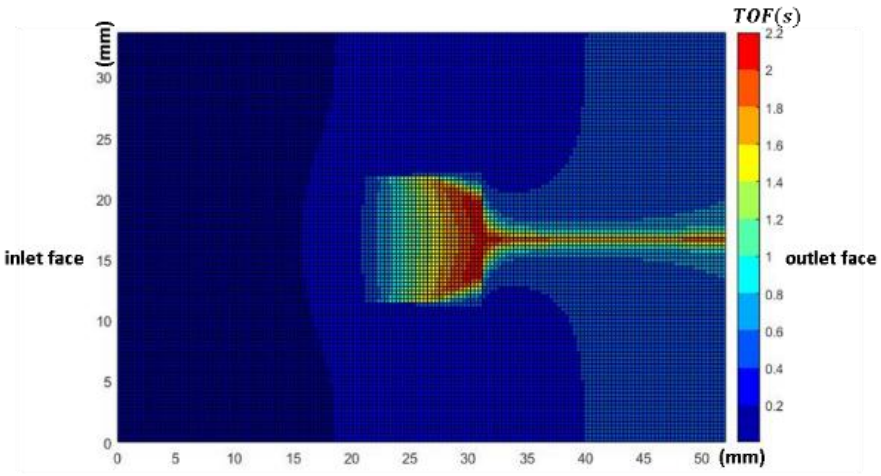

(c)

Figure 41 Time-of-flights for a) Case 3.1 with a heterogeneous area (1mm), (b) Case 3.2 with a heterogeneous area (5mm), (c) Case 3.3 with a heterogeneous area (10mm)

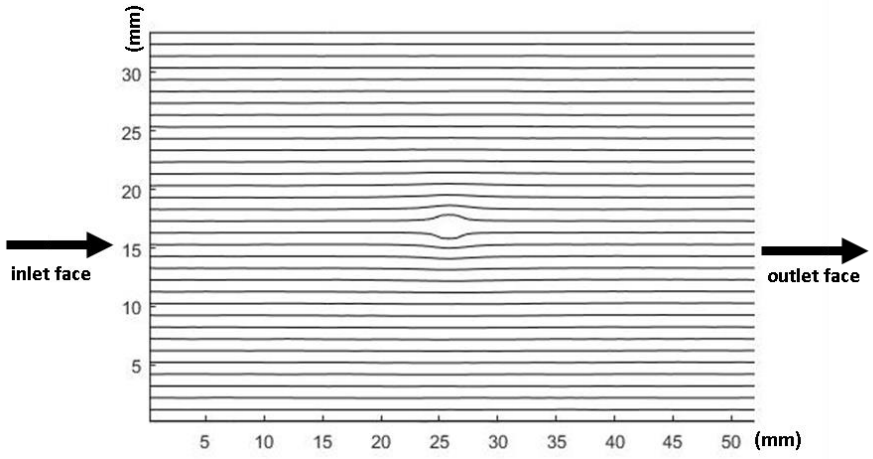

(a)

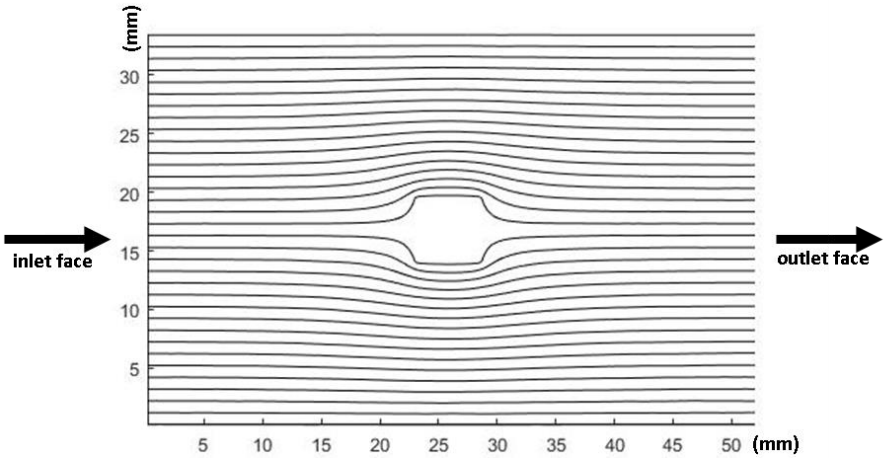

(b)

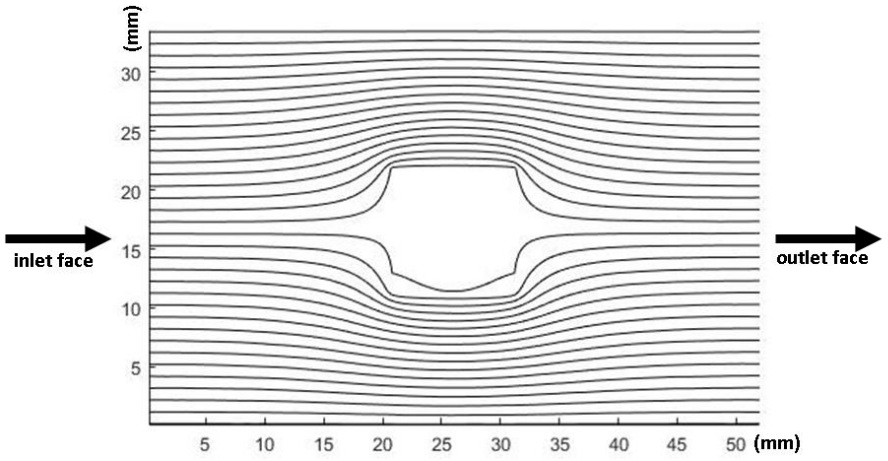

(c)

Figure 42 Streamlines for a) Case 3.1 with a heterogeneous area (1mm), (b) Case 3.2 with a heterogeneous area (5mm), (c) Case 3.3 with a heterogeneous area (10mm)

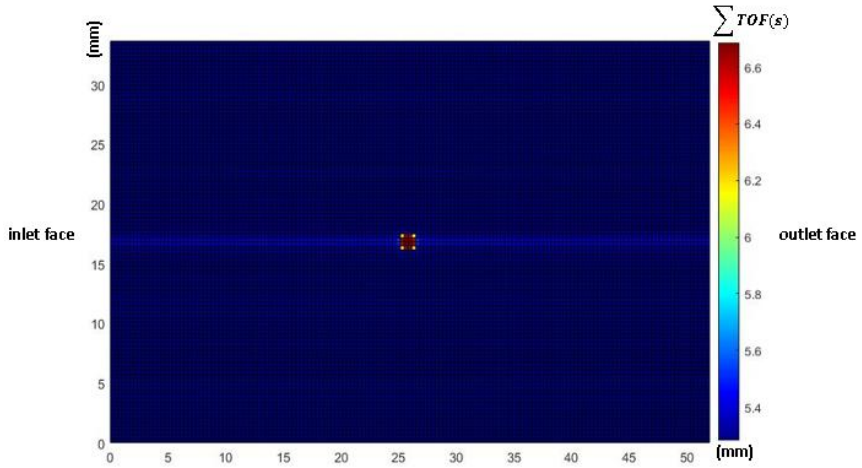
∑TOF(s)
(mm)
inlet face
outlet face
(mm)

(a)

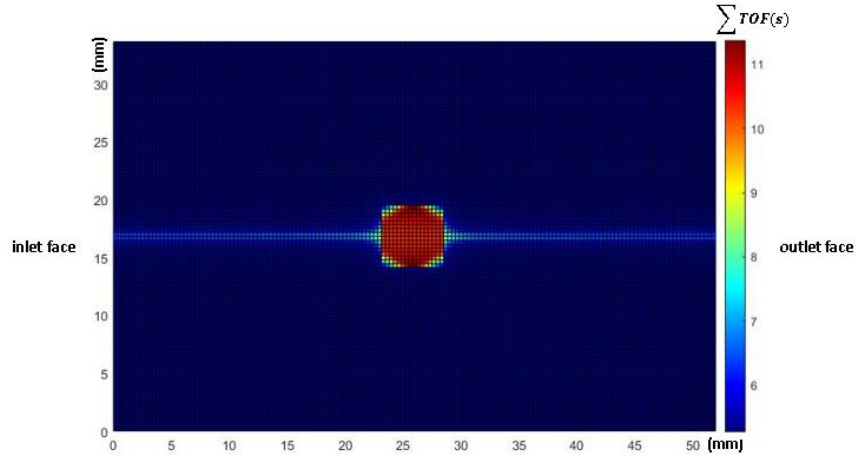
∑TOF(s)
(mm)
inlet face
outlet face
(mm)

(b)

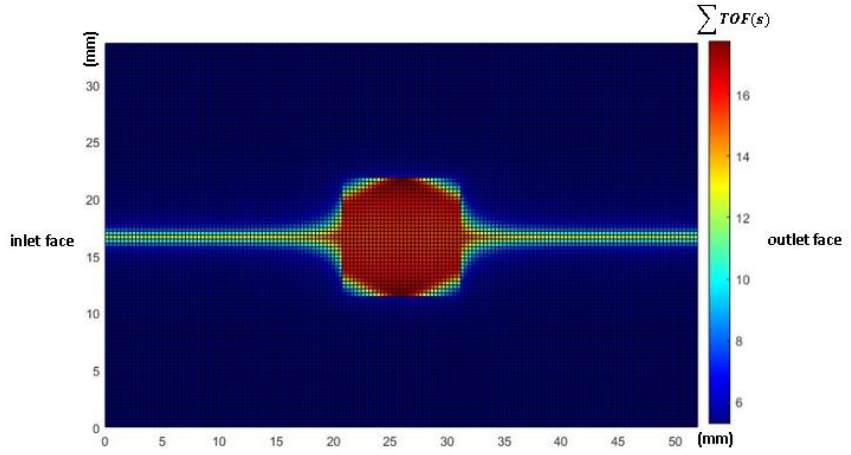
∑TOF(s)
(mm)
inlet face
outlet face
(mm)

(c)

Figure 43 High flow and stagnant regions for (a) Case 3.1 with a heterogeneous area (1mm), (b) Case 3.2 with a heterogeneous area (5mm), (c) Case 3.3 with a heterogeneous area (10mm)

Table 15 compares the simulation results of Heterogeneous Case 3 with Randomly Distributed Case 2 calculated in **Step 14**, which can show the deviation from the case with no heterogeneous areas. The equations that are used to calculate $aveS_w$ and Pc are introduced in Section 4.1.1. The SSEs of these three simulations range from 3.4×10^{-5} to 1.44×10^{-2} and the MSEs range from 3.8×10^{-6} to 1.3×10^{-3}. The $aveS_w$ for the Case with a bigger heterogeneous area (no flow area) is larger than that for the Case with a smaller heterogeneous area at same capillary pressure. This is reasonable since more water are retained in the digital model instead of being displaced by oil if the area of no flow region becomes grows larger.

Table 15 Comparisons of simulation results for Heterogeneous Case 3 and Randomly Distributed Case 2

Capillary pressure (bar)	**aveSw for Randomly Distributed Case 2 (frac.)**	**aveSw for Heterogeneous Case**			**σ^2**		
		Case 3.1 (1 mm)	**Case 3.2 (5 mm)**	**Case 3.3 (10 mm)**	**Case 3.1 (1 mm)**	**Case 3.2 (5 mm)**	**Case 3.3 (10 mm)**
4.116	0.272	0.275	0.292	0.334	8.410E-06	0.0004	0.0035
3.251	0.324	0.326	0.337	0.376	4.000E-06	0.0002	0.0025
2.489	0.381	0.383	0.395	0.431	1.690E-06	0.0002	0.0023
1.830	0.436	0.436	0.450	0.475	1.000E-08	0.0002	0.0016
1.270	0.671	0.676	0.685	0.698	1.764E-05	0.0002	0.0005
0.811	0.790	0.790	0.804	0.812	4.000E-08	0.0002	0.0005
0.427	0.875	0.876	0.889	0.894	6.400E-07	0.0002	0.0003
0.204	0.934	0.936	0.946	0.951	1.960E-06	0.0001	0.0002
0.051	1.000	1.000	1.000	1.000	0.0000	0.0000	0.0000
SSE:					3.439E-05	0.0017	0.0114
MSE:					3.821E-06	0.0002	0.0013

Figure 44 shows the corresponding $P_c(aveSw)$ curves and $P_c(aveS_w)$ curves. The equations that used for calculation are introduced in Section 4.1.1. When the heterogenous area (no flow area) grows bigger, higher water saturation can be obtained at same capillary pressure value. This is due

to the fact that a bigger heterogeneous area can retain more wetting phase (water) in the core; therefore, less wetting phase is produced. Lower numerical average phase saturations can be calculated from centrifuge simulations that only consider one-dimensional flow, which contributes to a negative bias of the interpreted capillary pressure curve as compared to the accurate capillary pressure. According to the comparison, it is known that if the low permeability area is small, its impact on the produced fluids and capillary pressure curves can be neglected ($\mathrm{MSE} = 3.821 \times 10^{-6}$*)*. As the heterogeneous area grows larger, its influence on capillary pressure curves becomes significant. Therefore, to investigate influences of the permeability in the heterogeneous area on fluid flow and capillary pressure curves, the length of the heterogeneous area can be taken as $5\ \mathrm{mm}$. The centrifuge simulations in the following cases have been conducted assuming a heterogeneous area with a length of $5\mathrm{mm}$.

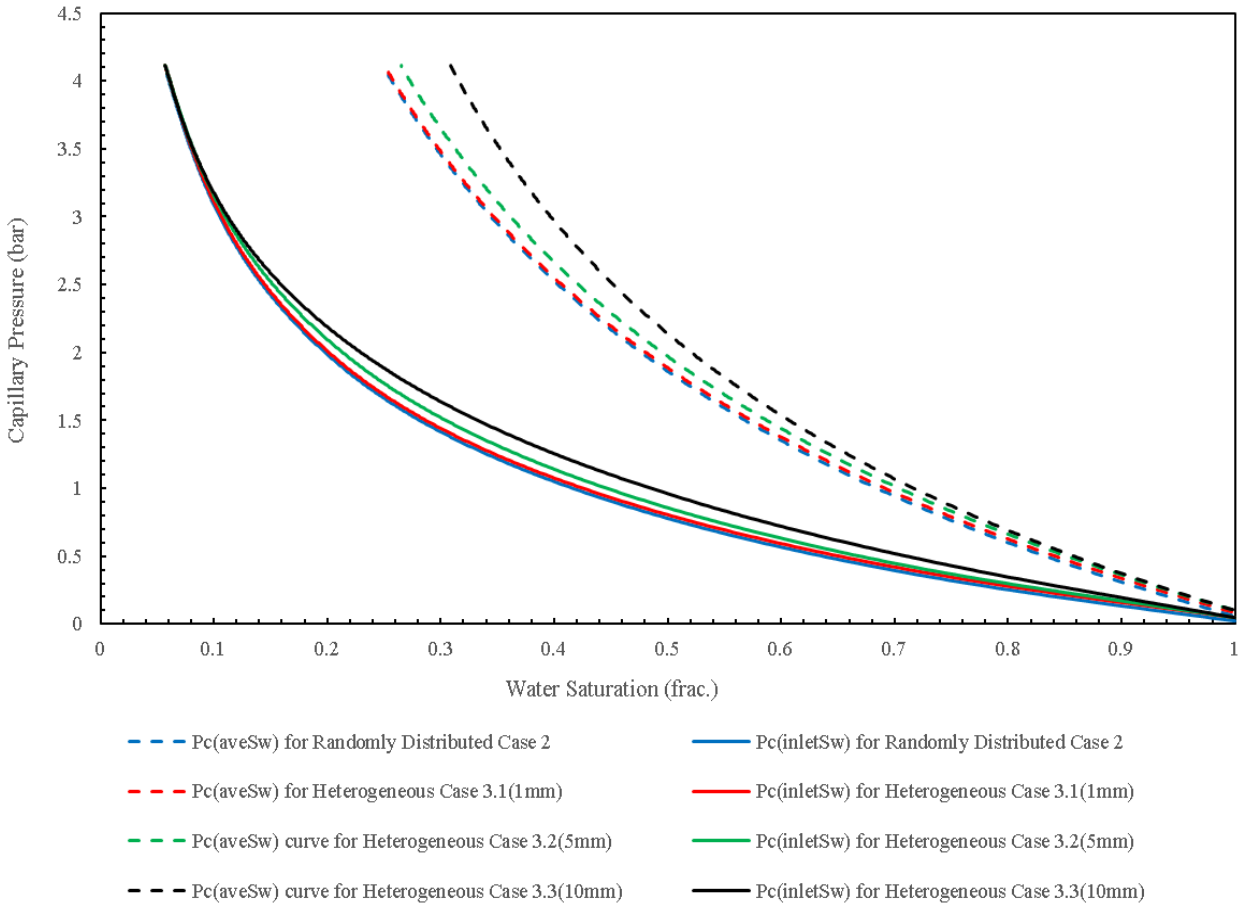

Figure 44 Pc ($aveS_w$) curves and Pc ($inletS_w$) curves for Heterogeneous Case 3.1(1mm), 3.2(5mm) and 3.3(10mm), the average permeability of the core is 360mD

4.1.4 Heterogeneous Case 4: 2D heterogeneous case with a low permeability area

The objective of this case is to study how low permeability value in the heterogeneous area will affect the fluid flow, phase saturation and capillary pressure curves from centrifuge.

Heterogeneities often exist in cores extracted from oil fields. It is very difficult to have a full understanding of the permeability distribution of an extracted core without using the tomography technique. Even though the heterogeneity distribution is known, the method to model it in a numerical model will be very complex. Therefore, an area of low permeability with a length of

5 mm is assumed to be placed in the center of the core in Heterogeneous Case 4. In Heterogeneous Case 4.1 the ratio of permeabilities between the heterogeneity and the matrix is approximately 5/9, and in Heterogeneous Case 4.2 the ratio is approximately 5/18. To make the Heterogeneous Cases comparable with the Randomly Distributed Case 2, mean permeabilities of all the cases were set to be the same. The petrophysical properties of the numerical models used in the two Cases remained unchanged other than the permeability distributions. Detailed parameters used are shown in Table 16 and the permeability field is shown in Figure 45. The blue region represents the low permeability area and the permeability in other areas is distributed randomly with a mean permeability as 360 mD.

Table 16 Parameters used for Heterogeneous Case 4 with a low permeability area

Parameters	**Units**	**Values**	
		Case 4.1	**Case 4.2**
Radial Blocks		100	100
Axial Blocks		155	155
Block size	cm	0.034	
Radial Blocks with Low Permeability		43-58	43-58
Axial Blocks with Low Permeability		70-85	70-85
Permeability of heterogeneity	mD	200	100
Mean permeability	mD	360	360

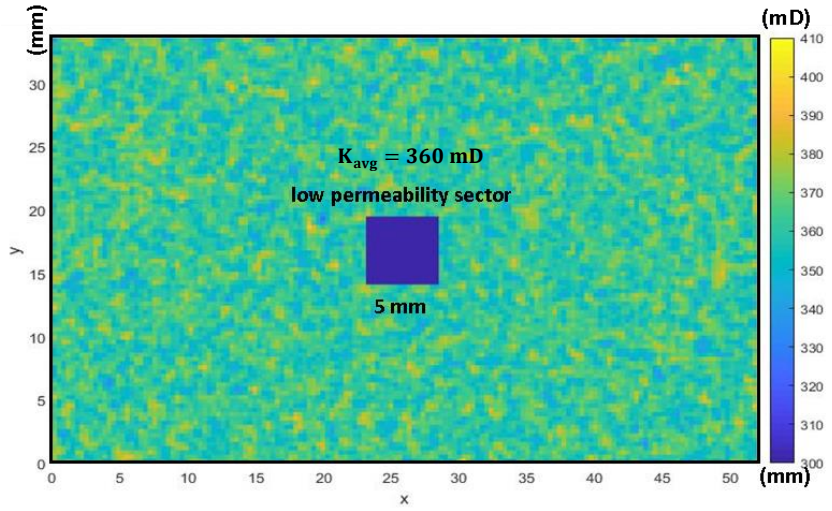

Figure 45 Permeability distribution for Heterogeneous Case 4 with a low permeability area

Figure 46 shows the centrifuge displacement front and the saturation profile when the capillary pressure is 4.116 bar for Heterogeneous Case 4.1 with a low permeability area calculated in **Step 13**. The equations that were used for calculation are introduced in Section 4.1.1. In part (a), The displacement front is curved in the center as opposite to the displacing direction since less wetting phase (water) is displaced in the heterogeneous area (no flow area). In part (b), the water saturations are distributed more dispersedly in the front as compared to part (b) of Figure 36 for the existence of the low permeability area.

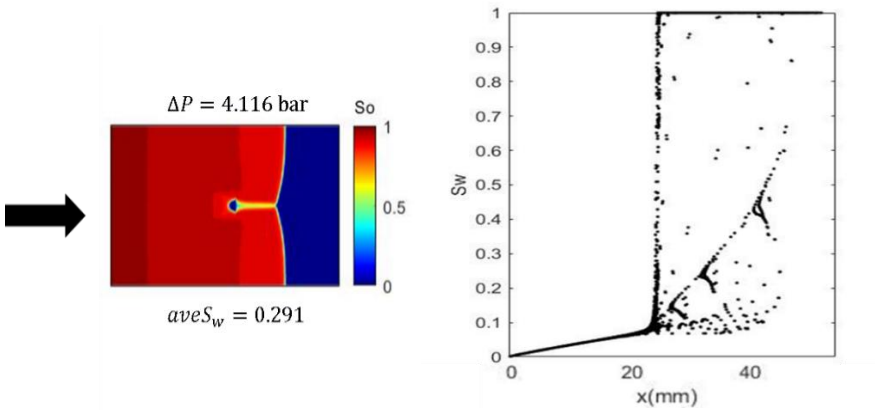

(a) (b)

Figure 46 Heterogeneous Case 4.1(200mD) when capillary pressure is 4.116 bar (a) Two-phase displacement, (b) Water saturation distribution

Table 17 shows the results of centrifuge simulations for Heterogeneous Case 4.1 (200 mD) and 4.2 (100 mD) calculated in **Step 14**. The equations for calculations are introduced in Section 4.1.1. The $aveS_w$ of the Heterogeneous Cases are larger than that of the Randomly Distributed Case 2. The MSEs of the two simulations are 0.0002 and 0.0005 respectively. For the Heterogeneous Case 4.2 (100 mD), the SSE and MSE are larger than that of the Heterogeneous Case 4.1 (200 mD) and thus, higher average saturation value can be obtained at same capillary presure in Heterogeneous Case 4.2 (100 mD). This is because the lower permeability value in the heterogeneous area can make the displacement of the wetting phase (water) harder. Thus, less water is displaced to the graduated tube.

Table 17 Comparisons of simulation results for Heterogeneous Case 4 with a low permeability area and Randomly Distributed Case 2

Capillary pressure (bar)	**aveSw for Randomly Distributed Case 2 (frac.)**	**aveSw for heterogeneous core (frac.)**		σ^2	
		Case 4.1 (200 mD)	**Case 4.2 (100 mD)**	**Case 4.1 (200 mD)**	**Case 4.2 (100 mD)**
4.116	0.272	0.291	0.301	0.0003	0.0009
3.251	0.324	0.336	0.347	0.0001	0.0005
2.489	0.381	0.397	0.401	0.0002	0.0004
1.83	0.436	0.445	0.456	0.0001	0.0004
1.27	0.671	0.684	0.699	0.0002	0.0008
0.811	0.790	0.802	0.815	0.0001	0.0007
0.427	0.875	0.889	0.894	0.0002	0.0004
0.204	0.934	0.946	0.954	0.0001	0.0004
0.051	1.000	1.000	1.000	0	0
SSE:				0.0015	0.0043
MSE:				0.0002	0.0005

Figure 47 displays $P_c(aveSw)$ curves and $P_c(inletS_w)$ curves for all the Cases. The equations that are used in calculation are introduced in Section 4.1.1. For same capillary pressure, the case with lower permeability value in the heterogeneous area has larger $aveS_w$ compared to the case with higher permeability value in the heterogenous area. The $P_c(aveSw)$ curve and $P_c(inletS_w)$ curve with lower permeability in the heterogeneous region will be shifted to the right compared to the curves with higher permeability. The capillary pressure curves of the heterogeneous cases are both at the right side of the capillary pressure curves of the Randomly Distributed Case 2. Therefore, for the same capillary pressure, higher saturation values can be obtained. The results make sense because the area with lower permeability can retain more wetting phase fluid and then less wetting phase fluid is produced in the graduated tube.

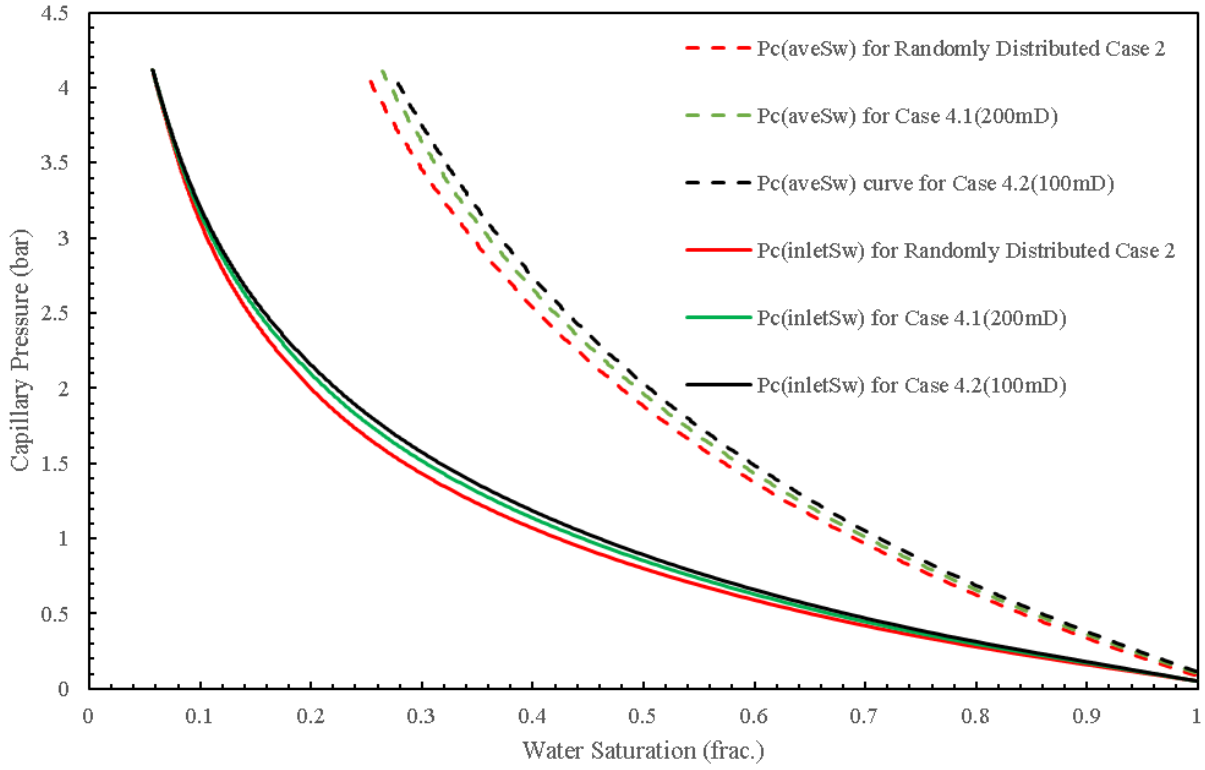

Figure 47 Pc ($aveS_w$) curves and Pc ($inletS_w$) curves for Heterogeneous Case 4 with a low permeability area, the length of the low permeability area is 5mm, the average permeability of the core is 360mD

4.1.5 Heterogeneous Case 5: 2D heterogeneous case with a high permeability area

The objective of this case is to study how high permeability value in the heterogeneous area will affect the fluid flow, phase saturation and capillary pressure curves from centrifuge.

In Heterogeneous Case 5, an area with high permeability was placed in the center of the core. In Heterogeneous Case 5.1(500mD), the ratio of permeability between the heterogeneity and the matrix is about 1.4 and in Case 5.2(700mD) the ratio is about 2. All other parameters used in this case are the same as the Randomly Distributed Case 2. Figure 48 shows the permeability distribution and detailed parameters used are shown in Table 18.

Table 18 Parameters used for Heterogeneous Case 5 with a high permeability area

Parameters	Units	Values

		Case 5.1 (500mD)	Case 5.2 (700mD)
Radial Blocks		100	100
Axial Blocks		155	155
Block size	cm	0.036	
Radial Blocks with High Permeability		43-58	43-58
Axial Blocks with High Permeability		70-85	70-85
Permeability of heterogeneity	mD	500	700
Mean Permeability	mD	360	360

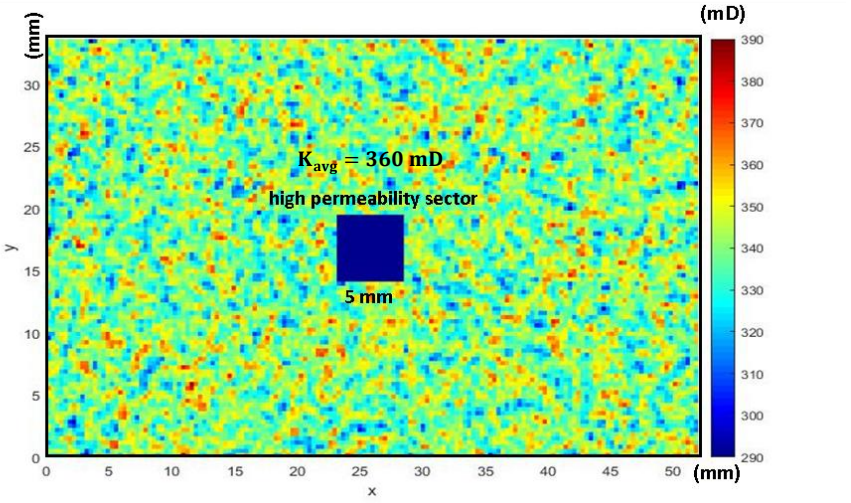

Figure 48 Permeability distribution for Heterogeneous Case 5 with a high permeability area

Figure 49 shows the corresponding streamlines for this case by using Equation (3.80) and (3.81) in Section 3.3.6 (**Step 10**). It can be observed that more streamlines can be found in the high permeability area since this area allows more fluids to pass through it compared to other areas in the core. Figure 50 shows the centrifuge displacement front and the saturation profile when the capillary pressure is 4.116 bar for Heterogeneous Case 5.1(500mD) calculated in **Step 13**. Equations for calculation are introduced in Section 4.1.1.In part (a), the displacement front is curved towards the outlet face as compared to part (a) of Figure 36 since the high permeability area

enhances the displacement efficiency and the water retained in the model decreases.

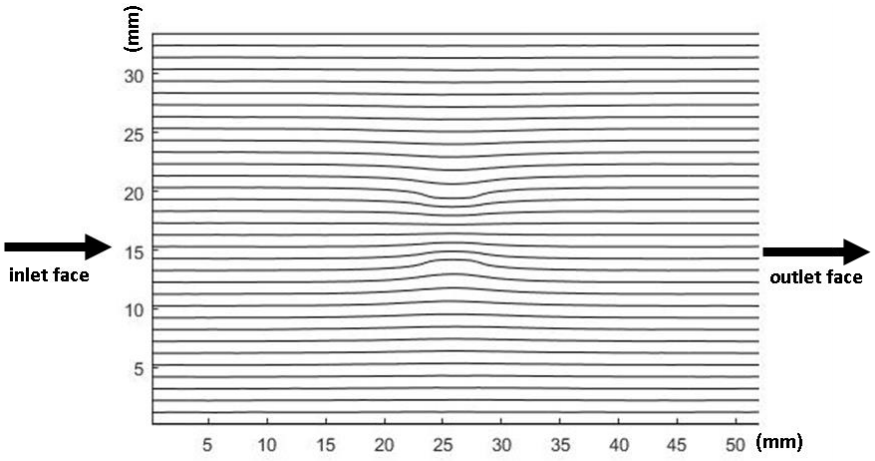

Figure 49 Streamlines for Heterogeneous Case 5 with a high permeability area

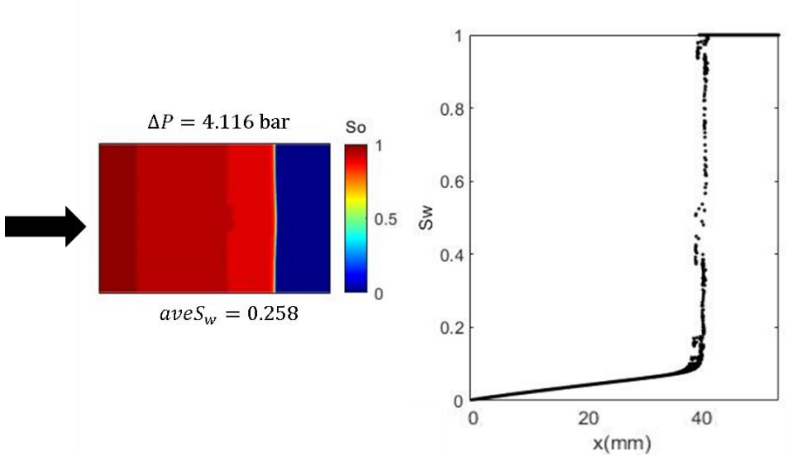

(a) (b)

Figure 50 Heterogeneous Case 5.1(500 mD) when capillary pressure is 4.116 bar (a) the two-phase displacement front, (b) the water saturation distribution

Table 19 shows the results of centrifuge simulation for Heterogeneous Case 5.1(500 mD) and 5.2(700 mD) calculated in **Step 14**. The equations that used for calculation are introduced in Section 4.1.1. From this table, we see that the $aveS_w$ of the Heterogeneous Cases 5 with a high permeability area is less than that of the Randomly Distributed Case 2 at the same capillary pressure. The deviation of the $aveS_w$ between the heterogeneous case and the randomly distributed case

increases if the permeability of heterogeneous region is increased. The results make sense because the heterogeneous area with higher permeability value can allow more wetting phase (water) to be displaced out of the core. Therefore, more water is produced and $aveS_w$ in the model decreases.

Table 19 Comparisons of simulation results for Heterogeneous Case 5 with a high permeability area and Randomly Distributed Case 2

Capillary pressure (bar)	**aveSw for randomly distributed Case 2 (frac.)**	**aveSw for heterogeneous core (frac.)**		σ^2	
		Case 5.1 (500mD)	**Case 5.2 (700mD)**	**Case 5.1 (500mD)**	**Case 5.2 (700mD)**
4.116	0.272	0.258	0.248	0.0002	0.0006
3.251	0.324	0.314	0.306	0.0001	0.0003
2.489	0.381	0.375	0.370	0.0000	0.0001
1.83	0.436	0.422	0.416	0.0002	0.0004
1.27	0.671	0.669	0.658	0.0000	0.0002
0.811	0.790	0.779	0.767	0.0001	0.0005
0.427	0.875	0.864	0.850	0.0001	0.0007
0.204	0.934	0.926	0.902	0.0001	0.0011
0.051	1.000	1.000	1.000	0.0000	0.0000
SSE:				0.0008	0.0039
MSE:				0.0001	0.0004

Figure 51 displays the $P_c(aveS_w)$ curves and $P_c(inletS_w)$ curves for Heterogeneous Case 5 with a high permeability area. The equations for calculations are introduced in Section 4.1.1. The $P_c(aveS_w)$ curve and $P_c(inletS_w)$ curve with higher permeability in the heterogeneous region are shifted to the left compared to the curves with lower permeability. The capillary pressure curves of the heterogeneous cases with a high permeability area are both at the left side of the capillary pressure curves of the Randomly Distributed Case 2. Therefore, for the same capillary pressure, lower saturation values can be obtained. This is reasonable since more wetting phase (water) is displaced by nonwetting phase (oil) through the high permeability area.

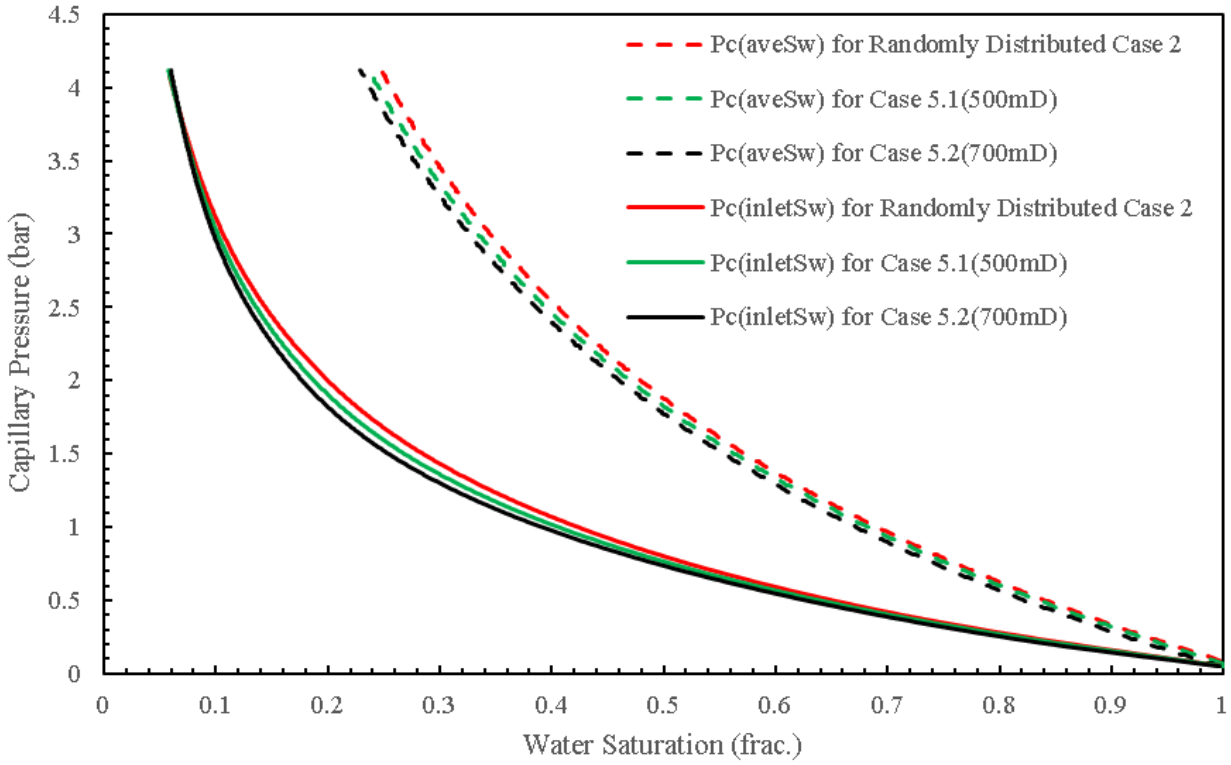

Figure 51 Pc ($aveS_w$) Curves and Pc ($inletS_w$) Curves for Heterogeneous Case 5 with a high permeability area, the length of the low permeability area is 5mm, the average permeability of the core is 360mD

4.1.6 Comparisons and Discussions

The results of Homogeneous Case 1 clearly indicate the justification and reasonability of the centrifuge simulation method used in this research since the calculated numerical $aveS_w$ curves and capillary pressure curves are in a good agreement with the experimental curves. This provides confidence in the application of the simulation method to the consideration of heterogeneity in the following cases. The deviations between the $aveS_w$ of Randomly Distributed Case 2 and that of Homogeneous Case 1.1 are negligible; therefore, it is more realistic and rational to apply randomly distributed permeability fields to the matrix areas without high/low permeability areas in the digital models (Shikhov and Arns, 2015). It is important to be noted that the average permeabilities of the randomly distributed field and the homogeneous field should be kept as the same for comparison.

As we observe in the Heterogeneous Case 3 with different lengths of heterogeneous areas, the influence of a fracture can be neglected when the length of the heterogeneous area has been reduced to $1\ mm$. In contrast, a large heterogeneous area can give rise to substantial deviations in the calculated capillary pressure curves compared to the Randomly Distributed Case 2. This makes sense because less wetting phase (water) is allowed to be displaced in a larger low permeability area. Thus, to better investigate impacts of permeability in heterogeneous areas, the lengths of the heterogenous areas were kept as $5\ mm$ in the subsequent simulations.

The obtained $aveS_w$ for Heterogeneous Case 4 with a low permeability area are found to be larger than the Randomly Distributed Case 2, which means the heterogeneous regions with low permeability hamper the fluid flow in the core during centrifuge and the hindered fluids in the core contribute to larger values of water saturations. This can also be validated intuitively by comparing the displacement front and water saturation distribution of Heterogeneous Case 4 with a low permeability area with that of Randomly Distributed Case 2. In part (a) of Figure 46, the displacing front is curved towards the inlet face in the middle of the core and the area with higher water saturation (blue area) is larger than that of Randomly Distributed Case 2. Additionally, the capillary pressure curves calculated from the larger saturation values in Heterogeneous Case 4 with a low permeability area are shifted to the right side as compared to the Randomly Distributed Case 2. The increase in the values of $aveS_w$ is subject to the permeability of the heterogeneous area. Reducing permeability in heterogeneous areas can increase the deviations of $aveS_w$ between the heterogenous case with a low permeability area and the randomly distributed case. The existence

of a low permeability area in the core contributes to a capillary pressure curve with a positive bias. The results are reasonable because the area with lower permeability can retain more wetting phase and less wetting phase is produced in the graduated tube.

The calculated $aveS_w$ of Heterogeneous Case 5 with a high permeability area are less than the Randomly Distributed Case 2. In part(a) of Figure 50, the displacement front is curved in the middle towards the outlet face of the core and the area with higher water saturation (blue area) is smaller than that of Randomly Distributed Case 2. The capillary pressure curves calculated based on the lower water saturation values in Heterogeneous Case 5 with a high permeability area are shifted to the left compared to Randomly Distributed Case 2. It is also found that a higher permeability value in the heterogeneous area can increase the deviations of $aveS_w$ between the heterogenous case and the randomly distributed case. However, no distinct rules could be found between the rotational speeds and the saturation deviations in Heterogeneous Case 4 and 5. The presence of a high permeability area in the core led to a capillary pressure with a negative bias. The results make sense since more wetting phase (water) is displaced by nonwetting phase (oil) in the high permeability area.

4.2 Research Significance

The typical centrifuge simulation methods that are widely used in the petroleum industry assume a one-dimensional fluid flow in the core without the consideration of heterogeneity. To investigate the impacts of core-scale heterogeneity on phase saturation predictions for centrifuge experiments, a centrifuge simulation method is presented in this thesis allowing a two-dimensional fluid flow, which is significant and vital in the core analysis field.

The proposed method to model the centrifuge experiments can describe the fluid flow in two dimensions by using streamline simulation method that considers capillary pressure numerically. The core heterogeneities have been accounted for in the centrifuge simulations by observing the streamline distributions with constant capillary pressure boundary conditions, which can also be validated by the displacing fronts and the saturation distributions at equilibrium. The two-dimensional centrifuge simulation method has been validated to be able to predict accurate average wetting phase saturation when the system has reached equilibrium at a given rotational speed/capillary pressure. The impacts of core-scale heterogeneity on phase saturation predictions and capillary pressure curves are studied using the proposed two-dimensional centrifuge simulation method. According to the results, the heterogeneity that is generated randomly by a Gaussian field does not have much impact on fluid flow, phase saturations and capillary pressure curves as compared to other heterogeneous model. It has also been proved that if a low permeability area is present in the model during centrifuge simulation, less wetting phase will be displaced, and the average wetting phase (water) saturations will increase. Thus, the resulting capillary pressure curve will have a positive bias as compared to the homogeneous/ randomly distributed model. The deviations in the average phase saturations can be enlarged by increasing the length of the heterogeneous area or by decreasing the permeability value in the heterogeneous area. It has been proved that a high permeability area can contribute to lower average wetting phase (water) saturation, and the resulting capillary pressure curve will have a negative bias as compared to the homogeneous/ randomly distributed model. Considering the choice of capillary pressure curve can significantly affect the results of reservoir simulation, the significance of this thesis lies in that it

can provide accurate capillary pressure curves for reservoir engineers to predict the oil recovery process and describe the fluid distribution.

For a reservoir engineer, capillary pressure is often used in the model initialization of the reservoir simulation where fluids are distributed all over the model initially (Shams et al., 2013). The effects of capillary pressure on the numerical simulation of reservoirs are significant in both fractured and non-fractured reservoirs. An accurate capillary pressure curve is crucial to accurately estimate the initial state of equilibrium by determining reservoir fluid distributions and fluid contacts. One-dimensional flow assumption may arise to errors in average saturation measurements if the core has heterogenieites in it. For example, if a low heterogeneity area is present in the core, one may underpredict the average wetting phases without the consideration of heterogeneity like Heterogeneous Case 4. Consequently, an underestimated capillary pressure curve that is calculated from average wetting phase saturations can lead to inaccurate determination of transition zones and thus, volumes of original fluids in place, which has significant influences on the economic target of a project (Shams et al., 2015). In contrast, an overpredicted capillary pressure curve may lead to problems that the reservoir geology model becomes unstable, high CPU time and convergence problems (Haddad, 2011). Capillary pressure curves measured from core samples are often used to estimated rock permeability when the direct measurement of permeability is not available. For example, Swanson's parameter has been widely used to estimate permeability from capillary pressure curves (Swanson, 1981). Guo et al. (2004) has also developed a parameter called Capillary Parachor for permeability estimation from capillary pressure curve and they found that the

permeability is proportional to the Capillary Parachor squared. If a high permeability area exists in the core like Heterogeneous Case 5, the capillary pressure may be overpredicted at the same water saturation by assuming a one-dimensional flow without the consideration of heterogeneity. Consequently. the permeability can be underestimated if Capillary Parachor is used for prediction. Since the capillary pressure and permeability are both crucial inputs for many reservoir simulators, a shift in capillary pressure curve without the heterogeneity consideration can produce results with considerable errors in simulations.

4.3 Limitations

The centrifuge simulation approach discussed in this research has its limitations. The simulation was conducted in a two-dimensional digital model; however, three-dimensional fluid flow can exist in the centrifuge experiments, so a three-dimensional model is needed. It is assumed that more deviations of phase saturations can be found in a three-dimensional model as compared to two-dimensional model since fluid flow in three dimensions is considered. The centrifuge simulation in this research applied the orthogonal Cartesian grid blocks without considering the geometry of the core plug. Radial grid blocks or curvilinear grid blocks would be better to model the core plug and fluid flows. The fluid flow in all the cases is assumed to be under steady state flow and the other kind of fluid flow conditions are not considered. Additionally, the permeabilities in the digital model are all assumed to be isotropic but most cores in reservoirs are heterogeneous with anisotropy. Only a few patterns of heterogeneity distributions in the cores were considered in the case studies, which may be too idealistic. To know the heterogeneity distribution in the core plug precisely, the tomography technique can be invoked.

5 Conclusions and Future Work

5.1 Conclusions

The modeling of centrifuge experiments for capillary pressure curve measurements are shown in very little literature. For the known centrifuge simulation methods, the porous media is assumed homogeneous, and the fluid flow is assumed to be in one dimension. However, absolute permeability may often vary spatially within a core plug, which will have impact on the flow pattern within the core and on the measured quantities. To fill the gap in this area, the centrifuge simulation method presented in this research thesis shows the advantage in allowing the fluids in the core to flow in two dimensions; therefore, core-scale heterogeneity can be accounted for when the fluids can flow more than one dimension. The centrifuge simulation method applied in this thesis is superior in describing the fluid flow compared to the standard numerical simulation methods (CYDAR, PORLAB etc.) for the determination of capillary pressure from SCAL experiments. This thesis applied streamline tracing method that considers capillary pressure to the modelling of centrifuge experiments; thus, core-scale heterogeneity can be characterized by streamline distributions. For the incompressible system without the consideration of gravity and diffusive effects, an elliptic pressure equation is derived and the pressure at the nodes are calculated. The pressure and velocity field are approximated and then the position of a particle at a specific point in time can be calculated and streamlines can then be traced. This thesis applied a semi-analytical Riemann solver along streamlines that can describe two-phase flow in the homogeneous and heterogeneous porous media under the constant differential pressure condition. Each streamline is treated as a one-dimensional system along which solution of mass conservation equations are

solved.

In this research, the lab-scale centrifuge experiments are performed for three core plugs from bay Du Nord on offshore Newfoundland and the U.S. The ability of the new centrifuge simulation method to model centrifuge experiments for phase saturation predictions is validated and demonstrated through comparing the numerical results with the experimental results. The influences of core-scale heterogeneity on fluid flow, phase saturation predictions and capillary pressure curves from centrifuge simulations can be summarized as:

1. A core with a permeability field generated randomly by the Gaussian field has produced equivalent simulated results (phase saturations, capillary pressure curves) as the core with a homogeneous permeability filed. The influences of the randomly generated heterogeneities by a Gaussian field on fluid flow, phase saturation and capillary pressure curves are negligible.
2. The size of heterogeneous area can have impacts on the numerical results of centrifuge simulations. As the low permeability area is growing larger, the hindrance of the fluid flow is becoming bigger. Consequently, less wetting phase is produced and a higher average wetting phase saturation at same capillary pressure can be obtained. A capillary pressure curve that is shifted to the right side compared to the homogeneous/randomly distributed case can be calculated and the shift can be increased by enlarging the area of the low permeability region.
3. When a low permeability area is present in a core plug during a drainage centrifuge

simulation, more wetting phase will be retained in the low permeability area of the core at some capillary pressure condition as compared to a homogeneous/randomly distributed core. Therefore, less wetting phase is produced from the core and higher average wetting phase saturation can be obtained. A capillary pressure curve with a positive bias as compared to homogeneous/randomly distributed case can be calculated. The difference between a heterogeneous and a homogeneous capillary pressure curve can be increased by decreasing the permeability values in the low permeability area.

4. When a high permeability area is present in a core plug during a drainage centrifuge simulation, more wetting phase will go through the high permeability area of the core at same capillary pressure condition as compared to a homogeneous/randomly distributed core. Thus, more wetting phase is displaced out of the core and lower average wetting phase saturation can be obtained. A capillary pressure curve with a negative bias as compared to homogeneous/randomly distributed case can be calculated. The difference between a heterogeneous and a homogeneous capillary pressure curve can be increased by increasing the permeability values in the high permeability area. There is no distinct rule can be found in the influence of rotational speeds on the saturation deviations.

The rock permeability is usually estimated from capillary pressures using an empirical correlation when direct measurement is not available. An overpredict/underpredict capillary pressure curves from centrifuge simulation may give rise to inaccurate relative permeability curves. Since the capillary pressure and permeability are both crucial inputs for many reservoir simulators, a shift in

capillary pressure curve without the heterogeneity consideration can produce results with considerable errors in simulations.

In conclusion, the effects of core-scale heterogeneity on phase saturation predictions and the resulting capillary pressure curves cannot be neglected and should be accounted for in the modelling of centrifuge experiments for capillary pressure curve measurements.

5.2 Future Work

The new centrifuge simulation method is developed to deliver more accurate simulations for centrifuge experiments. However, this method has only been performed in two dimensions throughout this research thesis. In other words, we can only handle the core with two-dimensional flow. This simulation method can be extended three-dimensional grid blocks, which can be achieved by tracing streamlines in three dimensions using cubic pressure approximation functions. This research thesis is based on Cartesian coordinate so errors may occur in the representation of the geometry of a core plug. Radial or cylindrical coordinate may better satisfy the complex geometry of a core plug. The permeabilities in the digital model are all assumed to be isotropic so the anisotropy can be considered by setting the permeability to be a full tensor. A full tensor permeability can better model local flow in directions at an angle to the coordinate axes. Only a limited patterns of heterogeneity distributions in the cores have been considered; thus, more permeability distribution patterns can be studied and investigated. The unsteady state flow condition and compressible fluid flow in the oil/gas case can also be studied as the future work.

References

Adachi, H. (1986). Research on one-dimensional two-phase flow. Theory on hydrodynamic balance in two fluid model and its application. *NASA STI/Recon Technical Report N*, *88*, 10290.

Alzayer, H., Jahanbakhsh, A., & Sohrabi, M. (2017, May). The role of capillary-pressure in improving the numerical simulation of multi-phase flow in porous media. In *SPE Reservoir Characterisation and Simulation Conference and Exhibition*. OnePetro.

Amyx, J., Bass, D., & Whiting, R. L. (1960). *Petroleum reservoir engineering physical properties*.

Andersen, P. Ø., Skjæveland, S. M., & Standnes, D. C. (2017). An Analytical Model for Analysis of Capillary Pressure Measurements by Centrifuge. *Petrophysics-The SPWLA Journal of Formation Evaluation and Reservoir Description*, *58*(04), 366-375.

Anderson, W. (1986). Wettability literature survey-part 2: Wettability measurement. *Journal of Petroleum Technology*, *38*(11), 1246-1262.

Andrew, M., Bijeljic, B., & Blunt, M. J. (2014). Pore-scale imaging of trapped supercritical carbon dioxide in sandstones and carbonates. *International Journal of Greenhouse Gas Control*, *22*, 1-14.

Araktingi, U. G., & Orr, F. M. (1988). Viscous fingering in heterogeneous porous media, paper SPE 18095. In *63rd Annual SPE Fall Meeting, Houston, TX*.

Ayappa, K. G., Davis, H. T., Davis, E. A., & Gordon, J. (1989). Capillary pressure: centrifuge method revisited. *AIChE Journal*, *35*(3), 365-372.

Batchelor, G. K. (1982). An introduction to fluid dynamics. Cambridge University Press (1967). *Bauer, HF" Natural frequencies and stability of circular cylindrical immiscible liquid*.

Bear, J. (2013). *Dynamics of fluids in porous media*. Courier Corporation.

Bentsen, R. G., & Anli, J. (1977). Using parameter estimation techniques to convert centrifuge data into a capillary-pressure curve. *Society of Petroleum Engineers Journal*, *17*(01), 57-64.

Bommer, P. M., & Schechter, R. S. (1979). Mathematical modeling of in-situ uranium leaching. *Society of Petroleum Engineers Journal*, *19*(06), 393-400.

Bratvedt, F., Bratvedt, K., Buchholz, C. F., Holden, L., Holden, H., & Risebro, N. H. (1992). A new front-tracking method for reservoir simulation. *SPE Reservoir Engineering*, *7*(01), 107-116.

Brooks, R. H. (1965). *Hydraulic properties of porous media*. Colorado State University.

Brooks, R. H., & Corey, A. T. (1966). Properties of porous media affecting fluid flow. *Journal of the Irrigation and Drainage Division*, *92*(2), 61-88.

Brusllovsky, A. L. (1992). Mathematical simulation of phase behavior of natural multicomponent systems at high pressure with an equation of state. *SPE Res Eng*, *7*(1), 117-122.

Buckley, S. E., & Leverett, M. (1942). Mechanism of fluid displacement in sands. *Transactions of the AIME*, *146*(01), 107-116.

Burdine, N. (1953). Relative permeability calculations from pore size distribution data. *Journal of Petroleum Technology*, *5*(03), 71-78.

Chang, J., & Yortsos, Y. C. (1992). Effect of capillary heterogeneity on Buckley-Leverett displacement. *SPE Reservoir Engineering*, *7*(02), 285-293.

Christiansen, R. L., & Cerise, K. S. (1992). Geometric Concerns for Accurate Measurement of Capillary Pressure Relationships with Centrifuge Methods (includes associated paper 27739). *SPE formation evaluation*, *7*(04), 311-314.

Cordes, C., & Kinzelbach, W. (1992). Continuous groundwater velocity fields and path lines in linear, bilinear, and trilinear finite elements. *Water Resources Research*, *28*(11), 2903-2911.

Dahle, H. K., Celia, M. A., & Hassanizadeh, S. M. (2005). Bundle-of-tubes model for calculating dynamic effects in the capillary-pressure-saturation relationship. *Transport in Porous media*, *58*(1), 5-22.

Datta-Gupta, A., & King, M. J. (1995). A semianalytic approach to tracer flow modeling in heterogeneous permeable media. *Advances in Water Resources*, *18*(1), 9-24.

Datta-Gupta, A., & King, M. J. (2007). *Streamline simulation: theory and practice* (Vol. 11). Richardson, Texas: Society of Petroleum Engineers.

de Lagrange, J. L. (1781). Mémoire sur la théorie du mouvement des fluides. *Acad. Roy. Sci. & Belles Lettres*, 151-198.

Dean, E. W., & Stark, D. D. (1920). A Convenient Method for the Determination of Water in Petroleum and Other Organic Emulsions. *Industrial & Engineering Chemistry*, *12*(5), 486-490.

Dernaika, M., Wilson, O. B., Skjæveland, S. M., & Ebeltoft, E. (2016). Drainage capillary pressure and resistivity index from short-wait porous-plate experiments. *Petrophysics-The SPWLA Journal of Formation Evaluation and Reservoir Description*, *57*(04), 369-376.

Donaldson, E. C., Kendall, R. F., Pavelka, E. A., & Crocker, M. E. (1980). *Equipment and procedures for fluid flow and wettability tests of geological materials* (No. DOE/BETC/IC-79/5). Department of Energy, Bartlesville, OK (USA). Bartlesville Energy Technology Center.

Dullien, F. A. (2012). *Porous media: fluid transport and pore structure*. Academic press.

Dyes, A. B., Caudle, B. H., & Erickson, R. A. (1954). Oil production after breakthrough as influenced by mobility ratio. *Journal of Petroleum Technology*, *6*(04), 27-32.

Friesen, W. I., & Mikula, R. J. (1987). Fractal dimensions of coal particles. *Journal of Colloid and Interface Science*, *120*(1), 263-271.

Ediriweera, M. P., & Halvorsen, B. (2015). A study of the effect of relative permeability and residual oil saturation on oil recovery.

Erkal, A., & Numbere, D. T. (1997, January). Relative permeability effects on the migration of steamflood saturation fronts. In *SPE Western Regional Meeting*. Society of Petroleum Engineers.

Evans, C. E., & Guerrero, E. T. (1979, June). Theory and application of capillary pressure. In *SPWLA 20th Annual Logging Symposium*. OnePetro.

Forbes, P. (1994). Simple and accurate methods for converting centrifuge data into drainage and imbibition capillary pressure curves. *The Log Analyst*, *35*(04).

Forbes, P. (2000). The H&B boundary condition in centrifuge Pc experiments (or why there is not experimental evidence that the pressure field model ever failed). In *International symposium of the society of core analysts, Abu Dhabi, UAE* (Vol. 64).

Fayers, F. J., Blunt, M. J., & Christie, M. A. (1990, September). Accurate calibration of empirical viscous fingering models. In *ECMOR II-2nd European conference on the mathematics of Oil Recovery* (pp. cp-231). European Association of Geoscientists & Engineers.

Firoozabadi, A., Soroosh, H., & Hasanpour, G. (1988). Drainage performance and capillary-pressure curves with a new centrifuge. *Journal of Petroleum Technology*, *40*(07), 913-919.

Firincioglu, T., Ozkan, E., & Ozgen, C. (2012, October). Thermodynamics of multiphase flow in unconventional liquids-rich reservoirs. In *SPE Annual Technical Conference and Exhibition*. OnePetro.

Fleury, M., Doevle, M., & Longeron, D. (1997). Full imbibition capillary pressure measurements on preserved samples using the micropore membrane technique. *SCA Paper*.

Fleury, M., Egermann, P., & Goglin, E. (2000). A model of capillary equilibrium for the centrifuge technique. *paper SCA2000-31*.

Forbes, P. (1994). Simple and accurate methods for converting centrifuge data into drainage and imbibition capillary pressure curves. *The Log Analyst*, *35*(04).

Forbes, P. L. (1997). Centrifuge data analysis techniques—a survey from the Society of Core Analysis. *SCA, Dallas*.

Gates, J. I., & Lietz, W. T. (1950, January). Relative permeabilities of California cores by the capillary-pressure method. In *Drilling and production practice*. OnePetro.

Glimm, J., Isaacson, E., Marchesin, D., & McBryan, O. (1981). Front tracking for hyperbolic systems. *Advances in Applied Mathematics*, *2*(1), 91-119.

Glimm, J., Grove, J., Li, X., & Zhao, N. (1999). Simple Front Tracking, Nonlinear Partial Differential Equations, edited by Chen, DiBenedetto. *American Mathematical Society*, 1-21.

Guo, B., Ghalambor, A., & Duan, S. (2004). Correlation between sandstone permeability and capillary pressure curves. *Journal of Petroleum Science and Engineering*, *43*(3-4), 239-246.

Haddad, R. (2011). Capillary Pressure Estimation and Reservoir Simulation.

Hagoort, J. (1980). Oil recovery by gravity drainage. *Society of Petroleum Engineers Journal*, *20*(03), 139-150.

Hamon, G., & Vidal, J. (1986, October). Scaling-up the capillary imbibition process from laboratory experiments on homogeneous and heterogeneous samples. In *European petroleum conference*. OnePetro.

Harrison, N. W. (1972). Diverting agents-history and application. *Journal of Petroleum Technology*, *24*(05), 593-598.

Hassler, G. L., & Brunner, E. (1945). Measurement of capillary pressures in small core samples. *Transactions of the AIME*, *160*(01), 114-123.

Higgins, R. V., & Leighton, A. J. (1962a). A computer method to calculate two-phase flow in any irregularly bounded porous medium. *Journal of Petroleum Technology*, *14*(06), 679-683.

Higgins, R. V., & Leighton, A. J. (1962b). Computer prediction of water drive of oil and gas mixtures through irregularly bounded porous media three-phase flow. *Journal of Petroleum Technology*, *14*(09), 1048-1054.

Higgins, R. V., Boley, D. W., & Leighton, A. J. (1964). Aids to forecasting the performance of water floods. *Journal of Petroleum Technology*, *16*(09), 1076-1082.

Hirasaki, G. J., O'Meara, D. J., & Rohan, J. A. (1988, October). Centrifuge Measurements of Capillary Pressure: Part 2-Cavitation. In *SPE Annual Technical Conference and Exhibition*. OnePetro.

Hoffman, R. N. (1963). A technique for the determination of capillary pressure curves using a constantly accelerated centrifuge. *Society of Petroleum Engineers Journal*, *3*(03), 227-235.

Johansen, T.E. (2010). A new semi-analytical method for streamline simulation. Unpublished manuscript, (www.petreng-thormod.ca).

Honarpour, M., Koederitz, L., & Harvey, A. H. (2018). *Relative permeability of petroleum reservoirs*. CRC press.

Johansen, T. E., Hender, D. G., & James, L. A. (2017). Productivity index for arbitrary well trajectories in laterally isotropic, spatially anisotropic porous media. *SPE Journal*, *22*(02), 699-711.

Johansen, T. E., & Liu, X. (2017). Solution of Riemann problems for hyperbolic systems of conservation laws modeling two-phase flow in general stream tube geometries. *Journal of Engineering Mathematics*, *105*(1), 137-155.

Kansas Geological Survey, & Baars, D. L. (1989). *Petroleum: A Primer for Kansas*. Kansas Geological Survey.

Kelkar, M., & Gupta, S. P. (1991). A numerical study of viscous instabilities: Effect of controlling parameters and scaling considerations. *SPE reservoir engineering*, *6*(01), 121-128.

Kewen, L. (2004, April). Theoretical development of the Brooks-Corey capillary pressure model from fractal modeling of porous media. In *SPE/DOE Symposium on Improved Oil Recovery*. OnePetro.

King, F. H. (1899). *Principles and conditions of the movements of ground water*. US Government Printing Office.

Kjosavik, A., Ringen, J. K., & Skjaeveland, S. M. (2002). Relative permeability correlation for mixed-wet reservoirs. *SPE Journal*, *7*(01), 49-58.

Lake, L. W., Carroll, H. B., & Wesson, T. C. (Eds.). (1991). *Reservoir characterization II* (Vol. 2). Academic Press.

Land, C. S. (1968). Calculation of imbibition relative permeability for two-and three-phase flow from rock properties. *Society of Petroleum Engineers Journal*, *8*(02), 149-156.

Leal, L., Barbato, R., Quaglia, A., Porras, J. C., & Lazarde, H. (2001, March). Bimodal behavior of mercury-injection capillary pressure curve and its relationship to pore geometry, rock-quality and production performance in a laminated and heterogeneous reservoir. In *SPE Latin American and Caribbean Petroleum Engineering Conference*. OnePetro.

LeBlanc, J. L., & Caudle, B. H. (1971). A streamline model for secondary recovery. *Society of Petroleum Engineers Journal*, *11*(01), 7-12.

Lenormand, R., Lorentzen, K., Maas, J. G., & Ruth, D. (2017). Comparison of four numerical simulators for SCAL experiments. *Petrophysics-The SPWLA Journal of Formation Evaluation and Reservoir Description*, *58*(01), 48-56.

Leverett, M. (1941). Capillary behavior in porous solids. *Transactions of the AIME*, *142*(01), 152-169.

Li, K., & Horne, R. N. (2002, May). Experimental verification of methods to calculate relative permeability using capillary pressure data. In *SPE Western Regional/AAPG Pacific Section Joint Meeting*. OnePetro.

Li, K., & Horne, R. N. (2003, February). Numerical simulation with input consistency between capillary pressure and relative permeability. In *SPE Reservoir Simulation Symposium*. OnePetro.

Li, K., & Williams, W. (2007). Determination of capillary pressure function from resistivity data. *Transport in porous media*, *67*(1), 1-15.

Lie, K. A. (2019). *An introduction to reservoir simulation using MATLAB/GNU Octave: User guide for the MATLAB Reservoir Simulation Toolbox (MRST)*. Cambridge University Press.

Linz, P. (1985). *Analytical and numerical methods for Volterra equations*. Society for Industrial and Applied Mathematics.

Lomeland, F., Ebeltoft, E., & Thomas, W. H. (2008, October). A new versatile capillary pressure correlation. In *Paper SCA 2008-08 presented at the International Symposium of the Society of Core Analysts held in Abu Dhabi, UAE* (Vol. 29).

Luffel, D. L. (1964). A TECHNIQUE FOR THE DETERMINATION OF CAPILLARY PRESSURE CURVES USING A CONSTANTLY ACCELERATED CENTRIFUGE-DISCUSSION. *SOCIETY OF PETROLEUM ENGINEERS JOURNAL*, *4*(2), 191-192.

Mannseth, T., Mykkeltveit, J., Nordtvedt, J. E., & Sylte, A. (1998, October). Effects of rock heterogeneities on capillary pressure and relative permeabilities. In *European Petroleum Conference*. OnePetro.

MANUAL, C. S. U. CYDAR-SCAL USER MANUAL.

Marle, C. (1981). *Multiphase flow in porous media*. Éditions technip.

Marquardt, D. W. (1963). An algorithm for least-squares estimation of nonlinear parameters. *Journal of the society for Industrial and Applied Mathematics*, *11*(2), 431-441.

Martin, J. C., Woo, P. T., & Wagner, R. E. (1973). Failure of stream tube methods to predict waterflood performance of an isolated inverted five-spot at favorable mobility ratios. *Journal of Petroleum Technology*, *25*(02), 151-153.

Martin, J. C., & Wegner, R. E. (1979). Numerical solution of multiphase, two-dimensional incompressible flow using stream-tube relationships. *Society of Petroleum Engineers Journal*, *19*(05), 313-323.

Matringe, S. F., Juanes, R., & Tchelepi, H. A. (2006). Robust streamline tracing for the simulation of porous media flow on general triangular and quadrilateral grids. *Journal of Computational Physics*, *219*(2), 992-1012.

McDonald, M. G., & Harbaugh, A. W. (1988). *A modular three-dimensional finite-difference ground-water flow model*. US Geological Survey.

McPhee, C., Reed, J., & Zubizarreta, I. (2015). *Core analysis: a best practice guide*. Elsevier.

Melrose, J. C. (1986, June). Interpretation of centrifuge capillary pressure data. In *SPWLA 27th Annual Logging Symposium*. OnePetro.

Mikes, D., Barzandji, O. H. M., Bruining, J., & Geel, C. R. (2001, April). Upscaling of flow units for reservoir flow incorporating small-scale heterogeneities. In *SPE Asia Pacific Oil and Gas Conference and Exhibition*. OnePetro.

Miller, S. J. (2017). The method of least squares. In *The Probability Lifesaver* (pp. 625-635). Princeton University Press.

Mood, A. M. (1950). Introduction to the Theory of Statistics.

Muskat, M., & Wyckoff, R. D. (1934). A theoretical analysis of water-flooding networks. *Transactions of the AIME*, *107*(01), 62-76.

Muskat, M. (1938). The flow of homogeneous fluids through porous media. *Soil Science*, *46*(2), 169.

Ng, C. W., & Pang, Y. W. (2000). Experimental investigations of the soil-water characteristics of a volcanic soil. *Canadian Geotechnical Journal*, *37*(6), 1252-1264.

Nilsen, H. M., & Lie, K. A. (2009, February). Front tracking methods for use in streamline simulation of compressible flow. In *SPE Reservoir Simulation Symposium*. OnePetro.

Nimmo, J. R. (2004). Porosity and pore size distribution. *Encyclopedia of Soils in the Environment*, *3*(1),

295-303.

Nojabaei, B., Johns, R. T., & Chu, L. (2013). Effect of capillary pressure on phase behavior in tight rocks and shales. *SPE Reservoir Evaluation & Engineering*, *16*(03), 281-289.

Nordtvedt, J. E., & Kolltvelt, K. (1991). Capillary pressure curves from centrifuge data by use of spline functions. *SPE reservoir engineering*, *6*(04), 497-501.

Nordtvedt, J. E., Mejia, G., Yang, P. H., & Watson, A. T. (1993). Estimation of capillary pressure and relative permeability functions from centrifuge experiments. *SPE Reservoir Engineering*, *8*(04), 292-298.

O'Meara, D. J., & Crump, J. G. (1985, September). Measuring capillary pressure and relative permeability in a single centrifuge experiment. In *SPE Annual Technical Conference and Exhibition*. OnePetro.

O'Meara, D. J., Hirasaki, G. J., & Rohan, J. A. (1992). Centrifuge measurements of capillary pressure: Part 1-Outflow boundary condition. *SPE reservoir engineering*, *7*(01), 133-142.

Omoregle, Z. S. (1988). Factors affecting the equivalency of different capillary pressure measurement techniques. *SPE formation evaluation*, *3*(01), 146-155.

Panchuk, K. (2019). *Physical Geology, First University of Saskatchewan Edition*. University of Saskatchewan..

Papatzacos, P., & Skjæveland, S. M. (2002, January). Relative permeability from capillary pressure. In *SPE Annual Technical Conference and Exhibition*. Society of Petroleum Engineers.

Parsons, R. W. (1972). Directional permeability effects in developed and unconfined five-spots. *Journal of Petroleum Technology*, *24*(04), 487-494.

Pickell, J. J., Swanson, B. F., & Hickman, W. B. (1966). Application of air-mercury and oil-air capillary pressure data in the study of pore structure and fluid distribution. *Society of Petroleum Engineers Journal*, *6*(01), 55-61.

Pishro-Nik, H. (2016). Introduction to probability, statistics, and random processes.

Pollock, D. W. (1988). Semianalytical computation of path lines for finite‐difference models. *Groundwater*, *26*(6), 743-750.

Prats, H. F. (1951, May). The application of numerical methods to cycling and flooding problems. In *3rd World Petroleum Congress*. OnePetro.

Prevost, M., Edwards, M. G., & Blunt, M. J. (2002). Streamline tracing on curvilinear structured and unstructured grids. *Spe Journal*, *7*(02), 139-148.

Purcell, W. R. (1949). Capillary pressures-their measurement using mercury and the calculation of permeability therefrom. *Journal of Petroleum Technology*, *1*(02), 39-48.

Purcell, W. R. (1950). Interpretation of capillary pressure data. *Journal of Petroleum Technology*, *2*(08), 11-12.

Rajan, R. R. (1986, June). Theoretically correct analytical solution for calculating capillary pressure-saturation from centrifuge experiments. In *SPWLA 27th annual logging symposium*. OnePetro.

Ruth, D., & Wong, S. (1991). Calculation of Capillary-Pressure Curves from Data Obtained by the Centrifuge Method. *The Log Analyst*, *32*(05).

Ruth, D. (1997, September). Analysis of centrifuge relative permeability data. In *Proceedings of the International Symposium of the Society of Core Analysts* (pp. 7-10).

Schoenberg, I. J. (1988). Contributions to the problem of approximation of equidistant data by analytic functions. In *IJ Schoenberg Selected Papers* (pp. 3-57). Birkhäuser, Boston, MA.

Seth, S. (2006). *Increase in surface energy by drainage of sandstone and carbonate*. University of Wyoming.

Shafer, J. M. (1987). Reverse pathline calculation of time‐related capture zones in nonuniform flow. *Groundwater*, *25*(3), 283-289.

Shafer, J., & Lasswell, P. (2007, June). Modeling Porous Plate Capillary Pressure Production Data: Shortening Test Duration and Quality Controlling Data. In *SPWLA 48th Annual Logging Symposium*. OnePetro.

Shams, M., El-Banbi, A. H., & Khairy, M. (2013, April). Effect of Capillary Pressure on the Numerical Simulation of Conventional and Naturally Fractured Reservoirs. In *North Africa Technical Conference and Exhibition*. OnePetro.

Shams, M., El-Banbi, A. H., & Khairy, M. (2015, September). Capillary pressure considerations in numerical reservoir simulation studies-conclusion maps. In *SPE North Africa Technical Conference and Exhibition*. OnePetro.

Shikhov, I., & Arns, C. H. (2015). Evaluation of capillary pressure methods via digital rock simulations. *Transport in Porous Media*, *107*(2), 623-640.

Siddiqui, F. I. (1999, October). Defining fluid distribution and fluid contacts for dynamically charged reservoirs. In *SPE Annual Technical Conference and Exhibition*. OnePetro.

Skjaeveland, S. M., Siqveland, L. M., Kjosavik, A., Thomas, W. L., & Virnovsky, G. A. (2000). Capillary pressure correlation for mixed-wet reservoirs. *SPE Reservoir Evaluation & Engineering*, *3*(01), 60-67.

Skuse, B., Firoozabadi, A., & Ramey, H. J. (1988, October). Computation and interpretation of capillary pressure from a centrifuge, SPE paper 18297. In *Annual Technical Conference, Houston, Oct* (pp. 2-5).

Slobod, R. L., Chambers, A., & Prehn, W. L. (1951). Use of centrifuge for determining connate water, residual oil, and capillary pressure curves of small core samples. *Journal of Petroleum Technology*, *3*(04), 127-134.

Swanson, B. F. (1979). Visualizing pores and nonwetting phase in porous rock. *Journal of Petroleum Technology*, *31*(01), 10-18.

Swanson, B. F. (1981). A simple correlation between permeabilities and mercury capillary

pressures. *Journal of Petroleum Technology*, *33*(12), 2498-2504.

Tchelepi, H. A., Orr Jr, F. M., Rakotomalala, N., Salin, D., & Woumeni, R. (1993). Dispersion, permeability heterogeneity, and viscous fingering: Acoustic experimental observations and particle‐tracking simulations. *Physics of Fluids A: Fluid Dynamics*, *5*(7), 1558-1574.

Thiele, M. R. (1995). *Modeling multiphase flow in heterogeneous media using streamtubes* (Doctoral dissertation, stanford university).

Thiele, M. R., Batycky, R. P., Blunt, M. J., & Orr, F. M. (1996). Simulating flow in heterogeneous systems using streamtubes and streamlines. *SPE Reservoir Engineering*, *11*(01), 5-12.

Thiele, M. R. (2001, September). Streamline simulation. In *6th International Forum on Reservoir Simulation* (pp. 3-7). Society of Petroleum Engineers: Schloss Fuschl, Austria.

Tiab, D., & Donaldson, E. C. (2015). *Petrophysics: theory and practice of measuring reservoir rock and fluid transport properties*. Gulf professional publishing.

Van Domselaar, H. R. (1984). An exact equation to calculate actual saturations from centrifuge capillary pressure measurements.

Wang, Y., Bandal, M. S., Moreno, J. E., & Sakdilah, M. Z. (2006, September). A systematic approach to incorporate capillary pressure-saturation data into reservoir simulation. In *SPE Asia Pacific Oil & Gas Conference and Exhibition*. OnePetro.

Ward, J. S., & Morrow, N. R. (1987). Capillary pressures and gas relative permeabilities of low-permeability sandstone. *SPE Formation Evaluation*, *2*(03), 345-356.

Watson, A. T., Kerig, P. D., & Otter, R. W. (1985). A Test for Detecting Rock Property Nonuniformities in Core Samples (includes associated papers 15342 and 15842). *Society of Petroleum Engineers Journal*, *25*(06), 909-916.

Wilson, O. B., Tjetland, B. T., & Skauge, A. (2001). Drainage rates in capillary pressure experiments. In *15th International Symposium of the Society of Core Analysts, No. SCA2001-30* (pp. 1-12).

Wilson, O. B., & Skjæveland, S. M. (2002, September). Porous plate influence on effective imbibition rates in capillary pressure experiments. In *Paper SCA2002-016, presented at the SCA International Symposium, Monterey, California, USA* (pp. 22-25).

Wunderlich, R. W. (1985, September). Imaging of wetting and nonwetting phase distributions: Application to centrifuge capillary pressure measurements. In *SPE Annual Technical Conference and Exhibition*. OnePetro.

Yuan, H. H., & Swanson, B. F. (1989). Resolving pore-space characteristics by rate-controlled porosimetry. *SPE Formation Evaluation*, *4*(01), 17-24.

Zeybek, M., Gurakin, G., Donmez, A., & Onur, M. (1995, October). Effects of capillary heterogeneities on spontaneous imbibition. In *SPE Annual Technical Conference and Exhibition*. OnePetro.

Zhang, N. (2017). *A New Semi-analytical streamline simulator and its applications to modelling waterflooding experiments* (Doctoral dissertation, Memorial University of Newfoundland).

Zhang, N., Cao, J., James, L. A., & Johansen, T. E. (2021). High-order streamline simulation and macro-scale visualization experimental studies on waterflooding under given pressure boundaries. *Journal of Petroleum Science and Engineering*, *203*, 108617.

Zhang, Y., King, M. J., & Datta‐Gupta, A. (2012). Robust streamline tracing using inter‐cell fluxes in locally refined and unstructured grids. *Water Resources Research*, *48*(6).

Appendices

Appendix A: Two-dimensional Homogeneous Case Centrifuge Simulation

```
clear all
mrstModule add incomp diagnostics
%% Set up grid and petrophysical data
nx=155;ny=100;
lx=0.0520;ly=0.0336; domain = [lx ly];
G = cartGrid([nx,ny],[lx,ly]);
G = computeGeometry(G);
K=ones(nx,ny).*360.*milli*darcy;
rock = makeRock(G, K(:), 0.2828);
plotGrid(G);
%% computation of upscaled permeability
q   = ones(G.cells.num,1);
vol = G.cells.volumes;
coarse = [1 1];
cG = computeGeometry(cartGrid(coarse,G.cartDims));
for i=1:size(rock.perm,2)
dims = G.cartDims; dims(i)=coarse(i);
qq = partitionUI(G, dims);
K = accumarray(qq,vol)./accumarray(qq,vol./rock.perm(:,i));
crock.perm(:,i) = accumarray(q,K(qq).*vol)./accumarray(q,vol)
end
%% The histogram of the permeability distribution in 1D problem
K = convertTo(rock.perm,milli*darcy);
plotCellData(G,K,'EdgeColor','none');axis tight;
[h,az] = colorbarHist(K,[0 400],'South');
pv     = poreVolume(G, rock);
%% Compute half transmissibilities
hT = computeTrans(G, rock);
%% Fluid model
gravity reset off
fluid = initSimpleFluidJfunc('mu' , [   1.01,
5.9]*centi*poise     , ...
    'rho', [1040, 858]*kilogram/meter^3, ...
    'n'  , [   2,   2], ...
    'surf_tension',1, ...
    'rock', rock);
%% Impose boundary condition
```

```
[src,bc] = deal([]);
bc = pside(bc, G, 'EAST',0*barsa,'sat', [1 0]);
bc = pside(bc, G, 'WEST',4.116*barsa,'sat', [0 1]);

clf, plotGrid(G,'FaceColor', 'none'); view(2);
plotFaces(G, bc.face(strcmp(bc.type,'pressure')), 'b');
plotFaces(G, bc.face(strcmp(bc.type,'pressure')), 'r');
%% Construct reservoir state object
state = initResSol(G, 0.0, [1 0]);
%% Solve pressure and show the result
state = incompTPFA(state, G, hT, fluid, 'src', src,'bc',bc);

clf,
plotCellData(G, convertTo(state.pressure, barsa()), 'EdgeColor',
'k');
axis equal tight; colorbar;
%% Compute time-of-flight
mrstModule add diagnostics
tof = computeTimeOfFlight(state, G, rock,'bc',bc);

clf,
plotCellData(G, tof);
axis equal tight;
colormap(jet(11));colorbar;
caxis('auto');
%% Visualize high-flow and stagnant regions
tofb = computeTimeOfFlight(state, G, rock, 'bc', bc, 'reverse',
true);

clf,
plotCellData(G, tof+tofb);
axis equal tight;
colormap(jet(128));
%% Trace streamlines
mrstModule add streamlines;
j=1;
for i=0:ny-1
    seed(j) = 1+i.*nx;
    j=j+1;
end
seed=seed.';
```

```
clf,
Sf = pollock(G, state, seed, 'substeps', 1);
hf=streamline(Sf);
axis equal tight;
set([hf],'Color','k');
%% Compute solution and plot saturation evolution
% Figure, colormap and contour values
nval = 25;
cval = linspace(0,1,nval+1);
cval=.5*cval(1:end-1)+.5*cval(2:end);
T=0;
dT=ones(1,20).*(11.55/20);
% dT=ones(1,20).*(10^(-2)/20);
% dT=ones(1,20).*(2*10^8/20);
Swt=zeros(1,numel(dT));
flux=zeros(1,numel(dT));
a  = 1/(2*(sqrt(2)-1)); %water front propagation speed
% Compute time-of-flight for the single-phase flow field and
record the corresponding breakthrough time in the producer.
ii=1;
for i=1:ny
    tbf(ii) = tof(i.*ny)
    ii=ii+1;
end
tbf=min(tbf);

for k=1:numel(dT)
    T=T+dT(k);
% Initialize number of time intervals and array to hold the oil
in place
[N,M]    = deal(6,10);% main step is N, substep is M. number of
time intervals is M*N
oip      = zeros(N*M+1,1); oip(1) =
sum(state.s(:,2).*pv); %assume the initial pore volume is filled
with oil
for n=1:N
    fprintf(1,'Main step %d: ',n);
    for m=1:M
       state  = incompTPFA(state, G, hT, fluid,'bc',bc);
```

```
        state  = explicitTransport(state, G, dT(k)/(N*M), rock,
fluid,'bc',bc);
        fprintf(1,'%d, ',m);
    end
    fprintf(1,'\n');

    % Plot multiphase solution
    subplot(1,2,1);
    contourf(reshape(G.cells.centroids(:,1), G.cartDims),...
        reshape(G.cells.centroids(:,2), G.cartDims), ...
        reshape(state.s(:,2),G.cartDims),[0 cval
1],'EdgeColor','none');
    ch=colorbar; set(get(ch,'title'),'string','So');
%     title(sprintf('T: %.0f s', T/10^4));
    hold on;
    caxis([0 1]);
    axis equal; axis([0 domain(1) 0 domain(2)]);
    set(gca,'XTick',[],'YTick',[]);
    % Plot multiphase solution as function of single-phase time-
of-flight
    subplot(1,2,2);
%   set(gca,'position',get(gca,'position')+[0 1 1 1]);
    plot(tof(:,1)/tbf,state.s(:,1),'.k','MarkerSize',4);
    set(gca,'YLim',[0 1]);
    set(gca,'XTick',[]);
    xlabel('x'); ylabel('Sw');
    drawnow;
end
%Calculation of Sw
for i=1:(numel(state.s)./2)
    Swt(k)=Swt(k)+state.s(i,1)
end
aveSwt(k)=Swt(k)./(numel(state.s)./2);

%flux vs displacing time
e = bc.face(strcmp('pressure', bc.type));
for j=1:ny
    flux(k)=flux(k)+state.flux(e(j))
end
flux(k)=flux(k)./ny;
% if k>1
```

```
% dtime(k)=(dtime(k-1)+T)./10^4;
% else
%     dtime(k)=T./10^4;
% end
dtime(k)=T;
y(k)=flux(k);
end
xlabel('Final time for integration (s)');
ylabel('flow rate (m^3/s)');
plot(dtime,y);
```

Appendix B: Two-dimensional Randomly Distributed Case Centrifuge Simulation

```
clear all
mrstModule add incomp diagnostics
%% Set up grid and petrophysical data
nx=155;ny=100;
lx=0.0520;ly=0.0336; domain = [lx ly];
G = cartGrid([nx,ny],[lx,ly]);
G = computeGeometry(G);
%% Gaussina porosity and permeability field
K = gaussianField(G.cartDims, [322 400].*milli*darcy);
rock = makeRock(G, K(:), .2828);
%% computation of upscaled permeability
q   = ones(G.cells.num,1);
vol = G.cells.volumes;
% Arithmetic
for i=1:size(rock.perm,2)
crock.perm(:,i) =
accumarray(q,vol.*rock.perm(:,i)) ./accumarray(q,vol);
end
%% The histogram of the permeability distribution in 1D problem
KK = convertTo(rock.perm,milli*darcy);
plotCellData(G,KK,'EdgeColor','none');axis tight;
xlabel('x');ylabel('y');
% [h,az] = colorbarHist(KK,[300 400],'South');
% hist(KK,20);xlabel('Permeability, mD'); ylabel('Frequency')
ca=colorbar; caxis([290 390]);
% set(get(ca,'title'),'string','(mD)');
pv     = poreVolume(G, rock);
%% Compute half transmissibilities
hT = computeTrans(G, rock);
%% Fluid model
```

```
gravity reset off
fluid = initSimpleFluidJfunc('mu' , [   1.01,
5.9]*centi*poise     , ...
    'rho', [1040, 858]*kilogram/meter^3, ...
    'n'  , [   2,   2], ...
    'surf_tension',1, ...
    'rock', rock);
%% Impose boundary condition
[src,bc] = deal([]);
bc = pside(bc, G, 'EAST',0*barsa,'sat', [1 0]);
bc = pside(bc, G, 'WEST',4.116*barsa,'sat', [0 1]);

clf, plotGrid(G,'FaceColor', 'none'); view(2);
plotFaces(G, bc.face(strcmp(bc.type,'pressure')), 'b');
plotFaces(G, bc.face(strcmp(bc.type,'pressure')), 'r');
%% Construct reservoir state object
state = initResSol(G, 0.0, [1 0]);
%% Solve pressure and show the result
state = incompTPFA(state, G, hT, fluid, 'src', src,'bc',bc);
clf,
plotCellData(G, convertTo(state.pressure, barsa()), 'EdgeColor',
'k');
axis equal tight; colorbar;
%% Compute time-of-flight
mrstModule add diagnostics
tof = computeTimeOfFlight(state, G, rock,'bc',bc);

clf,
plotCellData(G, tof);
axis equal tight;
colormap(jet(11));
caxis('auto'); colorbar;
%% Visualize high-flow and stagnant regions
tofb = computeTimeOfFlight(state, G, rock, 'bc', bc, 'reverse',
true);

clf,
plotCellData(G, tof+tofb);
axis equal tight;
colormap(jet(128));
%% Trace streamlines
```

```
mrstModule add streamlines;
j=1;
for i=0:ny-1
    seed(j) = 1+i.*nx;
    j=j+1;
end
seed=seed.';

clf,
Sf = pollock(G, state, seed, 'substeps', 1);
hf=streamline(Sf);
axis equal tight;
set([hf],'Color','k');
%% Compute solution and plot saturation evolution
% Figure, colormap and contour values
nval = 25;
cval = linspace(0,1,nval+1);
cval=.5*cval(1:end-1)+.5*cval(2:end);
T=0;
% dT=ones(1,20).*(10^8/20);
dT=ones(1,20).*(11.55/20);
Swt=zeros(1,numel(dT));
flux=zeros(1,numel(dT));
a = 1/(2*(sqrt(2)-1)); %water front propagation speed
% Compute time-of-flight for the single-phase flow field and
record the corresponding breakthrough time in the producer.
ii=1;
for i=1:ny
    tbf(ii) = tof(i.*ny)
    ii=ii+1;
end
tbf=min(tbf);

for k=1:numel(dT)
    T=T+dT(k);
% Initialize number of time intervals and array to hold the oil
in place
[N,M]    = deal(6,10);% main step is N, substep is M. number of
time intervals is M*N
```

```
oip      = zeros(N*M+1,1); oip(1) =
sum(state.s(:,2).*pv); %assume the initial pore volume is filled
with oil
for n=1:N
    fprintf(1,'Main step %d: ',n);
    for m=1:M
       state  = incompTPFA(state, G, hT, fluid,'bc',bc);
       state  = explicitTransport(state, G, dT(k)/(N*M), rock,
fluid,'bc',bc);
       fprintf(1,'%d, ',m);
    end
    fprintf(1,'\n');

    % Plot multiphase solution
    subplot(1,2,1);
    contourf(reshape(G.cells.centroids(:,1), G.cartDims),...
        reshape(G.cells.centroids(:,2), G.cartDims), ...
        reshape(state.s(:,2),G.cartDims),[0 cval
1],'EdgeColor','none');
    ch=colorbar; set(get(ch,'title'),'string','So');
%     title(sprintf('T: %.0f s', T./10^4));
    hold on;
    % Plot corresponding time lines from single-phase solution
    contour(reshape(G.cells.centroids(:,1), G.cartDims),...
        reshape(G.cells.centroids(:,2), G.cartDims), ...
        reshape(tof,G.cartDims),a/N, '-k','LineWidth',1);
    caxis([0 1]);
    axis equal; axis([0 domain(1) 0 domain(2)]);
    set(gca,'XTick',[],'YTick',[]);
    % Plot multiphase solution as function of single-phase time-
of-flight
    subplot(1,2,2)
%     set(gca,'position',get(gca,'position')+[0 .12 0 0]);
    plot(tof(:,1)/tbf,state.s(:,1),'.k','MarkerSize',4);
%     set(gca,'XLim',[0 5.5]);  set(gca,'YLim',[0 1]);
    set(gca,'XTick',[]); xlabel('x'); ylabel('Sw');
    drawnow;
end
%Calculation of Sw
for i=1:(numel(state.s)./2)
    Swt(k)=Swt(k)+state.s(i,1)
```

```
end
aveSwt(k)=Swt(k)./(numel(state.s)./2);
%flux vs displacing time
e = bc.face(strcmp('pressure', bc.type));
for j=1:ny
    flux(k)=flux(k)+state.flux(e(j))
end
flux(k)=flux(k)./ny;
dtime(k)=T./10^4;
y(k)=flux(k);
end
plot(dtime,y);
```

Appendix C: Two-dimensional Heterogeneous Case with a Heterogeneous Area Centrifuge Simulation

```
clear all
mrstModule add incomp diagnostics
%% Set up grid and petrophysical data
nx=155;ny=100;
lx=0.0520;ly=0.0336; domain = [lx ly];
G = cartGrid([nx,ny],[lx,ly]);
G = computeGeometry(G);
%% fracture low/high perm case
f=1;
if f==1
    %Case 3.1
    K = gaussianField(G.cartDims, [322 400].*milli*darcy);
    K(76:79,49:52)=20.*milli*darcy;
    rock = makeRock(G, K(:), .2828);
elseif f==5
    %Case 3.2
    K = gaussianField(G.cartDims, [323 400].*milli*darcy);
    K(70:85,43:58)=20.*milli*darcy;
    rock = makeRock(G, K(:), .2828);
elseif f==10
    %Case 3.3
    K = gaussianField(G.cartDims, [324 400].*milli*darcy);
    K(63:93,35:65)=20.*milli*darcy;
    rock = makeRock(G, K(:), .2828);
end
%% computation of upscaled permeability
q   = ones(G.cells.num,1);
```

```
vol = G.cells.volumes;
% Arithmetic
for i=1:size(rock.perm,2)
crock.perm(:,i) =
accumarray(q,vol.*rock.perm(:,i)) ./accumarray(q,vol);
end
%% The histogram of the permeability distribution in 1D problem
KK = convertTo(rock.perm,milli*darcy);
plotCellData(G,KK,'EdgeColor','none');axis tight;
xlabel('x');ylabel('y');
% [h,az] = colorbarHist(KK,[300 400],'South');
% hist(KK,20);xlabel('Permeability, mD'); ylabel('Frequency')
% set(az,'Position',get(az,'Position')-[0 0 0 .02]);
ca=colorbar; caxis([290 390]);
% set(get(ca,'title'),'string','(mD)');
pv     = poreVolume(G, rock);
%% Compute half transmissibilities
hT = computeTrans(G, rock);
%% Fluid model
gravity reset off
fluid = initSimpleFluidJfunc('mu' , [   1.01,
5.9]*centi*poise     , ...
    'rho', [1040, 858]*kilogram/meter^3, ...
    'n'  , [   2,   2], ...
    'surf_tension',1, ...
    'rock', rock);
%% Impose boundary condition
[src,bc] = deal([]);
bc = pside(bc, G, 'EAST',0*barsa,'sat', [1 0]);
bc = pside(bc, G, 'WEST',4.116*barsa,'sat', [0 1]);

clf, plotGrid(G,'FaceColor', 'none'); view(2);
plotFaces(G, bc.face(strcmp(bc.type,'pressure')), 'b');
plotFaces(G, bc.face(strcmp(bc.type,'pressure')), 'r');
%% Construct reservoir state object
state = initResSol(G, 0.0, [1 0]);
%% Solve pressure and show the result
state = incompTPFA(state, G, hT, fluid, 'src', src,'bc',bc);
clf,
plotCellData(G, convertTo(state.pressure, barsa()), 'EdgeColor',
'k');
```

```
axis equal tight; colorbar;
%% Compute time-of-flight
mrstModule add diagnostics
tof = computeTimeOfFlight(state, G, rock,'bc',bc);

clf,
plotCellData(G, tof);
axis equal tight;
colormap(jet(11));
caxis('auto'); colorbar;
%% Visualize high-flow and stagnant regions
tofb = computeTimeOfFlight(state, G, rock, 'bc', bc, 'reverse',
true);

clf,
plotCellData(G, tof+tofb);
axis equal tight;
colormap(jet(128));
%% Trace streamlines
mrstModule add streamlines;
j=1;
for i=0:ny-1
    seed(j) = 1+i.*nx;
    j=j+1;
end
seed=seed.';

clf,
Sf = pollock(G, state, seed, 'substeps', 1);
hf=streamline(Sf);
axis equal tight;
set([hf],'Color','k');
%% Compute solution and plot saturation evolution
% Figure, colormap and contour values
nval = 25;
cval = linspace(0,1,nval+1);
cval=.5*cval(1:end-1)+.5*cval(2:end);
T=0;
% dT=ones(1,20).*(10^8/20);
dT=ones(1,20).*(11.55/20);
Swt=zeros(1,numel(dT));
```

```
flux=zeros(1,numel(dT));
a  = 1/(2*(sqrt(2)-1)); %water front propagation speed
% Compute time-of-flight for the single-phase flow field and
record the corresponding breakthrough time in the producer.
ii=1;
for i=1:ny
    tbf(ii) = tof(i.*ny)
    ii=ii+1;
end
tbf=min(tbf);

for k=1:numel(dT)
    T=T+dT(k);
% Initialize number of time intervals and array to hold the oil
in place
[N,M]    = deal(6,10);% main step is N, substep is M. number of
time intervals is M*N
oip      = zeros(N*M+1,1); oip(1) =
sum(state.s(:,2).*pv); %assume the initial pore volume is filled
with oil
for n=1:N
    fprintf(1,'Main step %d: ',n);
    for m=1:M
       state  = incompTPFA(state, G, hT, fluid,'bc',bc);
       state  = explicitTransport(state, G, dT(k)/(N*M), rock,
fluid,'bc',bc);
       fprintf(1,'%d, ',m);
    end
    fprintf(1,'\n');

    % Plot multiphase solution
    subplot(1,2,1);
    contourf(reshape(G.cells.centroids(:,1), G.cartDims),...
        reshape(G.cells.centroids(:,2), G.cartDims), ...
        reshape(state.s(:,2),G.cartDims),[0 cval
1],'EdgeColor','none');
    ch=colorbar; set(get(ch,'title'),'string','So');
%     title(sprintf('T: %.0f s', T./10^4));
    hold on;
    % Plot corresponding time lines from single-phase solution
    contour(reshape(G.cells.centroids(:,1), G.cartDims),...
```

```
        reshape(G.cells.centroids(:,2), G.cartDims), ...
        reshape(tof,G.cartDims),a/N, '-k','LineWidth',1);
    caxis([0 1]);
    axis equal; axis([0 domain(1) 0 domain(2)]);
    set(gca,'XTick',[],'YTick',[]);
    % Plot multiphase solution as function of single-phase time-
of-flight
    subplot(1,2,2)
%     set(gca,'position',get(gca,'position')+[0 .12 0 0]);
    plot(tof(:,1)/tbf,state.s(:,1),'.k','MarkerSize',4);
%     set(gca,'XLim',[0 5.5]);  set(gca,'YLim',[0 1]);
    set(gca,'XTick',[]); xlabel('x'); ylabel('Sw');
    drawnow;
end
%Calculation of Sw
for i=1:(numel(state.s)./2)
    Swt(k)=Swt(k)+state.s(i,1)
end
aveSwt(k)=Swt(k)./(numel(state.s)./2);
%flux vs displacing time
e = bc.face(strcmp('pressure', bc.type));
for j=1:ny
    flux(k)=flux(k)+state.flux(e(j))
end
flux(k)=flux(k)./ny;
dtime(k)=T./10^4;
y(k)=flux(k);
end
plot(dtime,y);
```

Appendix D: Streamline Tracing in Cartesian Grid

```
function varargout = pollock(G, state, varargin)
%Trace streamlines in logically Cartesian grid using Pollock
approximation.
%
% SYNOPSIS:
%   [S,T,C] = pollock(G, state)
%   [S,T,C] = pollock(G, state, startpos)
%   [S,T,C] = pollock(G, state, 'pn', pv, ...)
%   [S,T,C] = pollock(G, state, startpos, 'pn', pv, ...)
%
% PARAMETERS:
```

```
%
%   G         - Cartesian or logically Cartesian grid.
%
%   state     - State structure with field 'flux'.
%
% OPTIONAL PARAMETER
%
%   positions - Matrix of size (N, 1) or (N, d+1), where d is the
dimension
%               of the grid, used to indicate where the
streamlines should
%               start.
%
%               If the size is (N, 1), positions contains the
cell indices
%               in which streamlines should start. Each
streamline is
%               started in the the local coordinate (0.5,
0.5, ...). To be
%               precise, this is the mean of the corner points,
not the
%               centroid of the cell.
%
%               If the size is (N, d+1), the first column
contains cell
%               indices, and the d next columns contain the local
%               coordinates at which to start streamlines.
%
% OPTIONAL PARAMETERS:
%
%   substeps  - Number of substeps in each cell, to improve
visual quality.
%               Default 5.
%
%   maxsteps  - Maximal number of points in a streamline.
%               Default 1000.
%
%   reverse   - Reverse velocity field before tracing.
%               Default false.
%
```

```
%   pvol      - Pore-volume vector.  One positive scalar for each
active
%               cell in the grid `G`.  Makes the physical
interpretation of
%               time-of-flight appropriate for non-uniform
porosity fields.
%
%   isoutflow - Cell-wise boolean indicator which indicates if a
streamline
%               should terminate upon reaching that cell.
Defaults to
%               false(G.cells.num, 1) and is useful in the
presence of many
%               weak source terms (which do not lead to inflow or
outflow
%               over all faces for a given source term).
%
%   blocksize - Internal parameter indicating how many
streamlines are
%               processed simultaneously. Larger values give
faster
%               processing, at a higher memory cost. Default:
1000.
%
% RETURNS:
%
%  S      - Cell array of individual streamlines suitable for
calls like
%           streamline(pollock(...)) and
streamtube(pollock(...)).
%
%  T      - Time-of-flight of coordinate.
%
%  C      - Cell number of streamline segment, i.e, line segment
between
%           two streamline coordinates.
%
% EXAMPLE:
%
%   S = pollock(G, x);
%   % pad with nan's
```

```
%   S = reshape([S, repmat({[nan, nan]}, [numel(S),1])]',[], 1);
%   S = vertcat(S{:});
%   plot(S(:,1), S(:,2), 'r-');
%
%   streamline(pollock(G, x, 'pvol', poreVolume(G, rock)));
%
% SEE ALSO:
%   `streamline`.

%{
Copyright 2009-2020 SINTEF Digital, Mathematics & Cybernetics.

This file is part of The MATLAB Reservoir Simulation Toolbox
(MRST).

MRST is free software: you can redistribute it and/or modify
it under the terms of the GNU General Public License as published
by
the Free Software Foundation, either version 3 of the License, or
(at your option) any later version.

MRST is distributed in the hope that it will be useful,
but WITHOUT ANY WARRANTY; without even the implied warranty of
MERCHANTABILITY or FITNESS FOR A PARTICULAR PURPOSE.  See the
GNU General Public License for more details.

You should have received a copy of the GNU General Public License
along with MRST.  If not, see <http://www.gnu.org/licenses/>.
%}

% Written by Jostein R. Natvig, SINTEF ICT, 2010.

   d = size(G.nodes.coords, 2);
   if mod(nargin, 2) == 0
      positions = [(1:G.cells.num)', repmat(0.5, [G.cells.num,
d])];
   else
      positions = varargin{1};
      if size(positions, 2) == 1
         positions = [positions, repmat(0.5, [size(positions, 1),
d])];
```

```
      elseif size(positions, 2) ~= 1 + d
         error('Expected array of local positions of width 1 or
1+d.');
      end
      varargin = varargin(2:end);
   end

   opt = struct('substeps'  , 5,     ...
                'maxsteps'  , 1000,  ...
                'reverse'   , false, ...
                'isoutflow' , false(G.cells.num, 1), ...
                'blocksize' , 1000,  ...
                'pvol'      , ones([G.cells.num, 1]), ...
                'flux'      , [], ... % See
getInteriorFluxesStreamlines
                'neighbors' , []);    % See
findStreamlineNeighborshipCart
   opt = merge_options(opt, varargin{:});

   if ~all(opt.pvol > 0)
      error('PoreVol:NonPositive', ...
            'Rock pore-volume must be strictly positive in all
cells');
   end

   [varargout{1:nargout}] = trace(G, state, positions, opt);
end

%
================================================================
========

function varargout = trace(G, state, pos, opt)
   d              = size(G.nodes.coords, 2);
   numStreamlines = size(pos, 1);
   assert(size(pos, 2) == d + 1);

   if ~isfield(G, 'cellNodes')
      cn = cellNodes(G);
      G.cellNodes = accumarray(cn(:,1:2), cn(:,3));
   end
```

```
   % Make array face fluxes for each cell in grid (Not outer).
   flux = opt.flux;
   if isempty(flux)
      flux = getInteriorFluxesStreamlines(G, state, opt.pvol,
opt.reverse);
   end

   neighbors = opt.neighbors;
   if isempty(neighbors)
      neighbors  = findStreamlineNeighborshipCart(G);
   end

   magic  = opt.blocksize;
   XYZ    = nan(numStreamlines, d, magic);
   T      = nan(numStreamlines, magic);
   C      = nan(numStreamlines, magic);
   active = true(numStreamlines, 1);


   % Store crossing coordinates of active streamlines
   [XYZ(active,:,1)] = globalCoordinate(G, pos(active,1),
pos(active, 2:end));
   T(active, 1) = zeros(sum(active), 1);
   C(active, 1) = pos(active,1);

   i = 2;
   while any(active)
      % Realloc
      if i+opt.substeps+1 > size(XYZ, 3)
         magic = max(magic, opt.substeps+1);
         XYZ   = cat(3, XYZ, nan(numStreamlines, d, magic));
         T     = cat(2, T,   nan(numStreamlines, magic));
         C     = cat(2, C,   nan(numStreamlines, magic));
      end
      current_cell = pos(active,1);

      % Take another pollock step
      [pos(active, :), t, xyz] = step(pos(active,:), flux,
neighbors, opt.substeps);
```

```
      % Store crossing coordinates and, optionally, coordinates
along curve
      % trajectory in cell of active streamlines
      for k=1:opt.substeps
         [XYZ(active, :, i+k-1)] = globalCoordinate(G,
current_cell, xyz(:,:,k));
      end
      T(active, i-1+(1:opt.substeps)) = repmat(t/opt.substeps,
[1, opt.substeps]);
      C(active, i-1+(1:opt.substeps)) = repmat(pos(active, 1),
[1, opt.substeps]);

      % Update active flag
      active(active)    =  pos(active,1) ~= current_cell &
~opt.isoutflow(current_cell);

      i = i+opt.substeps;
      if i > opt.maxsteps
          break;
      end
   end

   % Pack coordinates in list with streamlines separated by NaN.
   p = reshape(permute(XYZ, [3,1,2]), [], d);

   i = ~isnan(p(:,1));
   j = i|[true;i(1:end-1)];
   p = p(j,:);

   % Pack streamline coordinates in a cell array suitable for use
with
   % Matlab streamline, i.e., as in 'streamline(pollock(G,
resSol));'
   flag = isnan(p(:,1));
   ix = find(flag);
   dd  = diff([0;ix])-1;
   varargout{1} = mat2cell(p(~flag,:), dd, d);
   if nargout > 1
      T = reshape(T', [], 1);
      T = T(j);
      varargout{2} = mat2cell(T(~flag), dd, 1);
```

```
   end
   if nargout > 2
      C = reshape(C', [], 1);
      C = C(j);
      varargout{3} = mat2cell(C(~flag), dd, 1);
   end
end

%
================================================================
========

function xyz = globalCoordinate(G, c, p)
% Compute global coordinate corresponding to local coordinate p
in cells c
% p  - local positions == [xi,eta,zeta] in 3D
% c  -

   if numel(c)==1, p = reshape(p, 1, []); end

   % Compute node weight for quadrilateral or hexahedron
   d = size(G.nodes.coords, 2);
   w = ones(size(p,1), 2^d);
   for i=1:d
      mask        = logical(bitget((0:2^d-1)', i));
      w(:, mask)  = w(:, mask).* repmat(  p(:,i), [1,
sum( mask)]);
      w(:,~mask)  = w(:,~mask).* repmat(1-p(:,i), [1,
sum(~mask)]);
   end

   % Compute weighted average of corner points
   xyz = zeros(size(p,1), d);
   for i=1:d
      xi       = G.nodes.coords(:,i);
      xyz(:,i) = sum(w .* reshape(xi(G.cellNodes(c, :))', 2^d,
[])', 2);
   end
end
```

```
%
================================================================
========

function [pos, tof, xyz] = step(pos, flux, neighbors, nsubsteps)
% Update pos array by computing new local coordinate and new
cell.
% In addition, compute curve within cell.

   f = flux(pos(:,1),:);
   n = neighbors(pos(:,1),:);

   dims = size(pos, 2)-1;
   T    = nan(size(pos,1),dims);
   for i=1:dims
      T(:,i) = computeTime(pos(:,1+i), f(:,2*i-1:2*i));
   end
   [tof, dir] = min(T, [], 2);

   xyz = zeros(size(pos,1), dims, nsubsteps);
   d   = zeros(size(pos, 1), 1);
   for s=1:nsubsteps
      for i=1:dims
         t = tof*s/nsubsteps;
         [xyz(:,i,s), d(:,i)] = computePosition(pos(:,1+i),
f(:,2*i-1:2*i), t);
      end
   end

   pos (:,2:end) = xyz(:,:,s);

   % Find direction to look up neighbor cell
   k  = 2*(dir-1)+d(sub2ind([numel(dir), 3], (1:numel(dir))',
dir));
   t  = sub2ind(size(n), (1:numel(k))', k);

   % Update cell number if NOT at boundary.
   % IF at boundary, mark dir with NaN to avoid changing local
coordinate
   % below.
   ind         = n(t)==0;
```

```
   % Also, if there is no finite time to escape the current cell,
set NaN
   % value to indicate that the streamline has terminated.
   ind         = ind | all(~isfinite(T), 2);
   pos(~ind,1) = n(t(~ind));
   dir (ind)   = nan;

   % Change local coordinate when moving to new cell
   k = sub2ind(size(d), (1:size(dir,1))', dir);
   k = k(~isnan(k));
   pos(numel(dir) + k ) = 2-d(k);
end

%
================================================================
========

function t = computeTime(xi, v)
% Compute time needed to reach xi=0 or xi=1 given velocities
v=[v1,v2] at
% xi=0 and xi=1.  The formula is
%
%   t = xi/ui  or t = (1-xi)/ui,    if v1 = v2 = ui, and
%
%   t = 1/(v2-v1)*log(ue/ui),       otherwise
%
% where ui=v2*xi+v1*(1-xi) is the velocity at xi, and ue=v2 if
ui>0 or
% ue=v1 if ui<0.

   tolerance = 100*eps;

   ui          = v(:,1) + xi.*diff(v, 1, 2);%(:,2)-v(:,1));
   ue          = v(:,    2);
   ue (ui<0)   = v(ui<0, 1);
   arg         = ue./ui;
   t           = inf(size(xi));

   % Linear velocity
   ind         = abs(diff(v, 1, 2)) > tolerance*abs(v(:,1));
   t(ind,:)    = 1./diff(v(ind,:), 1, 2).*log(arg(ind,:));
```

```
   % Constant velocity
   ds          = -xi;
   ds(ui > 0)  = 1-xi(ui>0);
   t(~ind)     = ds(~ind)./ui(~ind);

   % nan happens for ui=ui=0
   t(arg<=0 | isnan(arg))   = inf;
end

%
================================================================
========

function [x, i] = computePosition(xi, v, t)
% Compute position at time t given start point xi and velocities
v=[v1,v2].
%
%   x = xi + v*t,    if v is constant or
%
%   x = xi + (ui*exp((v2-v1)*t) - ui)/(v2-v1), otherwise
%
   tolerance = 100*eps;

   du          = diff(v, 1, 2);
   ui          = v(:,1) + xi.*du;
   i           = 1 + ~(ui<0);
   x           = inf(size(xi));

   ind         = abs(du) > tolerance*abs(v(:,1));

   % linear velocity
   x(ind)     = xi(ind) + ( ui(ind).*exp(du(ind).*t(ind)) -
ui(ind))./du(ind);

   % Constant velocity
   x(~ind,:) = xi(~ind,:) + v(~ind, 1).*t(~ind, :);
   x(~ind & t==inf) = xi(~ind & t==inf);
end
```

Appendix E: Explicit Two-phase Flow Transport Solver

```
function state = explicitTransport(state, G, tf, rock, fluid,
varargin)
%Explicit single-point upstream mobility-weighted transport
solver for two-phase flow.
%
% SYNOPSIS:
%   state = explicitTransport(state, G, tf, rock, fluid)
%   state = explicitTransport(state, G, tf, rock, fluid, 'pn1',
pv1, ...)
%
% DESCRIPTION:
%   Implicit discretization of the transport equation
%
%      s_t + div[f(s)(v + mo K((rho_w-rho_o)g + grad(P_c)))] =
f(s)q
%
%   where v is the sum of the phase Darcy fluxes, f is the
fractional
%   flow function,
%
%                  mw(s)
%        f(s) = -------------
%               mw(s) + mo(s)
%
%   mi = kr_i/mu_i is the phase mobility of phase i, mu_i and
rho_i are the
%   phase viscosity and density, respectively, g the (vector)
acceleration
%   of gravity, K the permeability, and P_c(s) the capillary
pressure.  The
%   source term f(s)q is a volumetric rate of water.
%
%   We use a first-order upstream mobility-weighted
discretization in space
%   and a backward Euler discretization in time. The transport
equation is
%   solved on the time interval [0,tf] by calling
twophaseJacobian to build
%   a function computing the residual of the discrete system in
addition to
```

```
%   a function taking care of the update of the solution during
the
%   time loop.
%
% REQUIRED PARAMETERS:
%   state - Reservoir and well solution structure either properly
%           initialized from function 'initState', or the results
from a
%           previous call to function 'solveIncompFlow' and,
possibly, a
%           transport solver such as function
'explicitTransport'.
%
%   G     - Grid data structure discretizing the reservoir model.
%
%   tf    - End point of time integration interval (i.e., final
time).
%           Measured in units of seconds.
%
%   rock  - Rock data structure.  Must contain the field
'rock.poro' and,
%           in the presence of gravity or capillary forces, valid
%           permeabilities measured in units of m^2 in field
'rock.perm'.
%
%   fluid - Fluid data structure as defined in 'fluid_structure'.
%
% OPTIONAL PARAMETERS:
%   W         - Well structure as defined by function 'addWell'.
This
%               structure accounts for all injection and
production well
%               contribution to the reservoir flow.
%               Default value: W = [], meaning a model without
any wells.
%
%   bc        - Boundary condition structure as defined by
function
%               'addBC'.  This structure accounts for all
external boundary
%               contributions to the reservoir flow.
```

```
%               Default value: bc = [] meaning all external no-
flow
%               (homogeneous Neumann) conditions.
%
%   src       - Explicit source contributions as defined by
function
%               'addSource'. Default value: src = [] meaning no
explicit
%               sources exist in the model.
%
%   onlygrav  - Ignore content of state.flux.         Default
false.
%
%   computedt - Estimate time step.                   Default
true.
%
%   max_dt    - If 'computedt', limit time step.      Default
inf.
%
%   dt_factor - Safety factor in time step estimate.  Default
0.5.
%
%   dt        - Set time step manually.  Overrides all other
options.
%
%   gravity   - The current gravity in vector form. Defaults to
gravity().
%
%   satwarn   - Issue a warning if saturation is more than
'satwarn'
%               outside the default interval of [0,1].
%
% RETURNS:
%   state     - Reservoir solution with updated saturation,
state.s.
%
% EXAMPLE:
%   See simple2phWellExample.m
%
% SEE ALSO:
%   `twophaseJacobian`, `implicitTransport`.
```

```
   opt = struct(...
      'verbose'  , false      , ...
      'onlygrav' , false      , ...
      'computedt', true       , ...
      'max_dt'   , inf        , ...
      'dt_factor', 0.5        , ...
      'wells'    , []         , ...
      'W'        , []         , ...
      'src'      , []         , ...
      'bc'       , []         , ...
      'dt'       , tf         , ...
      'Trans'    , []         , ...
      'gravity'  , gravity()  , ...
      'satwarn'  , sqrt(eps));

   opt = merge_options(opt, varargin{:});
   opt = treatLegacyForceOptions(opt);
```

```
   if opt.onlygrav
      flux = state.flux;
      state.flux = zeros(G.faces.num, 1);
   end

   [F,~,gf,q] = twophaseJacobian(G, state, rock, fluid, ...
                         'wells', opt.wells,    ...
                         'src'  , opt.src  ,    ...
                         'bc'   , opt.bc,       ...
                         'Trans', opt.Trans);


   if opt.computedt

      % ---------- Time step estimate from state ---------------
      compi = { 'use_compi', true };
      vsrc = computeTransportSourceTerm(state, G, opt.wells, ...
                                        opt.src, opt.bc,
compi{:});
      vsrc = assembleTransportSource(state, fluid, vsrc,
G.cells.num, compi{:});

      gflux = getFlux(G, rock,opt);
      getdt = @(state) min([...
                  opt.max_dt, ...
                  opt.dt_factor * estimate_dt(G, state, rock,
fluid, ...
                                              state.flux,
gflux, vsrc)]);
   else

      % ----------- Constant time step ------------------------
      getdt =@(state) opt.dt;

   end


   s  = state.s(:,1);
   t  = 0;
```

```
   dispif(opt.verbose, 'explicitTransport: Computing transport
step in %d substeps\n', ...
           ceil(tf/getdt(state)));
   while t < tf
      dt      = min(tf-t, getdt(state));

      s(:)    = s - F(state, state, dt);
      t       = t + dt;

      s       = correct_saturations(s, opt.satwarn);

      state.s = [s, 1-s];

      if isfield(state, 'extSat')
         % Save minimum saturation for use in modeling of
relative
         % permeability hysteresis.
         state.extSat(:,1) = min(state.s(:,1),
state.extSat(:,1));
         state.extSat(:,2) = max(state.s(:,1),
state.extSat(:,2));
      end
   end

   if opt.onlygrav
      state.flux = flux;
   end

   if any(any(isnan(state.s)))
      error('explicitTransport: Transport step failed')
   end
end

%-----------------------------------------------------------------
----------
% Private helpers follow.
%-----------------------------------------------------------------
----------

function gflux = getFlux(G, rock, opt)
%harmonic average of one-sided n \cdot K \cdot g on each face
```

```
   gvec   = -opt.gravity;
   gflux  = zeros([G.faces.num, 1]);

   dim    = size(G.nodes.coords, 2);
   if(isempty(opt.Trans))
      [K, r, c] = permTensor(rock, dim);

      assert (size(K,1) == G.cells.num, ...
              ['Permeability must be defined in active cells
only.\n', ...
               'Got %d tensors, expected %d (== number of
cells).'],   ...
               size(K,1), G.cells.num);
   end
   nc     = G.cells.num;
   cellNo = rldecode(1 : nc, diff(G.cells.facePos), 2) .';

   if norm(gvec) > 0

      % nKg == n' * K * g for all cellfaces.
      nKg    = sum(G.faces.normals(G.cells.faces(:,1), r) .* ...
                   bsxfun(@times, K(cellNo,:), gvec(c)), 2);

      % Compute harmonic average of one-sided nKg on all faces.
      gflux = 2 ./ accumarray(G.cells.faces(:,1), 1 ./ nKg,
[G.faces.num, 1]);
   end


end


%-----------------------------------------------------------------
----------

function dt = estimate_dt(G, state, rock, fluid, flux, gflux,
sources)
   [rho, kr, mu, dkr] = getIncompProps(state, fluid);

   % Compute cell mobility and its derivative
```

```
   sat       = state.s;
   mob       = bsxfun(@rdivide, kr, mu);

   % dkr is Jacobian of kr.  We need derivatives with respect to
s(:,1),
   % hence sign of 'dkr(:,end)'.
   dmob = bsxfun(@rdivide, [dkr(:,1), -dkr(:,end)], mu);

   % Compute face density as average of cell densities.
   i = all(G.faces.neighbors > 0, 2);
   N = G.faces.neighbors(i, :);

   % Find simple approximation to the maximal wave speed from
advective
   % term in reservoir based on derivative of flux on face.
   df = @(mob, dmob) ...
        (mob(:,2).*dmob(:,1) - mob(:,1).*dmob(:,2))./(sum(mob,
2).^2);
   d  = df(mob, dmob);
   m  = max(abs(d(N)), [], 2);

   wavespeed  = max(abs(m.*flux(i)));

   % Find max wave speed from segregation term
   g      = @(mob) mob(:,1).*mob(:,2)./sum(mob, 2);
   s      = linspace(0,1, 101)';
   ss     = struct('s',[s,1-s]);
   [rho_loc, kr_loc, mu_loc] = getIncompProps(ss,
fluid); %#ok<ASGLU>
   m      = bsxfun(@rdivide, kr_loc, min(mu_loc, [], 2));
   dg     = max(abs(diff(g(m)))./diff(s));

   wavespeed  = max([wavespeed;
abs(dg.*gflux(i).*max(diff(rho_loc, 1, 2), [], 1))]  );

   % Find max wave speed from advective term for positive sources
in
   % interval [s, 1],
   i      = sources > 0;
   if any(i)
      s     = (min(sat(i)) : 0.05 : 1.0)';
```

```
      ss    = struct('s',[s,1-s]);
      if numel(s) > 1
         [tmp, kr, mu_w] = getIncompProps(ss, fluid); %#ok<ASGLU>
         mob   = bsxfun(@rdivide,  kr, mu_w);
         f     = bsxfun(@rdivide, mob(:,1), sum(mob, 2));
         maxdf = max(diff(f)./diff(s));
         wavespeed  = max(wavespeed, max(abs(sources(i) .*
maxdf)));
      end
   end

   % Find max wave speed from advective term for negative sources
in
   % interval [0, s],
   i      = sources < 0;
   if any(i)
      s     = (max(sat(i)) : -0.05 : 0.0)';
      ss=struct('s',[s,1-s]);
      if numel(s) > 1
         [kr, mu] = getIncompProps(ss, fluid);
         mob   = bsxfun(@rdivide,  kr, mu);
         f     = bsxfun(@rdivide, mob(:,1), sum(mob, 2));
         maxdf = max(diff(f)./diff(s));
         wavespeed  = max(wavespeed, max(abs(sources(i) .*
maxdf)));
      end
   end

   dt = min(abs(poreVolume(G, rock)/wavespeed));
end

function s = correct_saturations(s, satwarn)
   % Display error if s > 1+satwarn
   % or s < 0 - satwarn
   i = find(s(:,1) > 1 + satwarn);
   if ~isempty(i)
      disp('Saturation exceeds 1 in cells:')
      fprintf('%5d %g\n', [i, s(i,1)] .');
      error('explicitTransport: Error larger than satwarn')
   end
```

```
    i = find(s(:,1) < -satwarn);
    if ~isempty(i)
       disp('Saturation less than 0 in cells:')
       fprintf('%5d %g\n', [i, s(i,1)] .');
       error('explicitTransport: Error larger than satwarn')
    end
    % Correct numerical errors
    s(s(:,1) > 1, 1) = 1 - eps;
    s(s(:,1) < 0, 1) = 0;
end
```